Universitetet i Stavanger

FACULTY OF SCIENCE AND TECHNOLOGY
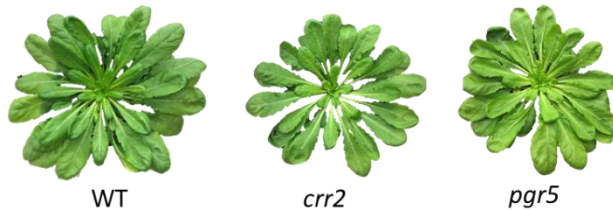
MASTER'S THESIS

Study programme/specialisation: MSc Biological Chemistry	Spring / Autumn semester, 20.19. Open Confidential
Author: Andrea Ramnath	………………………………………… (signature of author)
Programme coordinator: Hannah Kate Hondebrink Supervisor(s): Professor Lutz Andreas Eichacker and Stefanie Lackner	
Title of master's thesis: Mutants deficient in thylakoid membrane protein complexes characterize photosynthesis in Arabidopsis thaliana	
Credits: 60	
Keywords: Photosynthesis, free flow electrophoresis, native membrane complexes, cyclic electron flow	Number of pages: …………98……… + supplemental material/other: …None… Stavanger,…May 2019……………… date/year

Mutants deficient in thylakoid membrane protein complexes characterize photosynthesis in *Arabidopsis thaliana*

by

Andrea Ramnath

WT   crr2   pgr5

Master Thesis in Biological Chemistry

Supervised by Professor Lutz Andreas Eichacker and Stefanie Lackner

Submitted to the

Faculty of Science and Technology

Department of Biology, Chemistry and Environmental Engineering

May 2019

"Life is nothing but an electron looking for a place to rest."

— Albert Szent-Györgyi

Acknowledgements

I would like to express my sincere gratitude to Stefanie. Thank you for your endless patience and support. I have learnt so much from you, both within and beyond the academic setting. Thank you for making this experience so valuable for me and for taking the time to help me develop my skills and abilities. I appreciate your guidance and friendship so very much, and I will always cherish the many good memories we've made.

To Lutz, thank you for your mentorship and for supporting me in all academic aspects. Thank you for being so approachable and for investing so much time and energy towards my academic career. I will forever be grateful.

To my friends, both near and far, old and new; thank you for the encouragement and for helping to keep me motivated. Also, thank you to everyone at CORE who helped me when I needed it and gave me little words of support here and there.

Finally, I would like to thank my family. To my parents, Maya and Rajen, and to my sister, Andrecia; thank you for your unconditional love and support. I would not have achieved all that I have without your encouragement of the many bees in my bonnet. I am so very grateful to have you all in my life, even though there are great distances between us. I miss you every day, but I hope I've made you proud!

Abstract

Photosynthesis involves two major pathways through which light energy can be harvested and transformed into chemical energy. Light drives the flow of electrons through a chain of redox protein complexes to synthesize NADPH and is coupled to a flow of protons and ions across the thylakoid membrane of chloroplasts that drives ATP synthesis. The first route, namely linear electron flow begins at the reaction centre of Photosystem II (termed P680), couples to proton flow and the synthesis of ATP at the Cytochrome b_6f complex and ends at the reaction centre of Photosystem I (termed P700), where the terminal electron acceptor $NADP^+$ is reduced to NADPH. NADPH levels can consequently give us a comparative indication of how much linear electron flow is occurring. The second route, namely cyclic electron flow begins and ends at Photosystem I. Here, proton flow is also generated at the Cytochrome b_6f complex and ATP is synthesized. However, no accumulation of NADPH can occur since electrons are recycled from reduced ferredoxin from the acceptor side of Photosystem I. Alternatively, NADPH present inside the chloroplast can be used to reduce plastoquinone, the substrate of Cytochrome b_6f. Cyclic electron flow is believed to contribute to a regulation of photosynthesis and photoprotection in *Arabidopsis thaliana.* However, the components' importance and regulation is unclear. Two main partially redundant pathways are known, through which electrons are recycled back to plastoquinone: First, the "Proton Gradient Regulation 5" (PGR5) and "PGR5-Like Photosynthetic Phenotype 1" (PGRL1) and second, the "Chloroplast NADH dehydrogenase-like" (NDH) complex dependent pathways.

Here, photosystem complexes were isolated from the stroma thylakoid membrane of mutants *crr2* and *pgr5* in *A. thaliana*. Protein complexes were separated by free-flow interval zone electrophoresis, and analysed by spectroscopy, native-PAGE, dynamic light scattering and zeta potential measurements. Also, protein subunit composition was analysed by mass spectrometry. Further analysis of complex composition was done using SDS-PAGE and Western blotting. An indication towards a determination of the mode of electron transport was made using absorbance spectroscopy. It was shown that Photosystem I and Cytochrome b_6f complexes were found in complex together, and that this is a key complex in photosynthesis. Furthermore, it was shown that the absence of the PGR5 protein or NDH complex did not affect complex formation in the thylakoid stroma lamellae. Though, it could be shown that the ratio of complexes in the thylakoid stroma lamellae changed between the mutants and the wild-type. In addition, spectroscopic analysis of selected complexes suggested that the nature of PSI complexes was altered. Moreover, an increase in NADPH absorbance under light incubation suggested that both mutants show differences in linear electron flow rates.

Table of Contents

Abbreviations

β-DDM	n-Dodecyl β-D-Maltoside
Chl	Chlorophyll
CMC	Critical Micellar Concentration
crr2	chlororespiratory reduction (mutant)
Cytb$_6$f	Cytochrome b$_6$f
dH$_2$O	distilled water
FFE	free flow electrophoresis
FQR	ferredoxin-dependent plastoquinone reductase
hr(s)	hour(s)
hv	high voltage
kDa	kilo Dalton
LHCII	Light Harvesting Complex II
max	maximum
min	minutes
MS	Mass-Spectrometry
mV	milli Volts
NADH	Nicotinamide Adenine Dinucleotide
NADPH	Nicotinamide Adenine Dinucleotide Phosphate
NDH	NADH dehydrogenase-like
PAGE	polyacrylamide gel electrophoresis
pgr5	proton gradient regulation (mutant)
PS(I/II)	Photosystem (I/II)
rcf	relative centrifugal force
SDS	Sodium Dodecyl Sulphate
sec	seconds

SOP   Standard Operating Procedure

WT   Wild-Type

Introduction

Photosynthesis

In Photosynthesis, light drives the reduction of organic molecules and the synthesis of ATP. The molecular machinery that performs this process is found in the thylakoid membranes of chloroplasts where the photosynthetic process begins with the absorption of light energy by chlorophyll (Chl) (Hoober, 2016).

Photosystem I (PSI) and photosystem II (PSII) are the major protein complexes which control the light reactions of oxygenic photosynthesis. Light energy captured by PSI and PSII is eventually used to produce ATP and NADPH (absorbance at 340 nm). PSI and PSII are able to form super complexes with other photosynthetic proteins, in particular with the light harvesting antenna (LHCII) (Kouřil et al., 2005a, 2005b) and the NADH dehydrogenase-like complex (NDH) (Kouřil et al., 2005b). PSI was shown to bind one LHCII trimer at the site of the PsaK and PsaL subunits (Galka et al., 2012; Kouřil et al., 2005a)

The PSI super-complexes, in addition to light-harvesting, also contribute to regulating electron flow. There are two modes of electron flow that have been described, namely linear electron flow (LEF) and cyclic electron flow (CEF). For LEF, electrons flow from PSII to $Cytb_6f$ and then to PSI, and eventually produce ATP and NADPH. For CEF, electrons are cycled around PSI back to $Cytb_6f$, and ATP is eventually synthesised without an accumulation of NADPH. By regulating LEF and CEF, it is therefore possible to adjust the ratio of ATP/NADPH that is produced in response to changing metabolic and environmental conditions.

Under certain conditions, CEF appears to contribute substantially to photosynthetic electron flow, for example during induction of photosynthesis and under abiotic stress such as drought, high light and extreme temperatures (Johnson, 2011). There are two pathways responsible for CEF, which are thought to be partially redundant, through which electrons are recycled back to plastoquinone: 1. Proton Gradient Regulation (PGR5) and PGR5-Like Photosynthetic Phenotype1 (PGRL1) protein dependent pathway; 2. Chloroplast NADH dehydrogenase-like (NDH) complex dependent pathway. (DalCorso et al., 2008; Drop et al., 2014; Shikanai et al., 1998)

Plants must balance between an exploitation of light energy for production of ATP and NADPH in photosynthesis and a protection against photooxidation. Two major regulatory mechanisms are discussed, state transition and cyclic electron transfer. State transition contributes to balance light harvesting for maintaining electron flow between the two photosystems, by reversible redistribution of a mobile light-harvesting antenna (LHCII) between PSII and PSI (Bellafiore et al., 2005). Cyclic electron flow contributes to protect the plant from photooxidation and electrons are cycled around PSI (Yamori and Shikanai, 2016).

The function and structure of PSI super-complexes is thought to contribute to regulation of electron flow; however, this is not well understood. A super-complex composed of PSI and Cytb$_6$f complex was described in *Chlamydomonas reinhardtii* (Iwai et al., 2010; Steinbeck et al., 2018) and also found in *Arabidopsis thaliana* (Yadav et al., 2017). This super-complex is thought to play a role in the regulation of CEF. Another super-complex, composed of two PSI complexes held together by a centrally positioned NDH complex is also thought to play a part in CEF regulation (Kouril et al., 2005). It has been suggested that LHCs serve a role beyond light harvesting and energy dissipation, and that LHCA6 is important for NDH-PSI super-complex formation in *A. thaliana.* Analysis of the PSI-LHCI super-complex with putatively bound LHCII trimers showed that other LHC complexes could potentially competitively block Cytb$_6$f dimer binding (Steinbeck et al., 2018).

Chloroplast function and structure

Chloroplasts generate metabolic energy, which is also the case for mitochondria; however, chloroplasts are larger (5 – 10 μm long) and more complex than mitochondria and perform tasks in addition to ATP synthesis. Chloroplasts are responsible for the photosynthetic conversion of carbon dioxide to carbohydrates, but they also synthesize amino acids, fatty acids, and the lipid components of their own membranes. (Cooper, 2000)

The inner volume of chloroplasts is separated from the cells cytoplasm by two membranes – the chloroplast envelope membranes and contains an internal membrane system which harbours the photosynthetic machinery. This internal membrane system, called the thylakoid membrane, consists of grana stacks and the stromal lamellae (Cooper, 2000). The photosystems (which make up part of the photosynthetic machinery) are only close to one another in a small part of the thylakoid membrane. Typically, in higher plants, 80% of the thylakoid membrane is arranged in grana stacks which contains about 85% of PSII reaction centres associated with LHCII. The remaining 20% of the thylakoid membrane resembles the stromal lamellae which interconnect the grana stacks. PSI requires access to ferredoxin (Fd) and NADP$^+$ which are found in the stroma of the chloroplast; and it has been found that PSI and ATP synthase are localised mainly in the stromal lamellae and the edges and surfaces of the grana stacks. The stroma lamellae also contain some PSII but with smaller antenna. (Hoober, 2016). The distribution of the thylakoid membrane in distinct grana stacks and stromal lamellae is dependent on a family of proteins (curT – curvature thylakoid1) (Heinz et al., 2016).

It has been shown in higher plants such as *A. thaliana,* that the PSII-LHCII complexes as well as PSI oligomers have a molecular weight of about 720 kDa and complexes consisting of PSI-LHCI/II and PSI-LHCI fall within the range of 480 - 720 kDa (Yokono et al., 2015). It has also been shown in cyanobacteria *Synechococcus elongatus* that PSI exists as a trimer in its native state within the membrane and has a molecular mass of 1068 kDa and a super-complex estimated to have a molecular mass of 2400 kDa, was shown to contain PSI, PSII, LHCII and LHCI (Fromme et al., 2001). The individual LHC proteins have molecular masses between 22 and 25 kDa (Galetskiy et al., 2008).

Chloroplasts isolated in low-salt media have been shown to lose the thylakoid grana structure without release of Chl. These grana-free chloroplasts are noticeably swollen and consist almost entirely of continuous sheets of paired-membrane structures - the lamellae. Addition of salts (NaCl, MgCl$_2$ or methylaniline hydrochloride) to the grana-free low salt chloroplasts were found to provide strong interlamellar attractions. These attractions resulted in a sometimes almost random stacking of the lamellae and sometimes resulted in regular structures indistinguishable from the original grana. (Izawa and Good, 1966).

Physiological functions of cyclic electron transport around PSI

Cyclic electron transfer around PSI generates ATP without causing a build-up of NADPH in chloroplasts. As mentioned previously, there are two pathways *(Figure 1)* through which electrons are cycled back to the Cytb$_6$f complex: 1. PGR5-PGRL1 protein dependent pathway via the FQR complex and 2. Chloroplast NADH dehydrogenase-like complex dependent pathway via the NDH complex. Electrons are recycled from ferredoxin (Fd) to plastoquinone (PQ), consequently there is no accumulation of NADPH in the chloroplast (Yamori and Shikanai, 2016).
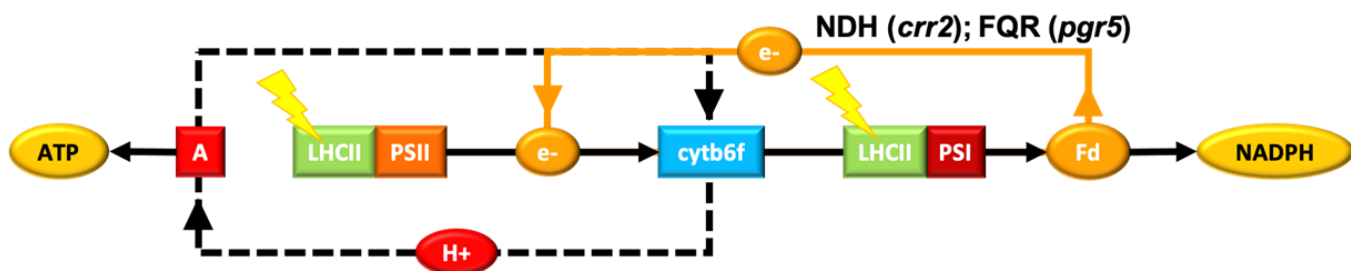
Figure 1. Model of electron and proton flow for coupling of light energy to the synthesis of ATP and NADPH in photosynthesis. Light harvesting (yellow arrows) by proteins (LHCII) drives electron (e$^-$) flow from photosystem II (PSII) to I (PSI). The Cytochrome b$_6$f (Cytb$_6$f) couples e$^-$ -flow to a flow of protons (H$^+$) to drive synthesis of ATP by ATPase (A). At PSI, e$^-$ flow is diverted at Ferredoxin (Fd) to synthesis of NADPH (linear) or back to the Cytb$_6$f (cyclic). Cyclic e- flow in mutants *crr2* and *pgr5* is disturbed at the NDH or FQR complex.

The function of CEF around PSI is mostly considered to be tightly coupled to the generation of a pH gradient (Δ pH) across the thylakoid membrane under conditions were LEF is not enough to generate the required Δ pH to drive ATP synthesis. Additionally, the Δ pH plays a regulatory role via the acidification of the thylakoid lumen which downregulates light energy utilization in PSII and electron transport through the Cytb$_6$f complex, which has been shown to be important to protect PSI from photodamage under fluctuating light (Yamori and Shikanai, 2016).

NDH complex

Chloroplast NADH dehydrogenase-like (NDH) in higher plants is homologous to the mitochondrial NADH:quinone oxidoreductase, it mediates cyclic electron transfer from ferredoxin to plastoquinone and may also act as a safety valve when the thylakoid stroma is highly reduced. It has been shown that in *A. thaliana,* the NDH complex is essential in the absence of PGR5 as the double mutant is unable to survive. (Shikanai, 2014). The accumulation of the NDH complex is impaired by the recessive alleles crr2-1 and crr2-2. The complete disruption of the NDH complex has been shown to not affect overall electron flow, thus it is not fully understood what role NDH plays in photoprotection (Shikanai et al., 1998).

PGR5/PGRL1-Dependent Cyclic Electron Flow - the FQR complex

The PGR5-dependent pathway is efficient in control of the ATP/NADPH ratio and essential to induce dissipation of energy by non-photochemical quenching. The NDH-dependent pathway is considered not to affect non-photochemical quenching. Rather it alleviates over-reduction of the stromal compartment and reduces photoinhibition (Munekage et al., 2004). The FQR complex also catalyses the reduction of plastoquinone by ferredoxin and has been shown to be sensitive to antimycin A (Shikanai, 2014; Tagawa et al., 1963). PGR5 functions to regulate PSI CEF and regulates LEF via control of Cytb$_6$f. It has been noted that *pgr5* plants grown under fluctuating light are specifically depleted in PSI proteins compared to the wild-type (WT) (Suorsa et al., 2012).

Solubilization of native membrane protein complexes

Efficient solubilisation of membrane complexes requires knowledge of the proteins, the membranes they are found in and the molecular structure of the detergents used. Membrane proteins are to date known to be divided into α-helical and β-barrel proteins (Reisinger and Eichacker, 2008; Wimley, 2003).

Transmembrane proteins are hydrophobic and are therefore usually found in direct interaction with the membrane's lipid bilayer. It is possible to solubilise the protein-lipid assemblies in aqueous solutions due to the amphipathic nature of the membrane lipids. Solubilisation in aqueous solutions however results in solubilised molecular assemblies composed of proteins and lipids that are too large for separation by electrophoretic methods. To resolve this problem, detergents are used to break up these large molecular assemblies into smaller assemblies which can then be separated and studied by electrophoretic methods. When solubilising transmembrane proteins, it is important to consider the critical micelle concentration (CMC) of the detergent used, as it is at this concentration that micelles begin to form that can sustain the solubilisation of hydrophobic and amphipathic molecules. (Garavito and Ferguson-Miller, 2001). Due to the highly hydrophobic nature of membrane proteins, they show a low solubility and a high propensity for aggregation in polar solvents (Reisinger and Eichacker, 2008).

Detergents are lipid-mimetic structures that are soluble in water as detergent monomers and in the form of micelles detergents dissolved in water do not show an inner aqueous compartment (Sanders et al., 2004; Speers and Wu, 2007).

The solubilisation strength of a detergent correlates to the size of the head group and the alkyl side chain volume. Detergents from one homologous series with longer alkyl chains are milder than the ones with short alkyl chains and also, the larger the head group the milder the detergent (Reisinger and Eichacker, 2008). Another factor to consider when solubilising membrane proteins with detergents are the chemical properties (anionic, non-ionic, zwitterionic) of the head group of the detergent monomers. This property affects the solubilization properties of a detergent regarding interactions with the proteins (Privé, 2007).

Anionic detergents like Sodium Dodecyl Sulphate (SDS) are used to disrupt protein-protein or intra-protein interactions directly (Kragh-Hansen et al., 1998; Speers and Wu, 2007). SDS is thus the ideal detergent for complete solubilisation of membrane proteins into individual protein units. Non-ionic detergents differ to ionic detergents in that they preferentially disrupt lipid-lipid and protein-lipid interactions (Speers and Wu, 2007). Consequently, non-ionic detergents, such as n-dodecyl-β-D-maltoside (β-DDM) and digitonin, allow for the solubilisation of native membrane protein complexes and are suitable for use in electrophoretic separations (Krause, 2006). Digitonin has the easiest access to the most exposed stroma lamellae and with an increase in concentration the solubilization proceeds deeper towards the grana margins (Grieco et al., 2015). Non-ionic detergents are usually used for the isolation of native membrane protein complexes as the stability of solubilized protein complexes has been shown to be dependent on the co-extraction of lipids with the proteins (Banerjee et al., 1995). Non-ionic detergents are ideal for isolation of membrane protein complexes from most membranes. For the isolation of protein super-complexes, digitonin is the best candidate since it shows a broad concentration range in which protein– protein interactions are hardly disintegrated. (Reisinger and Eichacker, 2008).

Free flow electrophoresis

Free flow electrophoresis (FFE) provides a means of separating particles by their electrophoretic mobility without any size restrictions in the molecular dimensions of the organelles of the cell, as is usually the case with polyacrylamide gel separations. FFE can be done in three ways:

1. Isoelectric focusing (IEF): separation of different molecules by their isoelectric point (pI)
2. Continuous zone electrophoresis: separation of different molecules by their net charge
3. Interval zone electrophoresis (IZE): a novel high-resolution separation technique for separating different molecules by their net charge.

The system allows for the separation of samples in a fast and consistent manner with highly reproducible results. The sample is applied using a peristaltic pump and is injected into a separation chamber consisting of two parallel plates. By laminar flow, the sample is transported upward within a

thin (0.4 mm) film of aqueous medium formed between the two plates. The plates are bordered by two electrodes that generate a high-voltage (hv) electric field perpendicular to the laminar flow. Charged particles (proteins, organelles, membrane fragments, or whole cells) are deflected, permitting subsequent separation and/or fractionation. (Weber and Wildgruber, 2008).

Spectroscopy

The Chl molecules bound in the photosynthetic machinery of the thylakoid membrane show fluorescent properties. Chloroplast complexes binding Chl absorb light at a wavelength of 435 nm. By exciting chloroplasts at this wavelength and determination of the wavelength spectrum of the emitted light, it is possible to discriminate between photosystem protein complexes. When light is emitted at 670 nm, this typically refers to small isolated particles containing free Chl. An emission wavelength of 680 nm is emitted from the inner and peripheral parts of LHCII. For the internal PSI antenna, an emission wavelength of 720 nm can be determined that strongly increases when the samples is frozen in liquid nitrogen. (Munekage et al., 2004).

Dynamic light scattering

Dynamic light scattering (DLS) is also known as photon correlation spectroscopy or quasi-elastic light scattering. Basis for the measurement is the change in the position of the sample in time relative to the exciting light particles. Basis of the change in position is the Brownian motion of the sample which allows to measure the size of the particles. Larger particles change their position less than smaller particles if measured over time. Brownian motion is the random movement of particles due to the bombardment by the solvent molecules that surround them. The larger the particle the lower the energy related effect of the solvent molecules on the motion of the particle. DLS measurements require an accurately known and constant temperature and viscosity. If the temperature is not stable and even, convection currents may emerge in the sample, thereby affecting the motion of the particles and subsequently the calculated size. Factors known to affect the diffusion speed of the particles in the solvent are: the ionic strength of the solvent (low conductivity can lead to an extended double layer of associated ions which reduces the diffusion speed), surface structure of the particles and the particles' shape especially when particles are non-spherical (Malvern instruments, 2014).

Zeta potential

The zeta potential is the potential that exists between the sample particle surface and the dispersing liquid, which varies depending on the distance from the particle surface. The zeta potential of a sample is measured by using a combination of electrophoresis and laser Doppler velocimetry. By using this method, it is possible to measure how fast a particle moves in a liquid when an electrical field is applied. When this velocity has been determined and the viscosity and dielectric constant of the sample medium is known, it is possible to calculate the zeta potential. (Malvern instruments, 2003).

Objectives

This project intends to study the complexes involved in the two CEF pathways around PSI: 1. The PGR5-PGRL1 protein dependent pathway via the FQR complex (*pgr5* mutant) and 2. The Chloroplast NADH dehydrogenase-like complex dependent pathway via the NDH complex (*crr2* mutant). The analysis is intended to better understand how plants can adapt their photosynthetic machinery to changing light conditions in order to optimise photosynthesis as well as prevent photodamage.

Materials and Methods

Solution preparation

All solutions were prepared using distilled water (Miele Aqua Purificator G 7795) or ultrapure water (Milli-Q water filtration machine, Arium mini from Sartorius)

6x SDS-PAGE sample buffer solution
30 % Glycerol
0.56 M Tris-HCl pH6.8
6 mM EDTA
10 % Sodium dodecyl sulphate (SDS)
179.11 µM Bromphenol blue
100 mM DTT (added just before use – prepared 1M stock solution)

1x SDS-PAGE Mes-Tris running buffer pH7.3
50 mM MES
50 mM Tris Base
0.1% SDS
1 mM EDTA

10x Concentrated Tris-buffered saline (TBS) for Western Blot
0.2 M Tris-HCl pH 7.5
1.5 M NaCl

1x Transfer Buffer for Western Blot
96 mM Glycine
10 mM Tris
Add freshly to buffer that is used in the transfer 1/10 methanol (100%)

5% (w/v) Milk in 1x TBS for Western Blot
5 g skim milk powder in 100 ml 1x TBS buffer

Enhanced Chemiluminescence (ECL) reaction mix 1   (15ml)
0.1 M Tris-HCl pH 8.3 (2 M stock)   750 µl
2.5 mM Luminol (250 mM stock in DMSO*)   150 µl
9 mM P-coumaric acid (90 mM stock in DMSO*)   150 µl
*DMSO: Dimethyl sulfoxide

Enhanced Chemiluminescence (ECL) reaction mix 2   (15ml)
0.1 M Tris-HCl pH 8.3   750 µl
0.0183 % H_2O_2 9.15 µl

Isolation media for chloroplast isolation
10 mM Hiba
300 mM Sorbitol
5 mM $MgCl_2$
5 mM KCl
5 mM $CaCl_2(x2H_2O)$
Titrated with Bistris to pH 6.8

10x TMK buffer
0.1 M Tris-HCl pH8.5
0.1 M $MgCl_2$
0.2 M KCl

5x Native-PAGE running buffer
250 mM Tricine
250 mM Bistris

4x Native-PAGE sample loading buffer
0.2 M BisTris
6 N HCl
40% (w/v) Glycerol
0.2 M NaCl
0.05 mM Ponceau S

Coomassie staining solution
0.23 mM Coomassie Brilliant Blue G250
75.03 mM Aluminium sulphate-(14-18)-hydrate
10% Ethanol
2% Orthophosphoric acid
  - Dissolve aluminium sulphate in 700ml dH_2O
  - Add ethanol
  - Dissolve Coomassie

- Add the orthophosphoric acid

Stable colloidal particles are formed so the Coomassie solution should be shaken before each use, it should also be stored in the dark. Protocol according to (Kang, 2002).

Hoagland's nutrient solution

Table 1. Micronutrient stock solution 1 L.

Chemical	Amount (g)
H_3BO_3	2.86
$MnCl_2 : 4H_2O$	1.81
$CuSO_4 : 5H_2O$	0.089
$ZnSO_4 : 7H_2O$	0.22
$Na_2MoO_4 : 2H_2O$	0.029

Table 2. 10x concentrated Hoagland's solution from the 6 stock solutions.

Stock Solution	1 L 10x solution	Final 1x concentration
1 M KH_2PO_4	10 ml	1 mM PO_4^{2-}
1 M KNO_3	50 ml	5 mM NO_3^-
1 M $Ca(NO_3)_2 : 4H_2O$	50 ml	10 mM NO_3^- 5 mM Ca^{2+}
1 M $MgSO_4 : 7H_2O$	20 ml	2 mM Mg^{2+} 2 mM SO_4^{2-}
1 % Fe-EDTA	10 ml	
Micronutrients	10 ml	

Table 3. Chemicals directory.

Full name	Common name	Formula	Company	Molecular weight g/mol	Density kg/l
2-Hydroxyisobutyric acid, 99% (dry wt.), water <2%	HiBa	$C_4H_8O_3$	Alfa Aesar	104.11	1.24
Acetic acid (glacial) 100%, anhydrous		CH_3COOH	Merck	60.05	1.05
Acetone		C_3H_6O	VWR chemicals	58.08	0.79
Aluminium sulphate-(14-18)-hydrate, 97+%, crystalline		$Al_2(SO_4)_3.xH_2O$ (x=14-18)-	Alfa Aesar	342.15	1.61
Bis		$C_8H_{19}NO_5$	VWR chemicals	209.2	
Boric acid		H_3BO_3	Roth	61.83	
Bromphenol blue		$C_{19}H_{10}Br_4O_5S$	Merck	669.96	
Calcium Chloride		$CaCl_2(x2H_2O)$	Merck		
Calcium nitrate tetrahydrate, 98%, extra pure		$CaN_2O_6.4H_2O$	Acros organics	236.15	1.86
Coomassie Brilliant Blue G250		$C_{47}H_{48}N_3O_7S_2Na$	Serva	854	
Copper sulphate pentahydrate		$CuSO_4.5H_2O$	Sigma-Aldrich	249.69	
D(-)-Sorbitol	Sorbitol	$C_6H_{14}O_6$	VWR chemicals	182.17	
Digitonin, high purity		$C_{56}H_{92}O_{29}$	Merck Calbiochem	1229.3	
Dimethyl sulfoxide	DMSO	$(CH_3)_2SO$	Lab-Scan analytical sciences	78.12	1.1
1,4 Dithiothreitol	DTT	$C_4H_{10}O_2S_2$	Biomol	154.25	
EDTA Disodium salt dihydrate	EDTA	$C_{10}H_{14}N_2O_8Na_2.2H_2O$	Amresco	372.24	
Ethanol		C_2H_5OH	Solveco	46.07	
Ferric EDTA	Fe-EDTA	$C_{10}H_{12}N_2FeNaO_8$	VWR chemicals	421.1	
Glycerol anhydrous		$C_3H_8O_3$	PanReac AppliChem	92.1	1.259
Glycine		H_2NCH_2COOH	Merck	75.06	
Hydrochloric acid fuming 37%		HCl	Merck		1.19
Hydrogen peroxide		H_2O_2	VWR chemicals	34.01	1.11
Hydroxypropyl methylcellulose	HPMC	$C_{56}H_{108}O_{30}$	BD (Becton, Dickinson and Company)	1261.45	

Lithium dodecyl sulphate	LDS	$C_{12}H_{25}LiO_4S$	Sigma-Aldrich	272.33	
Luminol		$C_8H_7N_3O_2$	PanReac AppliChem	177.17	
Magnesium Chloride anhydrous		$MgCl_2$	Merck	95.22	
Magnesium sulphate heptahydrate		$MgSO_4.7H_2O$	VWR chemicals	246.47	2.66
Manganese Chloride Tetrahydrate		$MnCl_2.4H_2O$	ICN Biomed	197.9	
2-Morpholinoethanesulphonic acid	MES	$C_6H_{13}NO_4S$	VWR chemicals	195.24	
Methanol		CH_3OH	Merck	32.04	0.792
Monopotassium phosphate		KH_2PO_4	Roth	136.09	2.34
n-Dodecyl β-D-maltoside	β-DDM	$C_{24}H_{46}O_{11}$	Sigma-Aldrich	510.62	
o-Phosphoric acid		H_3PO_4	Roth	98	1.69
p-Coumaric acid		$C_9H_8O_3$	Sigma-Aldrich	164.2	
Ponceau S		$C_{22}H_{12}N_4O_{13}S_4Na_4$	Sigma-Aldrich	760.6	
Potassium chloride		KCl	Roth	74.56	
Potassium nitrate		KNO_3	Merck	101.1	
Skim milk powder			VWR chemicals		
Sodium chloride		$NaCl$	VWR chemicals	58.44	2.16
Sodium dodecyl sulphate	SDS	$C_{12}H_{25}NaO_4S$	Merck-Schuchardt	288.38	
Sodium molybdate		$Na_2MoO_4.2H_2O$	Merck	241.95	
2,7-Naphthalenedisulfonic acid, 4,5-dihydroxy-3-[(4-sulfophenyl)azo]-, trisodiumsalt	SPADNS	$C_{16}H_9N_2Na_3O_{11}S_3$			
Tricine buffer		$C_6H_{13}NO_5$	Amresco	179.2	
Tris-(hydroxymethyl) aminomethane	Tris	$C_4H_{11}NO_3$	VWR chemicals	121.14	
Triton X-100		$C_{14}H_{22}O(C_2H_4O)_n(n=9-10)$	VWR chemicals	646.37	1.06
Zinc sulphate heptahydrate		$ZnSO_4.7H_2O$	VWR chemicals	287.54	1.97

Table 4. Consumables directory.

Consumable	Company
Amicon Ultra 0.5mL 100K centrifugal filters	Millipore
Antibodies (PetB, D2)	Agrisera
Anti-Rabbit IgG F (ab)2 fragment HRP	Sigma Life Science
Filter paper 3mm CHR	Whatman, GE Healthcare
MagicMark XP western protein standard	Invitrogen by Thermo Fisher Scientific
Microplate 96 well, UV-STAR, COC, F-bottom (chimney well), µClear	Greiner Bio-one
NativeMark unstained protein standard	Invitrogen by Thermo Fisher Scientific
NativePAGE 3-12% Bis-Tris gel (1mm x 10 well)	Invitrogen by Thermo Fisher Scientific
Nitrocellulose blotting membrane 0.45µm	Amersham Protran
NuPAGE 4-12% Bis-Tris gel (1.5mm x 15 well)	Invitrogen by Thermo Fisher Scientific
SeeBlue Plus2 prestained protein standard	Invitrogen by Thermo Fisher Scientific
Vivaspin 500 100K centricons	Sartorius Stedim Biotech
Planting soil (plantejord)	Tjerbo
Agra-vermiculite	LOG AS

Table 5. Instrument directory.

Instrument	Description	Manufacturer
Autoclave	SX-700E high-pressure steam sterilizer	Tomy
Blotter	PierceG2 Fast Blotter	Thermo Scientific
Centrifuge 1	Centrifuge 5430 R	Eppendorf
Centrifuge 2	Centrifuge 5415 R	Eppendorf
Chemiluminescence imager	ChemiDoc™ Touch Imaging System	BioRad
Dynamic Light Scattering, Zeta Potential analyser	Zetasizer Nano	Malvern Panalytical
Electrophoresis gel tank	Novex Mini Cell, Xcell SureLock	Invitrogen
Fluorescence imager	Odyssey® CLx	Licor
Fluorescence imager	Typhoon™ Variable Mode Imager	Amersham Biosciences
Free Flow Electrophoresis system	FFE advanced	FFE service GmbH, Munich, Germany
Freezer 1 (-20)		Miele
Freezer 2 (-20)		Liebherr
Fridge 1 (4)		Siemens
Fridge 2 (4)		Liebherr
Fume hood	120 cm, standard type	Kilab as
Heating block	HBT 130	HLC
Heating block	Thermoblock 220 V	Störk-Tronic
Image analysis software	Image studio	Licor
Image analysis software	Image lab	BioRad
Magnetic stirrer	Ikamag Reo	Drehzahl Electronic
Microplate reader	SpectraMax Paradigm Multi-Mode Microplate Reader	Molecular Devices
Mili-Q water filtration machine	Arium mini	Sartorius
pH-meter	pH 210 microprocessor pH meter	Hanna instruments
Pipettes	Pipetteman	Gilson
Scale 1	BP61S	Sartorius
Scale 2	72734 Reutlingen	Bachofer
Scanner (white-light)	CanoScan 9950F	Canon Solutions
Shaker 1	CH-4103 Bottmingen	Infors AG
Shaker 2	PMR-30 Mini Rocker-Shaker	Grant-bio
Spectrometer	UV-2401PC Spectrometer	Shimadzu
Voltmeter 1	Electrophoresis power supply - EPS 600	Pharmacia Biotech
Voltmeter 2	Electrophoresis power supply - EPS 301	Pharmacia Biotech
Water distiller	Aqua Purificator G 7795	Miele

Plant material

Arabidopsis thaliana seeds for wild-type columbia ecotype (WT-col) were supplied by Jean-David Rochaix from the Department of Molecular Biology, the University of Geneva, Switzerland. *A. thaliana* seeds for wild-type gli (WT-gli), *crr2* and *pgr5* were supplied by Toshiharu Shikanai from the Department of Botany, Kyoto University, Japan.

For planting of the seeds, a growth soil mix was prepared by mixing soil and agra-vermiculite 3:1 and adding 700 ml – 850 ml water. Seeds were then distributed evenly on the surface of the prepared soil mix and the pots were covered with a plastic sheet and stored in the dark at 4°C for 2 days following which the plants were then moved into the growth room. Philips de Luxe Pro TL5 HC 49W/965 lightbulbs were used as the light source and plants were grown in low light conditions (80-90 µmol m^{-2} s^{-1}) on an 8h/16h light/dark regime. After one week the plastic covering was removed and after 2-3 weeks the seedlings were transplanted into individual pots. All plants were watered every 2-3 days and were given Hoagland's solution once a week. Experiments were conducted using the plants when they were 12-16 weeks old.

Harvesting leaves for chloroplast isolation

Leaves were harvested from the plants after 1-2 hours of light exposure. Only leaves that had two-thirds of their surface area exposed to direct light were selected. To complete 2 runs on the FFE around 4.5 g fresh leaves were used.

Crude isolation of chloroplasts

All proceeding steps were conducted on ice. Cold isolation buffer was added (volume dependent on weight of the harvested sample; 5 ml used for 4.5 g of harvested leaves) and the leaves were then cut up using a razor blade until all large particles were broken down (estimated 10 min of cutting).

The solution was transferred using a pipette tip with the end cut off (allows for pipetting larger particles) and filtered through nylon gauze (pore size of 22 µm) into a 15 ml falcon tube. The solution was then distributed evenly into 4-5 Eppendorf tubes. More isolation media was added to tubes with smaller volumes to allow for balancing the centrifuge.

The sample tubes were centrifuged at 2000 rcf for 2 min 10°C using the centrifuge. The supernatant was poured off and the sample was resuspended in more isolation buffer (dependent on the size of the pellet, usually 500µl) before another round of centrifugation for 2 min at 2000 rcf 10 °C. The supernatant was discarded, and the pellets were resuspended in 50 – 60 µl separation medium 6 (inlet E7) from the FFE buffer solutions. All pellets were resuspended, and the samples were pooled into a single Eppendorf tube.

Isolation of chloroplasts with TMK lysis steps

TMK buffer washing steps were added to the "crude isolation of chloroplasts protocol" to osmotically lyse the chloroplasts and further remove unwanted cell debris.

The same procedure was followed up until the second centrifugation step of 2 min at 2000 rcf 10°C. Following which, the pellets were taken up in in 300 µl 1x TMK buffer and the samples were incubated on ice for 10 min. The samples were then centrifuged for 3 min at 5700 rcf at 10 °C and the supernatant was discarded. The samples were washed twice with resuspension in 300 µl 1x TMK and centrifugation for 3 min at 5700 rcf at 10 °C after each resuspension. Resuspension was done by pipetting slowly up and down and the supernatant was discarded after each centrifugation step. The pellets were then resuspended in 70 – 90 µl the E7 from the FFE buffers and the extracts were pooled into one tube.

Isolation of chloroplasts and freezing in liquid nitrogen

Whole chloroplasts were isolated following the "Isolation of chloroplasts with TMK lysis" protocol. However, the samples were resuspended in 70 µl of cold isolation buffer instead of 70 µl E7 FFE buffer. Following resuspension, the sample was frozen in liquid nitrogen, placed in -80 °C for a few min and then thawed on aluminium foil on ice. The sample was centrifuged for 5 min at 5700 rcf at 10°C and the supernatant was discarded. The sample was then taken up in 70 µl E7 FFE buffer and all tubes were pooled into one.

Determination of chlorophyll concentration

The concentrations of Chl a and Chl b of the isolated chloroplasts were determined by extraction using 80% acetone. 1 µl of the chloroplast sample was added to 99 µl of cold 80% acetone (1:100 solution), vortexed and then centrifuged for 10 min at max speed (30300 rcf) in centrifuge 1 (see instrument directory). If the pellet was still green after the 10 min centrifugation then the pellet was resuspended, and the centrifugation repeated (the extraction is not effective if the acetone is not cold). The extracted chlorophyll (supernatant) was diluted (50 µl to 250 µl 80% acetone, final dilution of 1:600). The absorbance was measured from 350 nm to 700 nm using the Shimadzu UV-Spectrophotometer (100 µl quartz-cuvettes; home-made), slit width 5 nm and medium scan speed was used. The Chl concentration was determined referring to Porra et al., 1989.

The Chl concentration of the solubilised proteins was determined using the same procedure as above, however the 1:100 solution was stored in -20 °C before extraction (centrifugation and measurement due to time constraints. The extracted Chl (supernatant) was diluted (50 µl to 100 µl 80% acetone, final dilution of 1:300).

Solubilisation of thylakoid membrane protein complexes

For the solubilisation mix, the final concentration of digitonin needed had to be more than 4 times greater than the lipid concentration (formula used: 1 µg/µl Chl = 1.65 g lipid). The standard protocol used for these experiments was 16mM of digitonin to ensure that the concentration was enough. The volume of sample added was calculated to get a final Chl concentration of 1.4 µg/µl in the final volume of 350 µl for the solubilisation mix. For a total volume of 350 µl, 70 µl of 80 mM digitonin was added and the remainder of the volume was made up using the E7 FFE buffer. The digitonin was the last component to be added to the solubilisation mix and the tube was inverted 3-4 times, flicked and placed directly into 10 °C. Once digitonin was added to all solubilisation mix tubes, the tubes were then incubated for 10 min at 10 °C. The tubes were then inverted twice and flicked a few times, following this the tubes were centrifuged for 30 min at 30300 rcf (max speed) at 10 °C.

The top 200 µl of each solubilisation mix was transferred into a new tube and kept in the dark on ice. This was the final sample used for the FFE separations.

Free flow electrophoresis (FFE)

The cooling system was turned on 30 - 40 min before assembly to cool down the separation chamber to 10 °C. The separation chamber was cleaned with dH_2O, then isopropanol and once again with dH_2O. The pre-soaked (in dH_2O) filter paper strips were aligned with the membrane strips (stored in diluted glycerol) and placed on the rubber strips in the separation chamber. The spacer was sprayed with dH_2O and put in place. The tubes were then slotted into place on the Ismatec IP high precision multichannel pump and the open ends placed in dH_2O. The media pump (240 ml/hr) was then started to make sure that all tubes were functioning, and no blockages were present. The chamber was then closed, starting with the loosened middle clamps (2 rotations loosened). As the chamber filled up, the respective clamps were closed. It was ensured that no bubbles were present in the chamber as it filled up. Once filled, the middle clamps were opened, tightened and shut again. To clear the sample collection tubes, dH_2O was fed through the waste tube until all 96 collection tubes were dripping. The counterflow clips were then closed and the counterflow tubes clicked into place to allow water to be pumped through them. Any bubbles were removed by opening the counter flow clips and gently tapping chamber. A stripe test was then done by placing tubes 2, 4, 6 and 8 into a 1:200 SPADNS solution. The media pump was left to run for 8 min and the sample collection was done for 2 min 10 sec. Absorbance readings at 517 nm were measured on the microtiter plate (*Figure 2*) to determine if all tubes were flowing evenly. A second test to ensure the even flow of all tubes was done by the same procedure however all tubes 2-8 were placed into the 1:200 SPADNS solution for this test.

The chamber was then washed by pumping dH_2O through the tubes for 30 min, exchanging the water source and washing for another 30 min with dH_2O.

If the system was assembled the day before running the separation experiments, then the cooling was turned off and the collection tubes were placed in a microtiter plate filled with dH_2O.

A final check and removal of any bubbles in the chamber was done. The chamber was then coated with 0.2% HPMC solution by filling it up for 8 min with the media pump set at 120 ml/hr and then leaving it to incubate for 30 min, with the media pump off and the collection tubes placed in the microtiter plate filled with dH$_2$O. The buffer tubes were then placed into their respective buffers and the counter flow tubes into the prepared 250 mM sorbitol solution. The chamber was filled with the buffers for 8 min and the sample tube was connected.

For separations with configured settings, 87 μl of the sample for separation was pipetted into the sample tube. For separations using continuous flow, the sample tube was placed directly into the sample.

The pI marker (lyophilized mixture of stable, salt-free, highly purified proteins) was used as a standard and run before each sample separation to ensure that the buffer steps were correct and to ensure consistency with the previous FFE separations experiments.
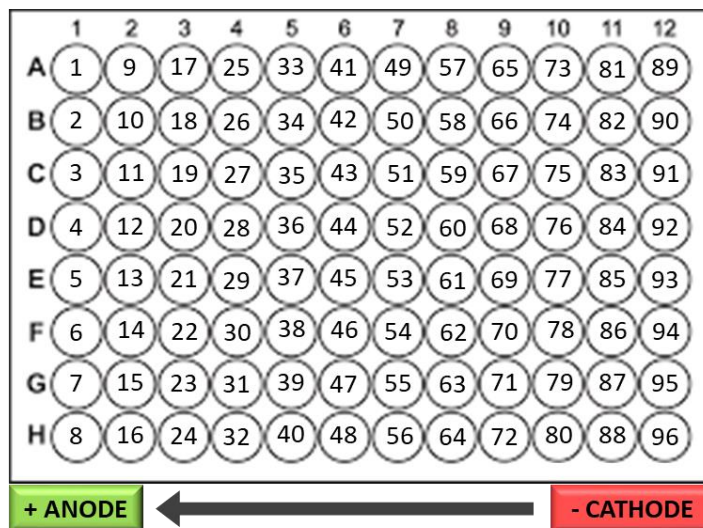

Figure 2. Schematic of the 96-well microtiter plate used to collect the separated protein complexes after separation by free flow electrophoresis. Each well contains at least 200 μl of sample after separation.

Table 6. Buffer systems used for the free flow electrophoresis experiments.

	20 mM Tris and Acetic acid	Hiba and Bistris	10 mM Tris and Acetic acid	10 mM Tris and Acetic acid
pH range	4.5 - 7	5.4 - 6.9	5 – 7; 5 & 7; 6.5 & 7; 7 & 7.5	6.5 - 7.5
Anodic electrode medium	200 mM Tris, Acetic acid to pH 7	100 mM H_3PO_4, Bistris to pH 6.9	200 mM Tris, Acetic acid to pH 7	200 mM Tris, Acetic acid to pH 7.5
Cathodic electrode medium		100 mM NaOH, 300 mM Tris, 200 mM Hiba		
Anodic stabilization medium (inlet E1)		150 mM HCl, Bistris to pH 6.9		
Cathodic stabilization medium (inlet E9)		100 mM KOH, 300 mM Tris, 200 mM Hiba, Bistris to pH 6.9		
Separation medium 1 (inlet E2)	20 mM Tris, 250 mM Sorbitol, Acetic acid to pH 4.5	20 mM Hiba, 250 mM Sorbitol, Bistris to pH 5.4	10 mM Tris, 250 mM sorbitol, Acetic acid to pH 5	20 mM Tris, 250 mM sorbitol, Acetic acid to pH 6.5
Separation medium 2 (inlet E3)	20 mM Tris, 250 mM Sorbitol, Acetic acid to pH 5			10 mM Tris, 250 mM sorbitol, Acetic acid to pH 6.5
Separation medium 3 (inlet E4)	20 mM Tris, 250 mM Sorbitol, Acetic acid to pH 5.5	10 mM Hiba, 250 mM Sorbitol, Bistris to pH 5.4	10 mM Tris, 250 mM sorbitol, Acetic acid to pH 5.5	10 mM Tris, 250 mM sorbitol, Acetic acid to pH 7
Separation medium 4 (inlet E5)	20 mM Tris, 250 mM Sorbitol, Acetic acid to pH 6		10 mM Tris, 250 mM sorbitol, Acetic acid to pH 6	
Separation medium 5 (inlet E6)	20 mM Tris, 250 mM Sorbitol, Acetic acid to pH 6.5		10 mM Tris, 250 mM sorbitol, Acetic acid to pH 6.5	10 mM Tris, 250 mM sorbitol, Acetic acid to pH 7.5
Separation medium 6 (inlet E7)	20 mM Tris, 250 mM Sorbitol, Acetic acid to pH 7, 10 mM KCl	10 mM Hiba, 250 mM Sorbitol, Bistris to pH 6.9	10 mM Tris, 250 mM sorbitol, Acetic acid to pH 7, 10 mM KCl	
Separation medium 7 (inlet E8)	20 mM Tris, 250 mM sorbitol, Acetic acid to pH 7	10 mM Hiba, 250 mM Sorbitol, Bistris to pH 6.9, 10 mM KCl	10 mM Tris, 250 mM sorbitol, Acetic acid to pH 7	
Counterflow medium (CC)	250 mM Sorbitol	250 mM Sorbitol	250 mM Sorbitol	250 mM Sorbitol

Detergents added:	150 µM β-DDM added to buffers E3 to E8 + CC	150 µM β-DDM added to buffers E2 to E8 + CC	150 µM β-DDM added to buffers E2 to E8 + CC	150 µM β-DDM added to buffers E2 and E3

Procedures for running the FFE separations:

Table 7. System parameters for isoelectric focusing free flow electrophoresis separations of membrane complexes solubilised from the thylakoid membrane stromal lamella of freshly isolated chloroplasts from *A. thaliana*. *Procedure 1* parameters for configured free flow electrophoresis separation **(left)** and *Procedure 2* for continuous flow free flow electrophoresis separation **(right)**.

Sample injection	
Sample	3000 µl/hr
Duration	100 s
Media	110 ml/hr
Separation	
Voltage	1500 V
Current	300 mA
Power	300 W
Pre separation	5 s
Media	40 ml/hr
Main separation	217 or 235 s
Collection	
Media	240 ml/hr
Time till collection	75 s
Collection time	130 s

Sample injection	
Sample	1700 µl/hr
Media	120 ml/hr
Separation	
Voltage	1500 V
Current	80 - 90 mA
Power	120 - 135 W
Media	120 ml/hr
Main separation	160 s
Collection	
Media	240 ml/hr
Time till collection	150 s
Collection time	290 s

Native Polyacrylamide Gel Electrophoresis

Invitrogen™ NativePAGE™ 3-12% Bis-Tris Protein Gels, 1.0 mm, 10-well pre-made gels were used for Native Polyacrylamide Gel Electrophoresis (N-PAGE) separation.

Sample preparation: Samples were kept cold using ice and cold boxes throughout the procedures.

Wells from the 96-well microtiter plate from the free flow electrophoresis separation were selected based on fluorescence spectra readings. Microtiter plates with 96 well of the label Greiner UV-Star (catalogue number: 655801) were used. The 200 µl sample from each selected well were concentrated by 100K centrifugal filters and the retentate was collected.

For the Sartorius centrifugal filters, the tubes were centrifuged for 3 min 30 sec at 15000 rcf at 10 °C. The retentate from each sample was then transferred to a new tube. For the Amicon centrifugal filters, the tubes were centrifuged for 3 min 30 sec at 14000 rcf at 10 °C. The filter tubes were then inverted and placed upside down into new tubes and centrifuged for 2 min at 1000 rcf at 10 °C.

A second solubilisation step was done using 5mM digitonin and Native-PAGE loading buffer was added to reach a final volume of 18 µl. 40 or 80 µM LDS was added to the 50 mM Bistris / 50 mM Tricine Native-PAGE running buffer for the cathode tank. 5 µl of Nativemark unstained protein standard was used as a marker and 18 µl of each sample was loaded by pipetting twice using the P10 pipette. The gels were run in a cold box at 17 V and 400 mA overnight (12 - 14 hrs) and the voltage was increased to 30 V in the morning, and run for another 4 - 5 hrs. The gels were left to run in the cold box until the dye front reached the bottom of the gel.

Fluorescent images of the gels were obtained using the Odyssey scanner and the Typhoon scanner and white light images were captured using the Canon scanner. After scanning, the Native-PAGE gels were stained overnight in colloidal Coomassie (Kang, 2002) solution. Following overnight staining, the gels were washed for 30 min in distilled water, with the water being exchanged every 10 min. Following the washing procedure, the gels were again scanned using the Odyssey scanner and Cannon scanner. Bands were selected and cut out for storage at -80 °C before being sent for MS sequencing.

For the quantification analysis of the N-PAGE gels, the emission at 700 nm was quantified using the Licor Image Studio software. Bands in the top part of the gel, greater than 720 kDa, were considered to be higher complexes, followed by PSI in the range of 480 to 720 kDa and finally by LHCII in the lower region, smaller than 480 kDa. The emission intensity of each section was quantified for each lane and then represented graphically for further interpretation.

Mass-spectrometry
Bands of interest were cut out from the Coomassie stained N-PAGE gels using a sterile blade, the excised bands were stored in sterile tubes at -80 °C. Mass-spectrometry (MS) analysis was done by Cambridge Centre for Proteomics at the University of Cambridge, England.

Sodium Dodecyl Sulphate Polyacrylamide Gel Electrophoresis and Western blotting
Sodium dodecyl sulphate polyacrylamide gel electrophoresis (SDS-PAGE):

Invitrogen™ NuPAGE™ 4-12% Bis-Tris Protein Gels, 1.0 mm, 15-well pre-made gels were used for SDS-PAGE separation. (Catalogue number: NP0336PK2)

Sample preparation standard protocol:

Selected wells from the 96-well microtiter plate were used for SDS-PAGE separation. 60 µl of the sample from the FFE separation was added to prepared 6x sample buffer (+ 100 mM DTT) to reach a final volume of 72 µl, 20 µl of which was loaded and run on the gels.

For later experiments using the Amicon centrifugal filters, 20 µl of the collected retentate was used for this sample preparation instead of 60 µl taken directly from the microtiter plate. Prepared 6x sample buffer (+ 100 mM DTT) was added to reach a final volume of 24 µl. When loading the sample into the gel, 18 µl of each sample was loaded onto 1 gel (for Coomassie staining) and 5 µl onto another gel (for western blotting).

The prepared sample solution was heated to 70 °C for 10 min and then centrifuged for approximately 15 sec at 12000 rcf at room temperature. Samples were stored at -20 °C before use.

MagicMark or SeeBlue protein standards were used. For the running buffer, MES-Tris buffer was used (separation of small-medium sized proteins: 200 kDa - 2.5 kDa). Gels were run at 200 V, 400 mA for 35-45 min (until dye front had reached the bottom of the gel).

Western Blot:

Transfer of proteins from SDS-PAGE to the nitrocellulose membrane was done using the Thermo Scientific PierceG2 Fast Blotter.

The filter paper layers and membrane were pre-soaked in the prepared transfer buffer (50 ml of transfer buffer was prepared by mixing 45 ml transfer buffer stock solution with 5 ml methanol) before placing into the blotting cassette. The membrane and gel were sandwiched on either side by three sheets of Wattman filter paper, i.e. three layers of soaked filter paper were placed on the cassette followed by the soaked nitrocellulose membrane and the SDS-PAGE gel, another three layers of soaked filter paper were then placed as the final layer on top of the gel. The remaining transfer buffer was poured onto the prepared layers and a roller was used to remove any air bubbles and distribute the buffer. The cassette was then closed and placed into the blotting machine.

The setting used for transfer on the PierceG2 Fast Blotter was for mixed range MW with a 25 V limit and a constant 2.5 A run for 7 min.

Following transfer of the proteins to the nitrocellulose membrane, blocking of binding sites was done by incubating the blot in 5% milk-TBS (w/v) for 45 min at room temperature on a shaker.

The primary antibody was then added to the milk solution. If fresh antibody wasn't used, the milk solution was poured off and replaced with the previously used antibody solution.

The blot was incubated overnight on a shaker in the 4 °C cold room. The antibody solution was removed the following morning and stored at -20 °C to be reused for future blots (up to 3 times).

For the washing procedure, the membrane was rinsed in 1x TBS solution and then washed three times for 5 min on the shaker with 1x TBS. After the washing procedure, the blot was incubated at room temperature in rabbit antibody IgG (1:5000) in 10 ml of 1x TBS for approximately 1 hr 15 min.

Following the secondary antibody incubation, the membrane was again rinsed and washed using 1x TBS as mentioned above. The enhanced chemiluminescent (ECL) reaction mixtures were prepared freshly and mixed in the dark. The blot was incubated in the mixture for approximately 1 min before chemiluminescent imaging was done. Chemiluminescent imaging was done using the Chemidoc instrument. Exposure and imaging were configured to take three images, the first after 40 sec and the last after 120 sec.

Dynamic Light Scattering measurements

Dynamic light scattering (DLS) measurements were done using the Zetasizer Nano. The quartz cuvette was rinsed with 99.99% ethanol and then with Milli-Q ultrapure water. Any remaining liquid was removed by pipetting. 50 µl of the selected sample from the microtiter plate collected from the FFE separation was then added to the cuvette. Measurements were taken with the following SOP:

> Sample: protein
>
> Dispersant: water
>
> Temperature: 25 °C
>
> Equilibration time: 2 min
>
> Cell type: Quartz cuvettes, ZEN2112

The instrument takes 3 measurements, if the curves did not align then another 3 measurements were taken as the particles sometimes take longer to settle than the equilibration time.

Zeta potential measurements

Measurements were done using the Zetasizer Nano. The cuvette was rinsed by using 2 syringes and washing each solution back and forth 5 times. First, the cuvette was washed with 99.99% ethanol, followed by washing with ultrapure water and finally washing with the buffer the sample was in (250 mM sorbitol was used for this purpose). Finally, the sample was filled into the cuvette. To fill the cuvette 750 µl of sample was needed, if one microtiter plate was used (200 µl of sample) then the missing 550 µl of volume was made up by using 250 mM sorbitol solution. Alternatively, wells from 5 microtiter plates were pooled together to make up the required volume. Measurements were taken with the following SOP:

Sample: protein

Dispersant: water

Temperature: 25 °C

Model: Smoluchowski

Cell type: disposable folded capillary cells, DTS1070

Absorbance spectroscopy

In vivo absorbance spectroscopy was done by using freshly cut whole leaves either harvested during the dark phase before the light turns on in the morning (use of a green headlamp) or during the light phase (mid-afternoon 13.00 - 16.00).

Procedure 1:

A leaf was cut from the selected plant and taped to the plate in the UV-2401PC spectrometer. Absorbance readings were measured from 190 – 750 nm at medium scan speed with a 1 nm sampling interval and a slit width of 5 nm. The instrument was set to change light sources at 350 nm. This was done 3 times for each genotype and repeated over the course of 3 days both for the dark and light phases, with a leaf taken from a different plant each time.

Procedure 2:

A leaf was cut from the selected plant. The stem was clamped with forceps and the leaf then taped to the plate in the UV-2401PC spectrometer. Absorbance readings were measured from 285 – 750 nm at slow scan speed with a 1 nm sampling interval and a slit width of 2 nm, 10 repetitions were recorded with a 1 sec time interval between each measurement. The instrument was set to change light sources at 285 nm. This was done 3 times for each genotype over the course of 3 days both for the dark and light phases, with a leaf taken from a different plant each time.

Results

Initial FFE separations of the cyclic electron flow (CEF) mutants

In several initial experiments, the experimental setup and analytical strategy was established. Experiments were directed to determine if differences in the protein complex composition can be found between two different cyclic electron flow (CEF) mutants – namely *crr2* and *pgr5,* when thylakoid stroma lamellae are selectively solubilized. First, chloroplasts were isolated from 14-week-old *crr2* and *pgr5 A. thaliana* mutant plants after 2 hrs of light exposure. Membrane complexes were solubilised from the isolated chloroplasts with 16 mM digitonin. Solubilised complexes were separated by FFE according to molecular charge and continuously fractionated with the electrophoretic buffer flow in 96-well microtiter plates. The FFE fractions were analysed for the presence of the Chl-binding photosystem complexes PSI, PSII, and LHCII by fluorescence spectroscopy. The composition of protein complexes was analysed by N-PAGE; the total composition of protein subunits was analysed by SDS-PAGE and Western blotting.

For separation of the protein complexes by FFE, the electrophoretic field was established in a buffer system composed of Tris and Acetic acid (see the 20 mM Tris and Acetic acid buffer system in *Table 6*, first column, of the methods section; E7 and E8 contained 10 mM KCl) and the instrument parameters were set according to 'Procedure 1' (see *Table 7* in methods section). The buffer was titrated to establish pH steps from 4.5 to pH 7 between the anode and cathode, respectively. For fluorescence spectroscopy, the collected FFE fractions were concentrated using Sartorius 100K centrifugation devices, and the retentate was used for separation of the protein complexes by Native-PAGE (N-PAGE) (*Figure 6* and quantification in *Figure 7*). Protein composition of the complexes was analysed by differential fluorescence analysis. With an excitation at 685 nm and an emission analysis at 700 nm PSII and LHCII bound to PSI were determined (*Figure 3*); whereas at excitation of 785 nm and an emission analysis at 800 nm primarily PSI was determined (*Figure 4*). The localization of the Cytb$_6$f complex was determined using antibodies against the Cytb$_6$ in gel-blots (blots in *Figure 8* and quantification in *Figure 9*).

In the initial separations comparing the two CEF mutants, it was found that approximately the same amount of protein complexes was solubilised when the two mutants were adjusted for Chl concentration in the solubilisation mix. Excitation/emission scanning at 685/700 nm upon FFE separation showed that the FFE separation profile of the *pgr5* mutant was shifted towards the anode compared to the *crr2* mutant (*Figure 3*). Lower fluorescence emission was found in the *pgr5* mutant between fractions 47 and 59 compared to *crr2,* which could have resulted from a tendency of the complexes in this region to move towards the anode. The separations showed a prominent peak in the 700 nm emission at fraction 35 for *pgr5* and fraction 38 for *crr2*, with the peak in *crr2* being slightly more intense in its emission. The emission at 700 nm was most likely dominated by fluorescence from LHCII and PSII, and to a lesser extent from LHCII to PSI. Interestingly, upon excitation/emission scanning at 785/800 nm, the appearance of a cathodic peak was determined in the range of fractions 56 to 69, which according to the fluorescence emission was due to the presence of PSI (*Figure 4*). It was also

noted that the intensity of the emission peaks at this wavelength were approximately the same. The shift of complexes towards the anode in the separation of complexes from *pgr5* compared to *crr2,* which was seen in the 700 nm emission, was again evident in the emission readings at 800 nm when excited at 785 nm.
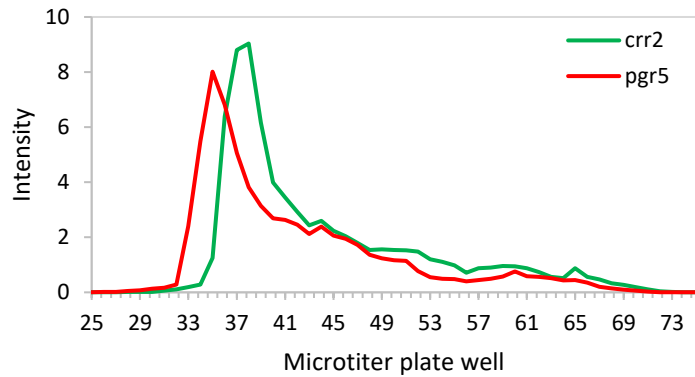
Figure 3. **Fluorescence intensity of the microtiter plates measured with excitation at 685 nm and emission at 700 nm.** Membrane complexes were solubilised from the stroma lamellae of isolated chloroplasts from *A. thaliana crr2* (green) and *pgr5* (red) mutants and separated by interval zone free flow electrophoresis with a pH range of 4.5 to 7. Intensity values times 10^6.


Figure 4. **Fluorescence intensity of the microtiter plates measured with excitation at 785 nm and emission at 800 nm.** Membrane complexes were solubilised from the stroma lamellae of isolated chloroplasts from *A. thaliana crr2* (green) and *pgr5* (red) mutants and separated by interval zone free flow electrophoresis with a pH range of 4.5 to 7. Intensity values times 10^2.
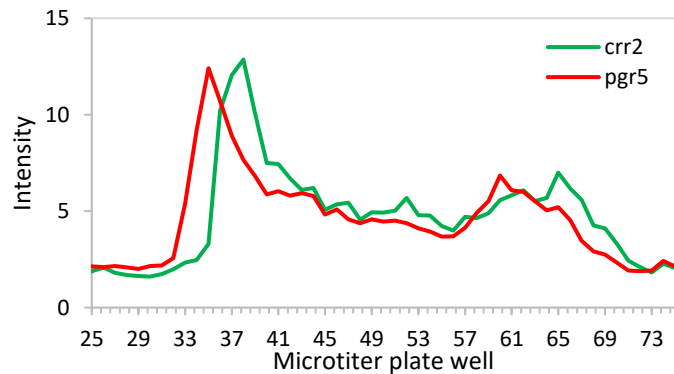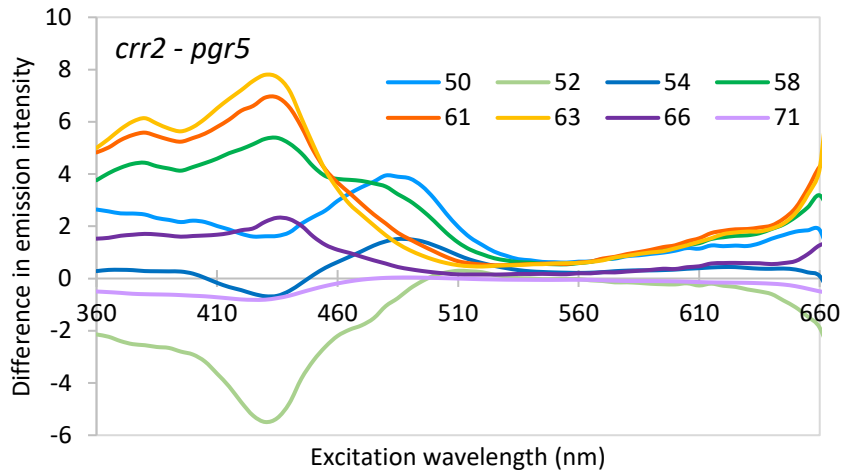
Figure 5. Difference in the excitation spectra for cathodic fractions (50 – 71) between *crr2* and *pgr5*. Excitation spectra data was measured for emission at 700 nm for selected cathodic fractions of the FFE separation of solubilised complexes from *crr2* and *pgr5* stroma thylakoid membranes. The difference in emission intensity between the two mutants is shown: *crr2 – pgr5* and values are given times 10^6.

The difference between the two mutants with respect to PSI was assessed by analysis of the excitation spectra for the selected cathodic fractions in the range of fractions 50 to 71. Measurements were recorded after FFE separation into the microtiter plate fractions for both *crr2* and *pgr5*. In the excitation spectra, the emission intensity values at 700 nm were reported for each of the excitation wavelengths. When the values for the *pgr5* fractions were subtracted from those for the *crr2* fractions, positive values showed a higher emission in the *crr2* mutant, while negative values conveyed a higher emission in the *pgr5* mutant (*Figure 5*). From the difference spectra, it was apparent that at an excitation of 430 nm, the *crr2* fractions showed an increase in the fluorescence emission with a peak in fractions 63, while *pgr5* showed a maximum relative to *crr2* in fraction 52 (*Figure 5*). In addition, *crr2* showed an excitation maximum at 485 nm, relative to *pgr5*. The wavelength specific differences indicated that in fractions 61, 63 and 66 more Chl a was detected in *crr2*; while in *pgr5* more Chl a was present in fraction 52. The relative increase in fraction 50 indicated that more Chl b or carotenoids were accumulated in *crr2* (*Figure 5*).
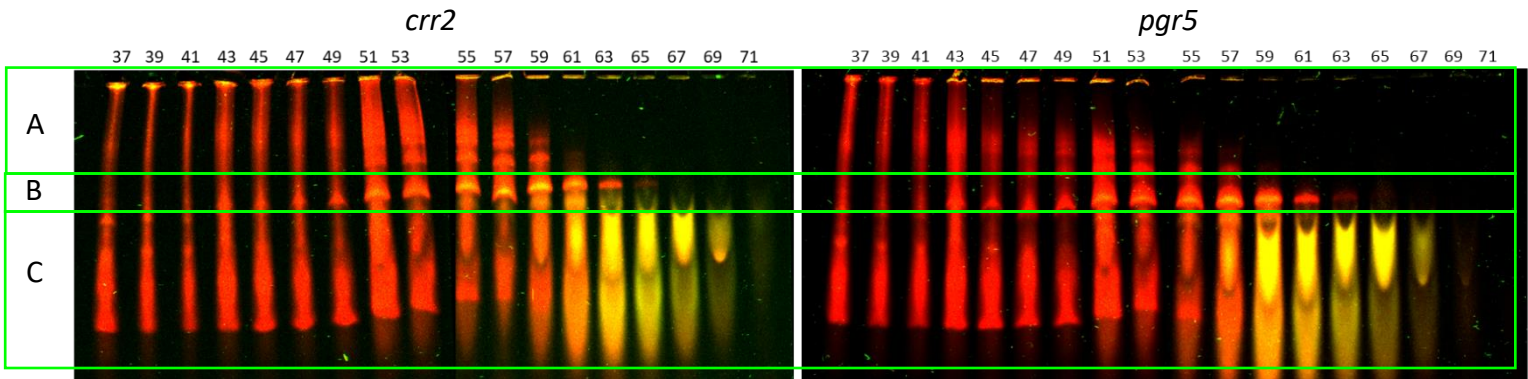
Figure 6. N-PAGE (fluorescence em700 and em800) separations of concentrated protein complexes after FFE separation (fractions (37 – 70). Membrane complexes from the stroma lamella were solubilised from freshly isolated chloroplasts of *A. thaliana crr2* and *pgr5* mutants. The solubilised complexes were separated by FFE, concentrated by centrifugal filtration using Sartorius 100K and further analysed by N-PAGE (40 µM LDS was added to the cathode buffer). Imaging was done by exciting at 685 nm and recording emission at 700 nm, and exciting at 785 nm and recording emission at 800 nm. Quantification analysis was done in the Licor Image Studio software to compare the intensity of the emission at 700 nm for the higher complexes **(A)**, PSI **(B)**, and LHCII **(C)** between the two cyclic electron flow mutants; see *Figure 7* for quantification analysis.
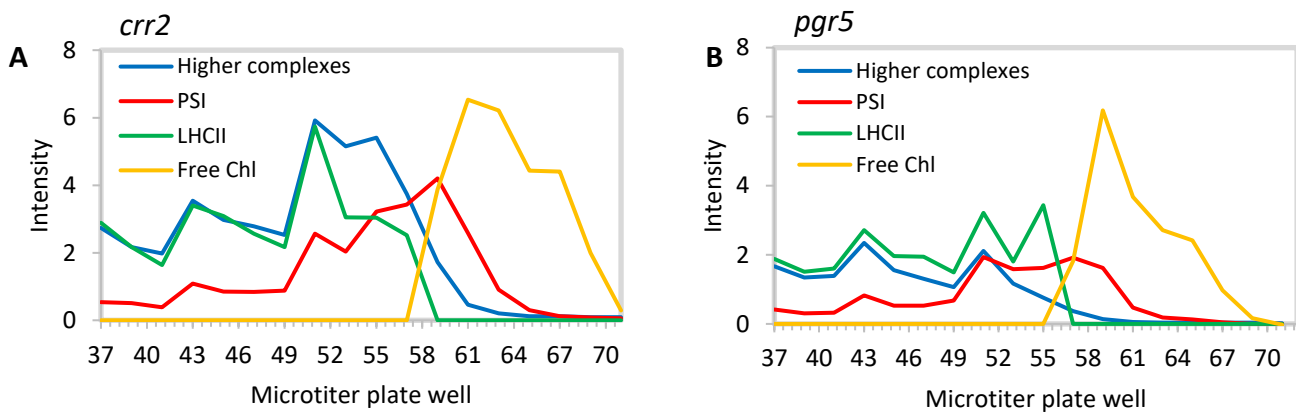

Figure 7. Quantification analysis of N-PAGE (fluorescence em700) separations of concentrated protein complexes after FFE separation (fractions (37 – 70). Membrane complexes from the stroma lamellae were solubilised from freshly isolated chloroplasts of *A. thaliana crr2* **(A)** and *pgr5* **(B)** mutants. The solubilised complexes were separated by FFE, concentrated by centrifugal filtration and further analysed by N-PAGE, 40 µM LDS was added to the cathode buffer. Higher aggregates (blue), PSI (red), LHCII (green) and free chlorophyll (Chl) (yellow); intensity values are shown times 10^5. See *Figure 6*.

The difference in the protein composition of the fractions from FFE separation were analysed using N-PAGE separation. The FFE fractions were subjected to centrifugal filtration and retentates larger than the 100K cut-off were loaded onto N-PAGE. Analysis of the concentrated fractions by fluorescence scanning of the native-gels showed a similar pattern of fluorescence signals at 700 nm and 800 nm. This indicated that both mutants have similar complexes, which also showed similar migration in the FFE separation (*Figure 6*). However, differences in the intensity of the fluorescence signal and the dispersed appearance of the gel-bands upon N-PAGE separation made it difficult to evaluate the result. Therefore, three molecular weight regions of the fluorescent gel were selected and the intensity of fluorescence quantified (*Figure 6*). This allowed to specify a diffuse high-molecular weight region, A, a PSI specific band, B, and a diffuse low molecular weight region, C. In the higher molecular weight complexes termed A, the *crr2* complexes showed a higher amount of fluorescent signal, compared to *pgr5* in fractions 45 to 57 (*Figure 6*, A and *Figure 7*). The molecular bands found in region B, characteristic for the distribution of PSI complexes, showed a similar fluorescence intensity in fractions 51 to 63 for both mutants; though, the signal intensity was increased between fractions 58 to 61 in *crr2*. The quantification of the lower molecular weight complexes found in region C, which represented mostly LHCII and free Chl, showed that the intensity distribution in this region was very similar to the higher molecular weight region (*Figure 6*, A and C, and *Figure 7*). It was also noted that the cathodic fractions from 57 to 69 contained free LHCII or free Chl in detergent micelles in both mutants. The analysis confirmed that *crr2* showed more of the higher molecular weight complexes and more PSI complexes compared to *pgr5*. Also, the distribution of LHCII complexes was more strictly correlated to the distribution of high molecular weight complexes in *crr2*.
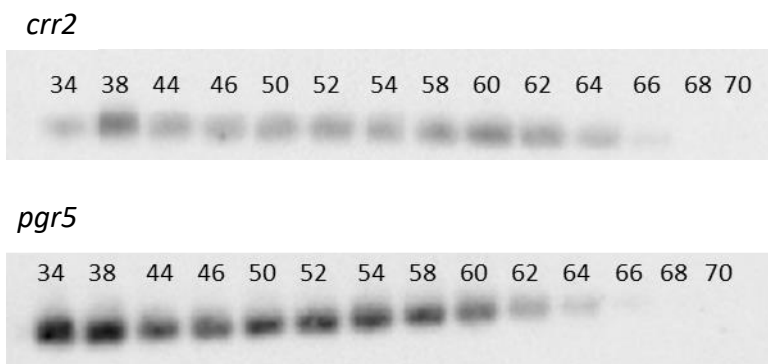
crr2

pgr5

Figure 8. Gel-blot analysis for Cytb$_6$ of fractions 34 – 70 after FFE separation. Antibodies directed against the Cytb$_6$ subunit were used to determine the distribution of the Cytb$_6$f complex in the cyclic electron transport mutants. The thylakoid stromal lamellae membrane complexes solubilised from *A. thaliana crr2* and *pgr5* mutants were separated by FFE before further separation by SDS-PAGE and gel-blot analysis. Chemiluminescence signal was shown and quantification analysis is shown in *Figure 9.*
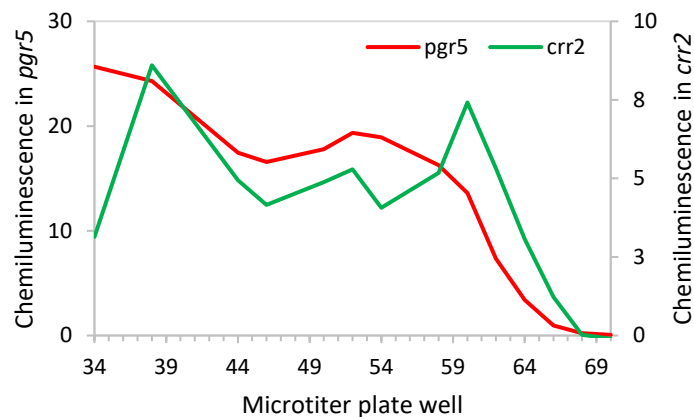
Figure 9. Quantification of chemiluminescent signal from gel-blot analysis for Cytb₆. Antibodies directed against the Cytb₆ subunit were used to determine the distribution of the Cytb₆f complex in the cyclic electron transport mutants. The thylakoid stromal lamellae membrane complexes solubilised from *A. thaliana crr2* (green) and *pgr5* (red) mutants were separated by FFE before further separation by SDS-PAGE and blot analysis. Chemiluminescence signal intensity values times 10^3. See *Figure 8*.

The distribution of PSI complexes in the FFE fractions was analysed further by investigation of the Cytb₆f complexes that may form a complex with PSI. The investigation was based on the concept that a complex between both complexes would result in a co-migration of both complexes during FFE separation. This would have subsequently resulted in an equal distribution of the protein complexes and the corresponding protein subunits. Upon FFE, fractions 34 to 70 from *crr2* and *pgr5* were subsequently denatured and protein subunits were separated by SDS-PAGE. The presence of the Cytb₆f complex in the FFE fractions was then detected using an antibody against the Cytb₆ subunit applying gel-blot analysis (*Figure 8*). The gel-blots showed a very broad distribution of antibody signal with two maxima seen at fractions 38 and 60 for *crr2*. In *pgr5* maxima were seen in fractions 34 and 38, and a broad maximum between fractions 50 to 58. This finding was corroborated by the quantification analysis of the gel-blot (*Figure 8* and *Figure 9*). The quantification showed a strong difference in the signal strength indicating that about three-fold more Cytb₆f complexes were present in *pgr5* relative to *crr2*.

The separation of membrane complexes solubilised from the two CEF mutants was then repeated with 16-week-old plants. The same procedures were conducted as in the initial separation experiments in order to confirm the results before beginning to optimise the FFE separation. Compared to the FFE separation analysed before, separation medium 6 (inlet E7) contained 10 mM KCl. For the analysis, the complexes were analysed exciting at 685 nm and measuring the emission at 700 nm. At this wavelength, both PSI and PSII as well as the connected LHCII would fluoresce. Again, the *pgr5* mutant showed an increased mobility of the Chl-containing complexes towards the anode compared to the *crr2* mutant (*Figure 10*). In *pgr5,* the anodic peak was seen at fraction 36; whereas in *crr2* it was seen at fraction 42 (*Figure 10*). Fluorescence readings were also taken by exciting at 435 nm and recording the emission at 680 nm (*Figure 11*). This is indicative of complexes containing Chl which includes PSII and PSI as well as any free LHCII or free Chl. These fluorescence readings showed that fluorescence intensity increased by about a factor of 80 compared to excitation 685 nm and emission 700 nm. In *crr2* two evident peaks were found at fractions 42 and 66 were found; whereas in *pgr5* an anodic peak

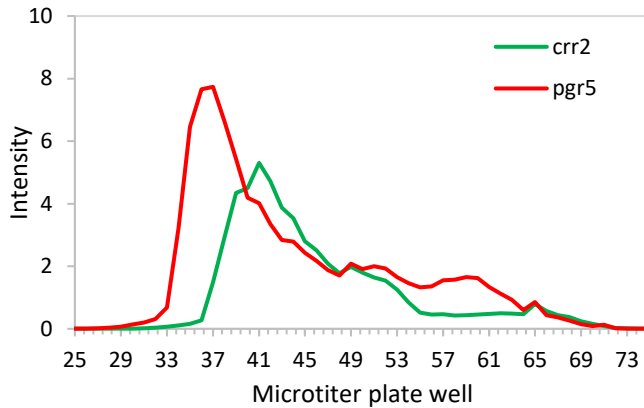at fraction 37 and a steadier and more evenly distributed emission from fraction 45 to 65 was found (*Figure 11*).

Figure 10. Fluorescence intensity of the microtiter plates measured with excitation at 685 nm and emission at 700 nm. Membrane complexes were solubilised from the stroma lamellae of isolated chloroplasts from *A. thaliana crr2* (green) and *pgr5* (red) mutants and separated by interval zone free flow electrophoresis with a pH range of 4.5 to 7. Intensity values times 10^6.
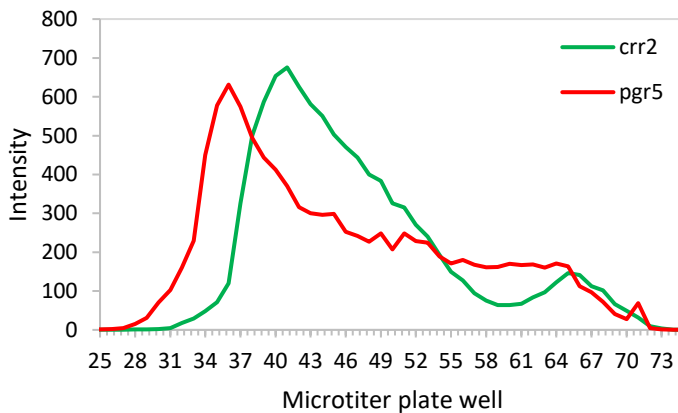

Figure 11. Fluorescence readings when exciting at 435 nm and emission at 680 nm. Fractions 25 – 75 are shown from the FFE separation of solubilised stromal lamellae membrane complexes from freshly isolated chloroplasts of *A. thaliana crr2* (green) and *pgr5* (red) plants. Intensity values given times 10^6.

Analysis of the protein composition by fluorescence analysis after N-PAGE corroborated the previous findings that more of the higher molecular weight complexes were extracted from the stroma thylakoid membrane of *crr2* relative to *pgr5.* However, an increase in 700 nm emission intensity was determined for *pgr5* using the 685 nm excitation analysis upon N-PAGE in fractions 40 to 48 (*Figure 12* and *Figure 13*). Interestingly, visual analysis of the selected molecular weight region B representing the PSI complex (*Figure 12*, B) indicated that *pgr5* contained a higher amount of fluorescence compared to *crr2* in fractions 51 to 63. This observation contrasted with the quantification of the fluorescence after N-PAGE. The increase in fluorescence may be indicative of a higher amount of PSI protein in the *pgr5* mutant. In terms of the migration of the various complexes during the FFE separation, both mutants

showed similar separation profiles. Quantification analysis of the fluorescent regions from the native gel image corroborated the higher molecular weight complexes in *crr2*, compared to *pgr5,* especially in the anodic peak near fraction 40 to 43. Both mutants showed the same distribution of PSI complexes, however the emission intensity in *pgr5* was more than twice that of *crr2.* In the former experiment it was seen that there were higher complexes/aggregates that did not enter the native-gel for the *pgr5* fractions (*Figure 6*, A, right side). In this separation the same phenomenon was found however it was reduced in this run from fractions 49 to 57 (*Figure 12*, A, right side). It was therefore speculated whether more PSI complexes had been released from higher molecular weight complexes in *pgr5* than in *crr2* in this N-PAGE separation. Additionally, in this separation *crr2* has two evident peaks in the distribution of LHCII whereas *pgr5* has three peaks. Although this differs from the previous separation experiment using the CEF mutants, *pgr5* still has an additional peak, which could indicate a different complex state compared to those found in *crr2.*
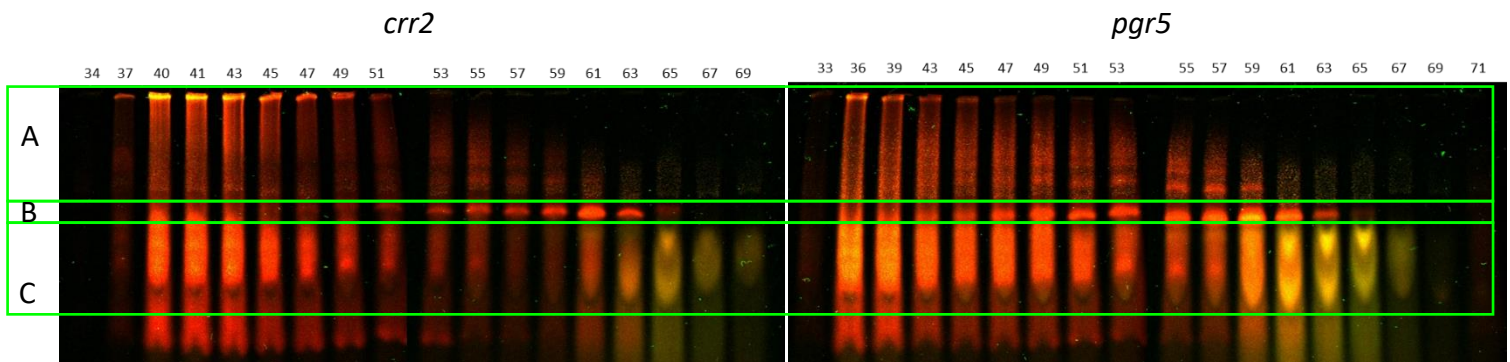

Figure 12. N-PAGE (fluorescence emission 700 nm, excited at 685 nm and emission 800 nm, excited at 785 nm) separations of concentrated protein complexes after FFE separation (fractions (34 – 71). Membrane complexes from the stroma lamellae were solubilised from freshly isolated chloroplasts of *A. thaliana crr2* and *pgr5* mutants. The solubilised complexes were separated by FFE, concentrated by centrifugal filtration using Sartorius 100K and further analysed by N-PAGE (40 µM LDS was added to the cathode buffer). Quantification analysis of higher complexes (A), PSI (B) and LHCII (C) is shown in *Figure 13.*
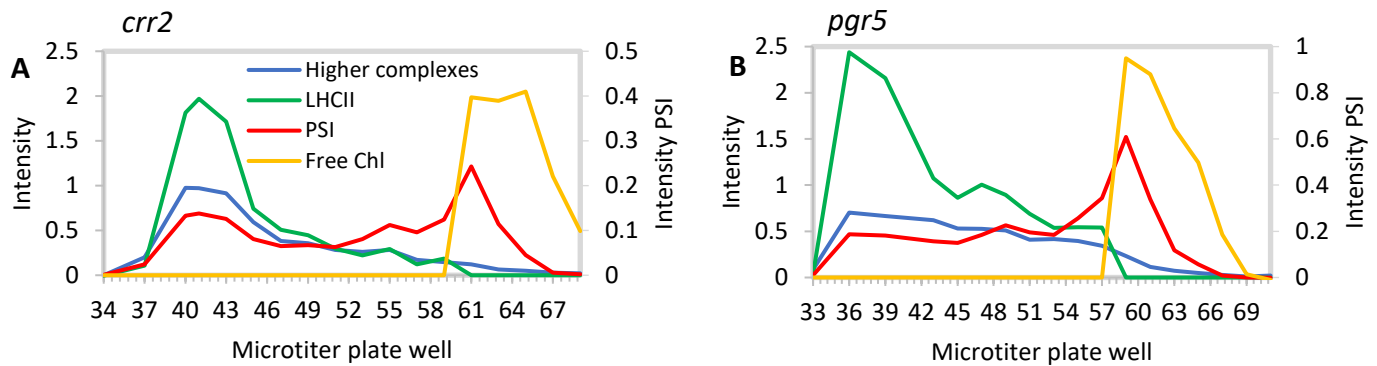
Figure 13. Quantification analysis of N-PAGE (fluorescence em700) separations of concentrated protein complexes after FFE separation (fractions (34 – 70). Membrane complexes from the stroma lamellae were solubilised from freshly isolated chloroplasts of *A. thaliana crr2* **(A)** and *pgr5* **(B)** mutants. The solubilised complexes were separated by FFE, concentrated by centrifugal filtration and further analysed by N-PAGE, 40 µM LDS was added to the cathode buffer. Higher aggregates are shown in blue, PSI in red, LHCII in green and free Chlorophyll (Chl) in yellow. Intensity values times 10^6. See *Figure 12*.
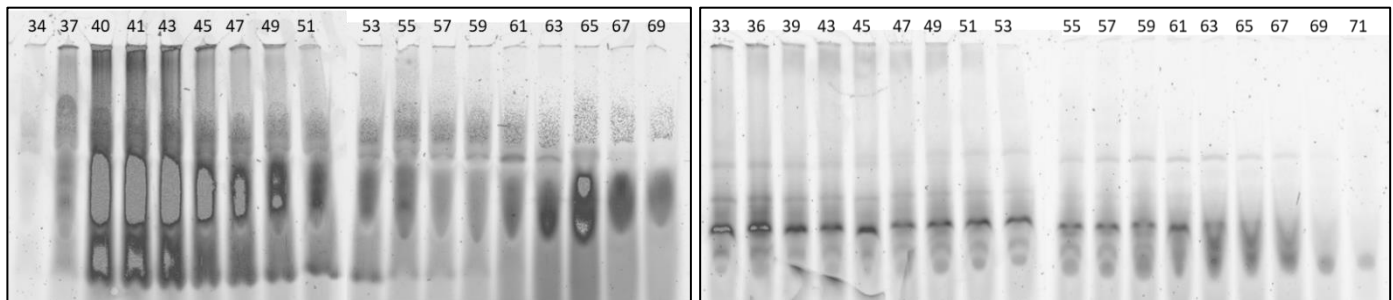

Figure 14. N-PAGE separation (fluorescence ex 633 em670) of concentrated protein complexes after FFE separation (fractions (33 – 71). Membrane complexes from the stromal lamella were solubilised from freshly isolated chloroplasts of *A. thaliana crr2* **(left)** and *pgr5* **(right)** mutants. The solubilised complexes were separated by FFE, concentrated by centrifugal filtration and further analysed by N-PAGE (40 µM LDS was added to the cathode buffer).

A very interesting observation was made when the fluorescence of the N-PAGE gels was investigated by exciting the Chla at 633 nm and recording the emission at 670 nm. Under these conditions, a clear difference was determined between the LHC, the PSI, and the high-molecular weight complexes solubilised from the two CEF mutants (*Figure 14*). While fluorescence from the trimeric and monomeric LHCs remained high in *crr2*, the emission nearly vanished in all but one band in the region of the LHCs from *pgr5*. In the molecular weight region of the PSI band, a molecular weight band larger than PSI was determined in all N-PAGE lanes from the FFE fractions; this band was absent in *pgr5*. However, the PSI band appeared at a lower molecular weight towards the anode fractions of FFE in fractions 33-47 (Figure 14). In the region of the high molecular weight bands, both mutants showed the accumulation of a diffuse band in the anode fractions of FFE. In *crr2* this band accumulated in fraction 40 and 41; whereas, in *pgr5* the band was distributed between fractions 36 to 51 (Figure 14). The reason for the

strong difference in fluorescence scanning upon excitation at 685 with emission at 700 nm (Figure 12) and excitation at 633 with emission at 670 nm (*Figure 14*) remained unclear.
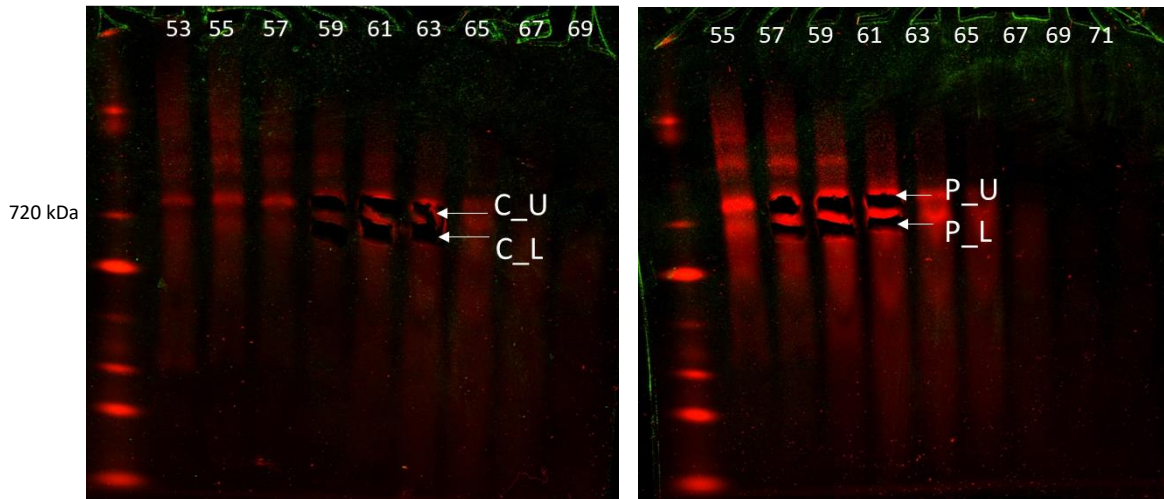

Figure 15. Bands excised for mass spectrometry analysis. A N-PAGE separation was done on the retentate of selected fractions after FFE separation of stroma lamellae complexes solubilised from *crr2* (left) and *pgr5* (right). Upper (U) and lower (L) bands, at a molecular mass of around 720 kDa, were pooled from fractions 59, 61 and 63 for *crr2* and from fractions 57, 59 and 61 for *pgr5*. NativeMark was used as a standard and loaded in lane 1. See Table *8* and *Table 9.*

Until this point in the experimentation, the PSI protein complex had been localized based on its fluorescence and mobility of the complex in the FFE separation and its fluorescence and molecular weight region upon separation as a band in N-PAGE. However, the identity of the protein complex had not been clarified. The proteins in the native-gel were therefore stained with Coomassie and the band corresponding to the fluorescent bands were cut out from the N-PAGE. Interestingly, upon staining not one but two bands were visible in all FFE fractions separated in the native-gel that showed a fluorescent band in the molecular weight region of the PSI complex. Hence, both stained bands that originated from a fluorescent and the non-fluorescent N-PAGE bands were cut from the gel and analysed by MS upon in-gel digestion (*Figure 15*, see methods section). Bands were cut from the 720 kDa region of fractions 59, 61 and 63 in the *crr2* separation and from fractions 57, 59 and 61 in the *pgr5* separation (*Figure 15*). The bands were categorised according to their molecular weight as 'upper' and 'lower' bands and the proteins were pooled from the three lanes originating from the three FFE fractions in each mutant to ensure that a high enough concentration of protein was available for the MS analysis (*Figure 15*, *Table 8*). Hereby, protein complexes were identified in the MS upon proteolytic digestion by analysis of the peptides originating from the complex's subunits. All identified subunits that originated from one of the crystallized complexes of the photosynthetic machinery were then pooled and divided by the number of identified subunits to normalize the dataset (*Table 8*). The results showed that both the upper and lower bands in both CEF mutants contained subunits for PSI and

Cytb$_6$f in about equal quantity. However, in the lower band also subunits of the PSII reaction centre were identified. Interestingly, also a small protein involved in the non-photochemical quenching of PSII termed PsbS was identified in the lower band of *pgr5* (*Table 8* and *Table 9*).

Table 8. Mass-spectrometry analysis of the in-gel digestion products from the upper (U) and lower (L) bands of *crr2* (C) and *pgr5* (P) mutants from the N-PAGE separation of concentrated protein fractions after separation by FFE. Protein complexes were separated by FFE, concentrated by centrifugal filtration, and separated by N-PAGE. Bands present at the same molecular weight in N-PAGE lanes, were pooled together from 3 different fractions/lanes and analysed by MS. Bands from *crr2* were labelled *as* upper (C_U) and lower (C_L) and from *pgr5 as* upper (P_U) and lower (P_L).

Identified Protein	Accession Number	Molecular Weight	C_L	C_U	P_L	P_U
Photosystem I reaction center subunit II-1, chloroplastic OS=Arabidopsis thaliana OX=3702 GN=psaD1 PE=1 SV=1	PSAD1_ARATH	23 kDa	13	11	12	15
Photosystem I reaction center subunit III, chloroplastic OS=Arabidopsis thaliana OX=3702 GN=PSAF PE=1 SV=1	PSAF_ARATH	24 kDa	8	8	8	8
Photosystem I reaction center subunit IV B, chloroplastic OS=Arabidopsis thaliana OX=3702 GN=PSAE2 PE=2 SV=1	PSAE2_ARATH	15 kDa	0	7	5	8
Photosystem I subunit l OS=Arabidopsis thaliana OX=3702 GN=PSAL PE=4 SV=1	A0A1P8B6D0_ARATH (+1)	30 kDa	6	5	6	6
Photosystem I iron-sulfur center OS=Arabidopsis thaliana OX=3702 GN=psaC PE=3 SV=2	PSAC_ARATH	9 kDa	5	5	6	6
Photosystem I reaction center subunit V, chloroplastic OS=Arabidopsis thaliana OX=3702 GN=PSAG PE=1 SV=1	PSAG_ARATH	17 kDa	0	0	0	5
Photosystem I reaction center subunit VI-2, chloroplastic OS=Arabidopsis thaliana OX=3702 GN=PSAH2 PE=2 SV=1	PSAH2_ARATH	15 kDa	0	4	4	0
Photosystem I reaction center subunit N, chloroplastic OS=Arabidopsis thaliana OX=3702 GN=PSAN PE=1 SV=2	PSAN_ARATH	18 kDa	0	0	4	7
ATP synthase subunit alpha, chloroplastic OS=Arabidopsis thaliana OX=3702 GN=atpA PE=1 SV=1	ATPA_ARATH	55 kDa	0	0	0	4
Cytochrome f OS=Arabidopsis thaliana OX=3702 GN=petA PE=3 SV=1	CYF_ARATH	35 kDa	20	10	20	15
Cytochrome b6 OS=Arabidopsis thaliana OX=3702 GN=petB PE=1 SV=1	CYB6_ARATH	24 kDa	6	0	7	4
Isoform 2 of Cytochrome b6-f complex iron-sulfur subunit, chloroplastic OS=Arabidopsis thaliana OX=3702 GN=petC	UCRIA_ARATH	23 kDa	5	0	6	0

Photosystem II CP43 reaction center protein OS=Arabidopsis thaliana OX=3702 GN=psbC PE=1 SV=3	PSBC_ARATH	52 kDa	0	0	8	0
Photosystem II CP47 reaction center protein OS=Arabidopsis thaliana OX=3702 GN=psbB PE=1 SV=1	PSBB_ARATH	56 kDa	6	0	7	0
Photosystem II 22 kDa protein, chloroplastic OS=Arabidopsis thaliana OX=3702 GN=PSBS PE=2 SV=1	PSBS_ARATH	28 kDa	0	0	4	0

Table 9. Normalization of peptide counts as shown in Table 8. Peptides assigned to photosystem I (PSI), Cytochrome b6f (Cytb6f) and photosystem II (PSII) were summarized (Total number of peptides) and the sum divided by the number of peptides contributing to the sum value (Quotient of total peptides/subunits).

	Total number of peptides				Quotient (tot. peptides/subunits)			
N-PAGE band	C_L	C_U	P_L	P_U	C_L	C_U	P_L	P_U
PSI	32	40	45	55	8	7	6	8
Cytb$_6$f	31	10	33	19	10	10	11	10
PSII	6	0	19	0	6	0	6	0

The number peptides identified to originate from PSII proteins in the lower of both bands containing PSI and Cytb6f proteins was low. This could indicate that the peptides identified by MS were not enough to conclude on the presence of the photosystem complex in this band or that a very low amount of the proteins were present in the band. Presence of PSII complexes was therefore re-investigated in addition by the distribution of PSII and Cytb$_6$f containing complexes in all FFE fractions by gel-blot analysis. For PSII, antibodies directed against subunit D2 and for Cytb$_6$f, antibodies directed against subunit Cytb$_6$ were used (*Figure 16* and *Figure 17*). Gel-blot analysis showed an almost equal distribution of Cytb$_6$ between fraction 54 to 66. This indicated that the separation of Cytb$_6$f at the cathode side of FFE was about similar in both mutants. However, at the anode of FFE, some of the Cytb$_6$f complexes solubilised from *pgr5* showed a higher mobility, which indicated that complexes in these fractions were more negatively charged (*Figure 18* A). In particular, quantification of the gel-blot signals from the Cytb$_6$ detection showed that both mutants showed two peaks, one at the cathodic end (fractions 59 to 63) and one at the anodic end (fractions 39 to 43) (*Figure 18* A). Interestingly, the shift of Cytb$_6$f complexes towards the anode for *pgr5* relative to *crr2* was not found when the distribution of PSII was determined using the D2 antibody (*Figure 18* B). Here, both mutants showed a peak for D2 in the range of fractions 38 to 42. The signal intensity in *crr2* was about half that of *pgr5* in both the Cytb$_6$ detection and the D2 detection (*Figure 18*). This indicated that the *pgr5* mutant contained more Cytb$_6$f and PSII containing complexes than the *crr2* mutant. This tendency was also observed during the former separation, when *pgr5* showed more than three times more signal in Cytb$_6$ detection than *crr2* (*Figure 8* and *Figure 9*). In addition, data showed very low signal for the D2 protein in the cathodic FFE fractions that showed co-mobility of the Cytb$_6$f and PSI complexes; although, the signal strength of D2 was several-fold increased relative to Cytb$_6$ signal at the anodic FFE fractions. This indicated that the pooled protein bands isolated in N-PAGE from FFE fractions 57-61 (*pgr5*) and 59-63 (*crr2*) were composed of PSI and Cytb6f and did not contain PSII.
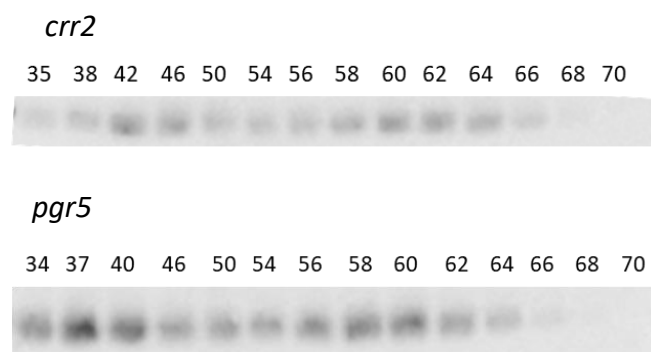
crr2

35 38 42 46 50 54 56 58 60 62 64 66 68 70

pgr5

34 37 40 46 50 54 56 58 60 62 64 66 68 70

Figure 16. Gel-blot analysis of fractions 34 – 70 after FFE separation. Antibodies directed against the Cytb$_6$ subunit were used to determine the distribution of the Cytb$_6$f complex in the cyclic electron transport mutants. The thylakoid stromal lamellae membrane complexes solubilised from *A. thaliana crr2* and *pgr5* mutants were separated by FFE before further separation by SDS-PAGE and gel-blot analysis. Quantification analysis shown in *Figure 18*.
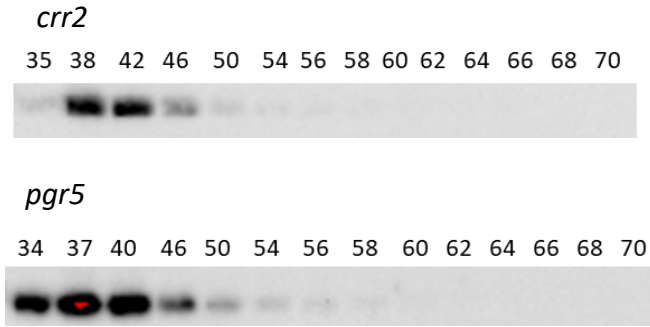
crr2

35 38   42   46   50   54 56 58 60 62 64 66 68 70

pgr5

34   37   40   46   50   54   56   58   60 62 64 66 68 70

Figure 17. Gel-blot analysis of fractions 34 – 70 after FFE separation. Antibodies directed against the D2 subunit were used to determine the distribution of PSII. The thylakoid stromal lamellae membrane complexes solubilised from *A. thaliana crr2* and *pgr5* mutants were separated by FFE before further separation by SDS-PAGE and gel-blot analysis. Quantification analysis shown in *Figure 18.*
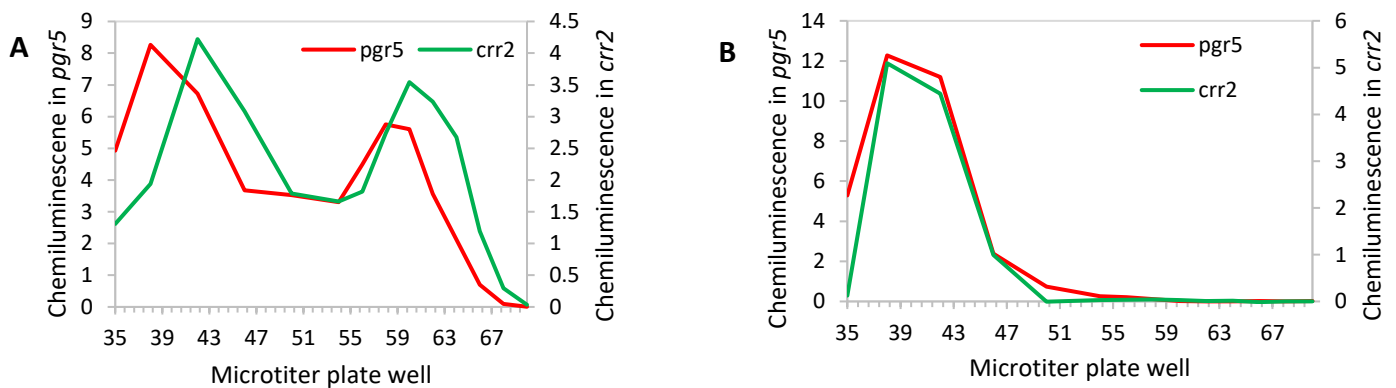

Figure 18. Quantification of chemiluminescent signal from gel-blot analysis. Antibodies directed against the $Cytb_6$ subunit were used to determine the distribution of the $Cytb_6f$ complex in the cyclic electron transport mutants **(A)** and against the D2 subunit to determine the distribution of PSII **(B)**. The thylakoid stromal lamellae membrane complexes solubilised from *A. thaliana crr2* (green) and *pgr5* (red) mutants were separated by FFE before further separation by SDS-PAGE and blot analysis. Chemiluminescence signal intensity values in times 10^3 (A) and times 10^6 (B). See gel-blots in *Figure 16* and *Figure 17*.

Optimisation experiments
Solubilisation of thylakoid stroma lamellae

To assess the difference in the complexes solubilised using different non-ionic detergents, chloroplasts were isolated freshly from 13-week-old WT-gli A. thaliana plants after 2 hrs of light exposure (see isolation protocol in the methods section). The isolated chloroplasts were treated with two different detergent concentrations to find the best treatment to solubilise as much of the membrane complexes found in the stroma lamellae of the thylakoid membrane as possible without solubilising the grana or the grana margins. In one solubilization 16 mM digitonin was used. In a second solubilization, 10 mM digitonin was combined with 94 µM β-DDM. Less digitonin was added when β -DDM was used to prevent solubilising the grana stacks due to too high overall concentration of detergent. It was expected that the second treatment may contain more PSII than the first treatment, due to the

extraction of PSII from the grana membranes using β-DDM. The solubilised complexes were separated by FFE and collected in microtiter plates and then further analysed by fluorescence spectroscopy, N-PAGE, SDS-PAGE and Western blotting.

For the FFE separation, the 20 mM Tris and Acetic acid buffer system was used with pH steps from pH 4.5 to pH 7 (see *Table 6* in methods section; E7 and E8 contained 10 mM KCl and E3 - E8 + CC contained β-DDM) and 'Procedure 1' was used for the FFE parameter settings (see *Table 7* in methods section). As done with the previous experiments, fluorescence spectroscopy was done on the collected FFE fractions (*Figure 19*) and selected protein complexes were concentrated using Sartorious 100K centricons. The retentate was then separated by N-PAGE and the fluorescence of complexes analysed by an excitation wavelength of 685 and 785 nm and an emission wavelength of 700 and 800 nm, respectively (*Figure 20*). The protein composition of complexes was also analysed by quantification of the fluorescence in the three molecular weight regions (*Figure 21*, ABC).
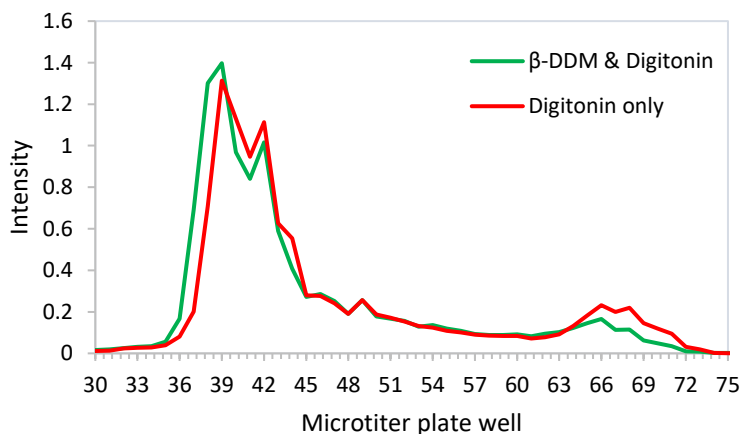

Figure 19. Fluorescence intensity of the microtiter plate measured with excitation at 685 nm and emission at 700 nm. Membrane complexes were solubilised from the stromal lamella of isolated chloroplasts from A. thaliana WT-col and separated by interval zone free flow electrophoresis with a pH range of 4.5 to 7. Solubilisation using only 16 mM digitonin (red) is compared to solubilisation using 10 mM digitonin and 94µM β-DDM (green). Intensity values times 10^6.

Both detergent treatments showed a similar separation profile among the FFE fractions of the solubilised complexes when the fluorescence of complexes was detected in the liquid state of the FFE buffers at 700 nm upon excitation at 685 nm were (*Figure 19*). The strongest peaks were seen in the anodic region at fraction 39 and 42 and a less intense peak was seen in the cathodic region at around fraction 66 for both separations (*Figure 19*). The only clear difference between both solubilisations was that the solubilization containing β-DDM resulted in a slightly stronger shift towards the anode. Generally, the strong peak in the anodic region indicated that most of the fluorescence was associated with the Chl binding negatively charged PSII, PSI and LHCII complexes.
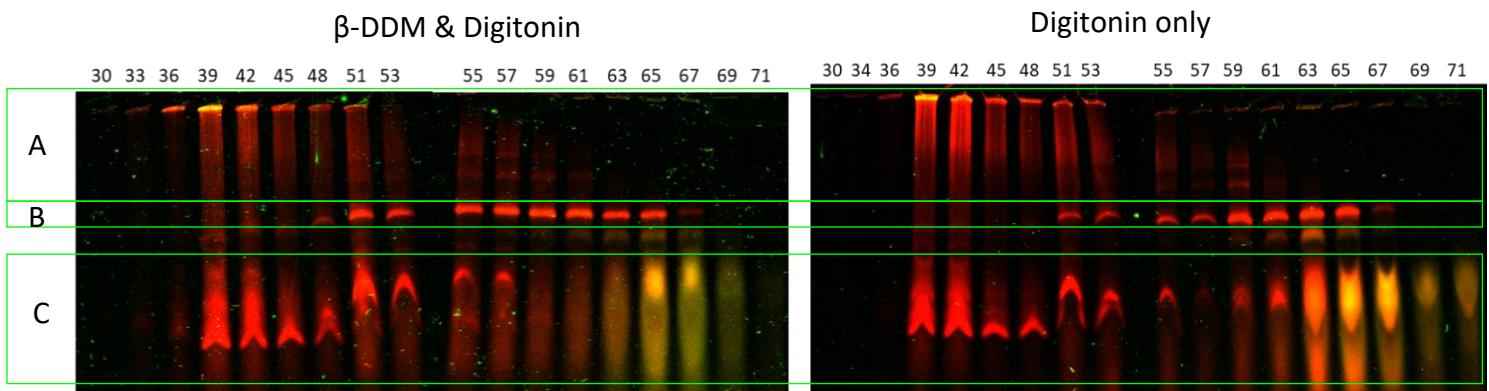
Figure 20. N-PAGE (fluorescence em700 and em800) separations of concentrated protein complexes after FFE separation (fractions 30 – 72). Chloroplasts isolated freshly from *A. thaliana* WT-col were treated with different detergents; (left) 10 mM digitonin and 94 µM β-DDM and (right) 16 mM digitonin. The solubilised membrane complexes were first separated by free flow electrophoresis (FFE) before further separation by N-PAGE, 80 µM LDS was added to the cathode buffer for the N-PAGE separation. Quantification analysis was done for the higher complexes (A), PSI (B) and LHCII (C) and is shown in *Figure 21.*

The separation of both solubilisations was further analysed via N-PAGE (*Figure 20*). In the presence of β-DDM, the fluorescence intensity among complexes in the molecular weight region B representing the PSI complexes, was changed. It was at first again remarkable that despite the determination of a dominating fluorescence maximum at the anode, upon N-PAGE separation of the FFE fractions 39 to 65 showed an about equally high overall fluorescence; although fluorescence was distributed in specific molecular weight regions, as already shown in the previous experiments. It was particularly noted that in fractions 51 to 57, the fluorescence intensity was increased when digitonin and β-DDM were used for solubilization. In addition, fluorescence in fractions 59 to 65 was increased in the presence of digitonin only (*Figure 20*). Interestingly, the molecular weight of the complexes remained unchanged when both solubilisations were compared. An increase in fluorescence could be interpreted to show that the presence of β-DDM altered the solubilization yield of these complexes from the membrane. It was noted that the molecular weight did not change between fractions 51 to 57 and fraction 59 to 65. Interestingly, the regions among both FFE fraction differed in that the second low molecular weight PSI band was only present in fractions 59 to 65 and fluorescence from increased in the presence of digitonin only. This indicated that the regions in both FFE fractions were representing complexes containing PSI and Cytb$_6$f that were binding different amounts of LHC complexes in addition (*Figure 20*). This thinking was supported by the observation that FFE region 51-57 also showed a distribution pattern of fluorescence from LHC proteins that was corresponding to the distribution of fluorescence from PSI complexes in the presence of β-DDM.

The quantification analysis of the N-PAGE separation of the concentrated FFE fractions showed that the distribution of the higher complexes, PSI and LHCII was similar for both separations with respect to the fractions in which complexes were found (*Figure 21*). However, there was a difference seen in the intensities of the various high molecular weight complexes. There was close to twice the emission intensity from the higher complexes in the peak at fraction 39 in the digitonin treatment compared to that of the β-DDM and digitonin treatment. PSI showed a very similar distribution in both treatments, with the higher emission intensities seen in fractions 51 to 57 for the β-DDM and digitonin treatment and in fractions 58 to 66 in the digitonin only treatment. Hence, PSI appeared to distribute much more uniformly in the presence of β-DDM relative to the digitonin only treatment. For both treatments, peaks for LHCII were seen in fractions 39 and 51; however, the yield in LHCII fluorescence was clearly increased in the presence of β-DDM. Free Chl showed a peak at fraction 65 for both treatments with an increase in the presence of digitonin only. In both treatments, the presence of free chlorophyll was concluded from a selective recording of 800 nm fluorescence in fractions 65-67 upon excitation at 785 (*Figure 20*). Basis for the conclusion was that an aggregation of Chl in detergent micelles typically results in a long-wavelength shift in fluorescence (Gottstein and Scheer, 1983).

Additionally, it appears quantification revealed that digitonin only treatment of the membranes alone increased the extraction of higher complex states that were separated in fraction 40 during FFE but decreased the amount of LHCII fluorescence in fraction 51 to 57. When this result is expressed in reverse, β-DDM contributed to released aggregation of higher molecular weight complexes in fraction 40 but was associated with a release of LHCII that showed mobility in fraction 50 and fraction 54/55. In the digitonin only separation, it appeared that PSI was more clearly associated with LHCII in fraction 64/65. But in the presence of β-DDM the PSI band was broader, stretching out to the anode, and this broadening was associated with a correlated LHCII distribution that was well determined especially in the native gel (*Figure 20*). In summary, results indicated that in the presence of digitonin only, complexes of PSI with $Cytb_6f$ and trimeric LHC were isolated in fractions 59 to 67; whereas, in fractions 51 to 57 the binding of $Cytb_6f$ to the PSI-LHC complexes had been lost. The PSI-$Cytb_6f$-LHC complex was less extracted in the presence of digitonin, which is indicating it is dominating the thylakoid membrane. Based on this conclusion, the binding of $Cytb_6f$ to the PSI complex decreased the mobility of the complex towards the anode. This indicated that $Cytb_6f$ was the least negatively charged of the three complex constituents.
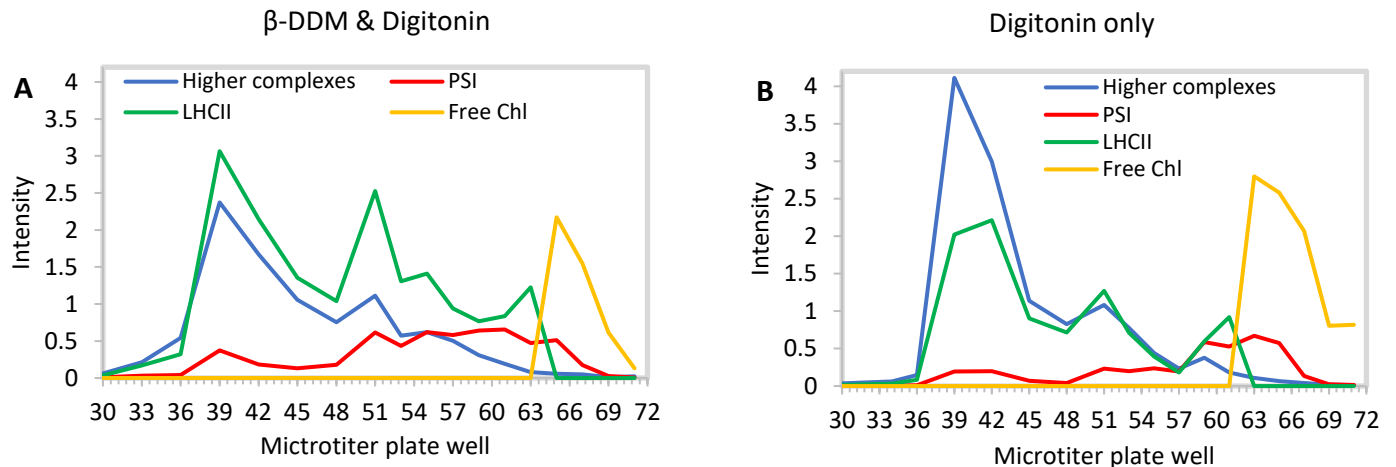
Figure 21. Quantification analysis of N-PAGE (fluorescence em700) separations of concentrated protein complexes after FFE separation (fractions 30 – 72). Chloroplasts isolated freshly from *A. thaliana* WT-col were treated with different detergents. **(A)** 10 mM digitonin and 94µM β-DDM **(B)** 16 mM digitonin. 80 µM LDS was added to the cathode buffer. Higher complexes (blue), PSI (red), LHCII (green), free chlorophyll (Chl) (yellow); intensity quantification values times 10^5. See *Figure 20*.

Comparison of buffer systems used for FFE

To assess if the concentration of ions in the buffers used for the FFE separation were affecting the native state and migration of the solubilised stroma lamellae complexes, different buffer systems were compared. The buffer systems used here were the Hiba - Bistris buffer system with pH steps pH 5.4 and 6.9 which had β-DDM in inlets E2 to E8 and 10 mM KCl in inlet E7; and the 10 mM Tris -Acetic acid pH 5 – 7 buffer system which had β-DDM in inlets E2 to E8 and 10 mM KCl in inlet E7 (see *Table 6* in the methods section). Chloroplasts were harvested freshly from 12-week-old WT-col *A. thaliana* plants after 2 hrs of light exposure (see isolation protocol in methods). Stroma lamellae complexes were solubilised by use of 16 mM digitonin (see solubilisation of thylakoid membrane protein complexes protocol in methods).

The Hiba – Bistris buffer system had a higher concentration of ions (due to the buffer component concentrations), compared to the 10 mM Tris – Acetic acid pH range 5 – 7 buffer system. It was expected to potentially increase the migration of the solubilised complexes but could have also potentially disrupted the interactions which keep the complexes together. Additionally, the Tris - Acetic acid system did not include a rise in molarity from 10 mM to 20 mM in the first anodic buffer (separation media 1, inlet E2), whereas the Hiba-Bistris included one. This means that the Tris - Acetic acid buffer system did not lead to a stronger barrier for larger complexes to move towards the anode, which would slow them down. A separation was also done just using two pH levels with the 10 mM Tris – Acetic acid buffers system, namely pH 5 and pH 7. The solubilised stroma lamellae membrane complexes were separated by FFE and collected in microtiter plates and then further analysed by fluorescence spectroscopy, N-PAGE, SDS-PAGE and Western blotting. Fluorescence spectroscopy was done on the collected FFE fractions and selected protein complexes were concentrated using Sartorious 100K centricons, the retentate was then separated by N-PAGE.
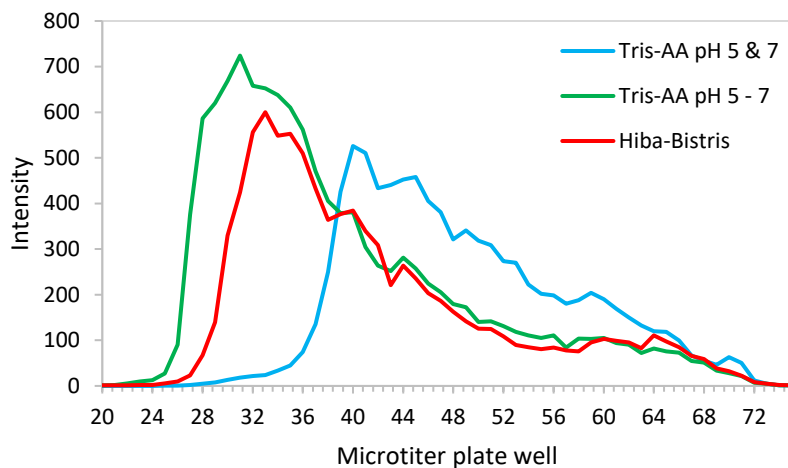
Figure 22. Fluorescence readings when exciting at 435 nm and emission at 680 nm. Fractions 20 – 75 are shown from the FFE separation of solubilised stroma lamellae membrane complexes from freshly isolated chloroplasts of *A. thaliana* WT-col. Different buffer systems were compared, Tris - Acetic acid pH 5 and pH 7 (red), Tris - Acetic acid pH range 5 – 7 (green) and Hiba – Bistris (blue). Intensity values times 10^6. See *Table 6* in methods section for details of the buffer systems used.

After the FFE separation, the FFE microtiter sample collection plate of three separations using different buffer systems were excited at 435 nm and the fluorescence recorded at 680 nm (*Figure 22*). The systems compared were: 1) 10 mM Tris – Acetic acid pH 5 and 7, to 2) 10 mM Tris – Acetic acid with pH range 5 to 7 and to 3) the Hiba – Bistris buffer system. All three separations showed a distinct peak in very distinct fraction numbers towards the anode and then a decrease in emission intensity as one moved towards the cathodic fractions (*Figure 22*). Evidently, regardless of the buffer system used complexes that showed emission at 680 nm were mostly found in the anodic region of the FFE separation. These would be Chl a and b-containing complexes and therefore mostly excite LHCII. Interestingly, when only using the two pH steps with the Tris – Acetic acid buffer (pH 5 and 7) the range of the separation was narrower and fell between fractions 36 to 71 (*Figure 22*, blue). With the other two systems however, the complexes were separated between fractions 25 to 71 in the Tris -Acetic acid (pH range 5 to 7) and fractions 28 to 71 in the Hiba – Bistris system (*Figure 22*, green and red). The emission intensity of the anodic peak at fraction 31 in the Tris – Acetic acid (pH range 5 to 7) separation was higher and closer towards the anode than the respective peak in the Hiba – Bistris system at fraction 33 (*Figure 22*, green and red). From fractions 35 to 71, the separation profiles of the Tris – Acetic acid (pH range 5 to 7) and the Hiba – Bistris systems were almost identical. However, the only significant difference observed in the separation profiles between the two systems was in the anodic fractions. Based on previous separations, it had been shown that these anodic fractions usually contain the higher complexes/aggregates. Consequently, the buffer components appeared to be affecting only the movement of higher complexes/aggregates found in the anodic fractions. The fractions from 35 to 71 were seemingly unaffected in terms of their migration during the FFE separation. A reason for this could have been that the Tris - Acetic acid system did not include an increase in molarity at the first anodic separation buffer from 10 mM to 20 mM, whereas the Hiba – Bistris buffer system did. This would mean that complexes were freer to move in the Tris – Acetic acid system, because no molar

barrier existed that would have required more net negative charge to overcome it. However, in the Hiba – Bistris system this barrier existed and consequently slowed down complexes.

To confirm the results of the comparison between the Hiba – Bistris buffer system (pH 6.9 and 5.4) and the 10 mM Tris – Acetic acid (pH range 5 – 7) buffer system another separation was performed. Optimisation on the FFE parameters were done to configure the separation time (with hv on), time until collection (after the hv has been turned off) and the time taken for sample collection into the microtiter plate. To begin with, the separation time was changed from 235 s to 217 s. The FFE separation was again analysed by fluorescence spectroscopy (excitation at 435 nm and emission at 680 nm) and fractions were further analysed via N-PAGE. The presence of $Cytb_6f$ in the FFE separation was tested via the detection of $Cytb_6$ after SDS-PAGE and Western blotting.

Figure 23. Fluorescence readings when exciting at 435 nm and emission at 680 nm. Fractions 30 – 75 are shown from the FFE separation of solubilised stroma lamellae membrane complexes from freshly isolated chloroplasts of *A. thaliana* WT-col. Different buffer systems were compared, 10 mM Tris - Acetic acid pH range 5 - pH 7 (red), and Hiba – Bistris (green). Intensity values times 10^6.

For the next separation with the two buffer systems the concentration of chloroplasts of only 0.86 µg/µl Chl a and b were loaded, solubilized in the Tris – Acetic acid system, compared to the solubilization of chloroplasts with 1.4 µg/µl Chl a and b content in the Hiba – Bistris system. The separation profiles were again very similar in terms of the distribution of the fluorescence between anode and cathode, in terms of having the strongest peak towards the anode and flattening out towards the cathode (*Figure 23*). However, differences were seen in the emission intensity when exciting at 435 nm and recording the fluorescence emission at 680 nm (*Figure 23*). Despite the observation that the anodic peaks of the two separations aligned better than with the previous experiment and both separations showed a peak at fraction 35/36; fractions 37 to 51 indicated a lower emission in the Hiba – Bistris system compared to that in the Tris – Acetic acid system. Again, fractions 52 to 64 aligned, whereas the emission in fractions 65 to 74 was once again lower in the Hiba – Bistris system compared to the Tris – Acetic acid system.

The N-PAGE separation of the concentrated proteins showed, at the anodic side between fractions 35 and 47, more detached antenna complexes in the Hiba – Bistris buffer system than Tris – Acetic acid buffer system (*Figure 24*). Additionally, in the Hiba – Bistris system, protein complexes above the detached antenna with a molecular weight between 480 kDa and 720 kDa also showed a higher fluorescence in the gel (*Figure 24*). Interestingly, these complexes contained mostly PSI complexes

that were split into a lower and higher PSI band. In contrast, in the Tris - Acetic acid separation this split PSI complex was found to a much lesser extent and in less anodic fractions. By analysing the Coomassie stained native-gels it was even more obvious that generally more complexes were visible on the native-gel in the Hiba – Bistris system than in the Tris – Acetic acid system (data not shown). Between fractions 52 and 64, which showed very similar emission at 680 nm when tested before N-PAGE separation (*Figure 23*), these fractions also showed a very similar protein complex distribution and fluorescence pattern in the native-gel (*Figure 24*). However, the Hiba – Bistris system showed a slight increase in 680nm emission in the liquid state and also showed more PSI complexes in the native-gel (*Figure 23* and *Figure 24*). Differences were also seen in fractions 63 to 69, where the Tris – Acetic acid system gel showed more liquid 680nm emission and fluorescent PSI complexes in the native-gel compared to the Hiba – Bistris system (*Figure 23* and *Figure 24*). Additionally, the amount of complexes that were excited at 785 nm and emitted light at 800 nm, visible in the gel as a more yellowish signal, was increased in the Tris – Acetic acid gel. It can be assumed that this signal originates from free chlorophylls and is therefore located underneath the trimeric antenna complex band around 240 kDa (*Figure 24*).

Interestingly, even when fewer chloroplasts were solubilized for the Tris – Acetic acid system compared to the Hiba – Bistris system, the former still showed a generally higher fluorescence emission after FFE separation (*Figure 23*). However, less fluorescence was visible towards the anode when analysing the protein complexes after N-PAGE (*Figure 24*). Therefore, it can be assumed that a smaller amount of protein complexes that moved in the Tris – Acetic acid buffer system led to a weaker fluorescence quench when measuring the liquid FFE fractions.
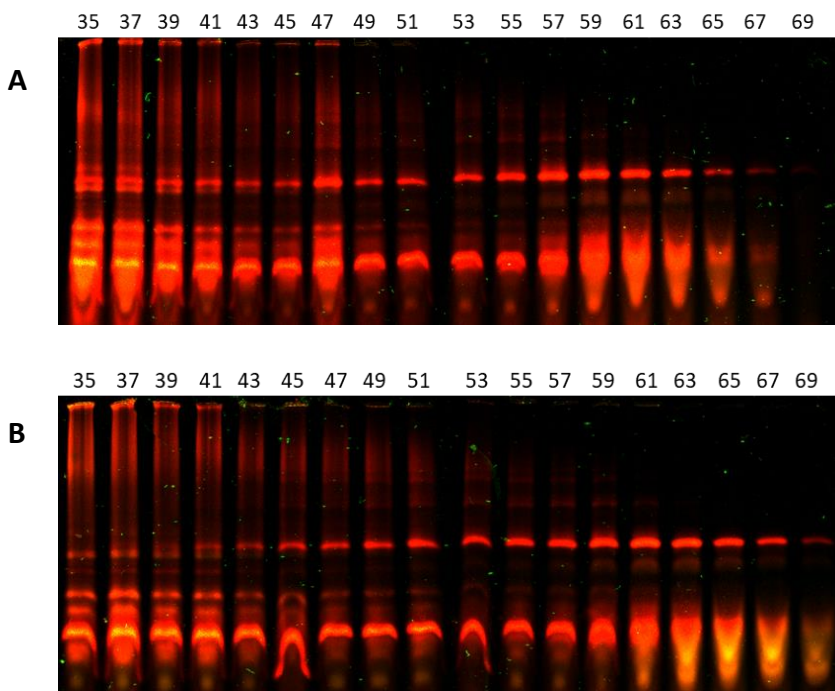

Figure 24. N-PAGE (fluorescence emission 700 nm and emission 800 nm) separations of concentrated protein complexes after FFE separation (fractions (35 – 69). Membrane complexes from the stroma lamellae were solubilised from freshly isolated chloroplasts of *A. thaliana* WT-col. FFE separations were done using the **A.** Hiba – Bistris buffer system (pH 5.4 and 6.9) and **B**. the 10 mM Tris – Acetic acid buffer system pH range 5 – 7. The solubilised complexes were separated by FFE, concentrated by centrifugal filtration and further analysed by N-PAGE (80 µM LDS was added to the cathode buffer). Fluorescence imaging was done by exciting at 685 nm and measuring the emission at 700 nm; and by exciting at 785 nm and measuring the emission at 800 nm.

Figure 25. Gel-blot analysis of FFE fractions 34 – 68 collected from separations using different buffer systems. Antibodies directed against the Cytb$_6$ subunit were used to determine the distribution of the Cytb$_6$f complex in the two FFE separation. **(A) H**iba – Bistris buffer system and **(B)** 10 mM Tris – Acetic acid pH range 5 – 7 buffer system. The thylakoid stromal lamellae membrane complexes solubilised from *A. thaliana* WT-col were separated by FFE before further separation by SDS-PAGE and blot analysis.
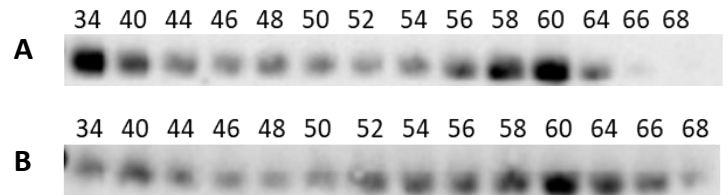
When analysing the FFE fractions via SDS-PAGE and Western blotting, Cytb$_6$ was detected in all tested fractions but showed two distinct peaks in both separations (*Figure 25)*. In the Hiba – Bistris separation, a peak was seen in fraction 34 and another peak in fraction 60 (*Figure 25* A). In the Tris – Acetic acid system an anodic peak was seen in fraction 40 and then another much stronger cathodic peak was detected in fraction 60 (*Figure 25* B). However, the cathodic peak in the Tris – Acetic acid separation was more spread out than that in the Hiba – Bistris separation, ranging from fraction 52 to 66 (*Figure 25* B). In contrast, the cathodic Cytb$_6$ peak in the Hiba – Bistris separation was very concentrated within fractions 58 to 60 (*Figure 25* A). Also, the anodic peak in the Hiba – Bistris separation was more concentrated than in the Tris – Acetic acid separation and also moved much closer to the anode (*Figure 25* A and B). From the gel blot analysis, it can be concluded that protein complexes containing Cytb$_6$ moved much faster towards the anode in the Hiba – Bistris system than in the Tris – Acetic acid system. Additionally, a stronger up-concentration of a cathodic complex with Cytb$_6$ was achieved in the Hiba – Bistris system. Therefore, the bigger difference in pH steps between the separation media in the Hiba – Bistris system (pH 6.9 and 5.4) compared to the narrower pH difference in the Tris – Acetic acid system (pH range over 7, 6.5, 6, 5.5, 5) led to a stronger and more focused separation of protein complexes containing Cytb$_6$f.
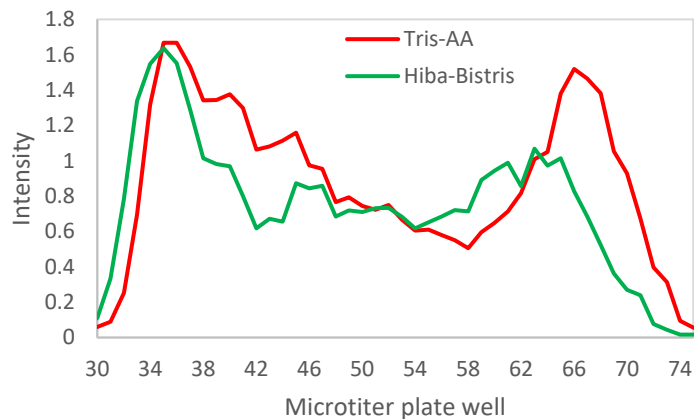
Figure 26. Fluorescence readings when exciting at 435 nm and emission at 630 nm (detection of the Cytb$_6$f complex). Fractions 30 – 75 are shown from the FFE separation of solubilised stroma lamellae membrane complexes from freshly isolated chloroplasts of *A. thaliana* WT-col. Different buffer systems were compared, Tris - Acetic acid pH range 5 - pH 7 (red), and Hiba – Bistris pH 5.4 and 6.9 (green). Intensity values given times 10^6.

Emission intensity at 630 nm was recorded for the FFE microtiter plates, in addition to the emission at 680 nm when exciting at 435 nm (*Figure 26*). Generally, anodic fractions 30 to 54 as well as cathodic fractions from 54 to 74 in both buffer systems correlated to 680 nm and 630 nm recording upon 435 nm excitation (comparing *Figure 23* and *Figure 26*). Interestingly, the 630 nm emission was about 100 - 200 times lower in intensity relative to the 680 nm emission (comparing *Figure 23* and *Figure 26*). However, the cathodic peaks between fraction 58 and fraction 74 in the Hiba – Bistris system and between fraction 54 and fraction 71 in the Tris – Acetic acid system were markedly increased at 630 nm emission relative to emission at 680 nm (*Figure 26*). Additionally, in the Hiba – Bistris separation the 630 nm emission peak was shifted more to the anode and not as clearly resolved as in the Tris – Acetic acid system (*Figure 26*). This indicated that the Chl excited in the most cathodic fraction was no longer bound to protein. Instead, the increased value at 630 nm could therefore have been caused by the preferential recording of the detergent bound fraction of Chl a and b. This interpretation is also supported by presence of bands that showed a lower fluorescent band located below the LHC bands in the cathodic fractions in the native-gel (*Figure 24*). When the Tris – Acetic acid systems showed a stronger fluorescence emission at 630 nm than the Hiba – Bistris system (*Figure 26*), also this additional band was especially strong (*Figure 26*). In addition to a stronger emission at 630 nm, when excited at 435 nm, it also showed a stronger emission at 800 nm when excited at 785 nm during gel analysis (*Figure 24*). Thus, it can be assumed that these fractions contained free Chl.

The effect of β-DDM on the FFE separation of native membrane complexes
Next, the migration and assembly state of the solubilised native membrane complexes was studied in absence of β-DDM detergent supplementation in the FFE buffers (*Figure 28*). Freshly isolated chloroplasts were isolated from 13-week-old *A. thaliana* WT-col after 2 hrs of light exposure. Experiments were run in the 10 mM Tris – Acetic acid buffer system with two different buffer ranges to test the effect of the detergent (see *Table 6* in methods section). First, a concentration of 150 μM β-DDM was added to all the separation media inlets from E2 to E8 and solubilized complexes were

separated with buffers ranging from pH 5 to pH 7, increasing in 0.5 steps (*Figure 28*, green). Then, in order to increase the separation range, complexes were separated at only two pH steps, namely pH 6.5 and pH 7. No detergent was added to the separation buffers firstly, but to avoid precipitation in the anodic region β-DDM was added to E1 and E2 only (*Figure 28*, red). The electrophoretic setting "Procedure 1"(see *Table 7* in methods section) with a separation time of 217 s was used. The distribution of Chl-protein complexes were monitored upon media fractionation in the microtiter plates by recording the fluorescence intensity distribution at 680 nm using an excitation of 435 nm (*Figure 28*).

The presence of β-DDM in all FFE-separation media inlet channels E2 to E8 over a range of pH 5 to 7 resulted in two well separated maxima. The main fluorescence intensity was recorded between fractions 30 to 55, while a smaller intensity peak was recorded between fractions 60 to 73 (*Figure 28*, green graph). The shift to only two pH steps (pH 6.5 and pH 7), resulted in a broadening of the fluorescence signals. Now, three peak intensity areas were recorded: in fractions 13, between fractions 55 to 70 and a very broad distribution increase between fractions 20 to 55 (*Figure 28*, red graph). Interestingly, the strongest fluorescence was recorded in the anodic region where β-DDM was supplemented to the separation media (*Figure 28*, red graph). When comparing the run with the wider pH range (pH 5 to 7) it was clear that the peak in fraction 37 moved towards the anode (fraction 13) when only pH 6.5 and 7 were used (*Figure 28*). In addition, the former peak area visible between fraction 38 and 56 separated already from fraction 19 when only the two pH steps (pH 6.5 and 7) were used (*Figure 28*). Generally, the fluorescence area underneath the broad range pH step and the two-pH step separation was the same. The only difference can be seen in the distribution of complexes. Furthermore, the mobility of protein complexes in the two-step pH separation at a decreased separation time of 157 s was evaluated (*Figure 29*). Generally, total fluorescence intensity remained unchanged. The anodic maximum shifted by four fractions closer towards the anode, but the cathodic maximum was no longer resolved (*Figure 29*, 157 s graph).

N-PAGE analysis of the 157 s FFE separation revealed a very concentrated PSI separation between fractions 59 to 65 (*Figure 27*). However, these PSI bands most likely showed a possible overlay with fractions containing free Chl. Evidence for this was given by the observation that FFE fractions between 61 and 67 analysed by N-PAGE showed bands, which emitted more light at 800 nm when excited at 785 nm during gel analysis (*Figure 27*). Additionally, the same fractions increasingly emitted at 680 nm when excited at 435 nm (*Figure 29*, green graph). Though, both of these overlaying signals that showed a peak at fraction 66/67 are not correlating with the peak at fraction 62 to 64 of the PSI complex band observed in the N-PAGE (*Figure 27*). A stronger separation of the PSI complex from the cathodic fractions was obtained via a longer separation time (*Figure 29*, red graph 217 s). Data indicated that the separation time was an effective parameter to direct separation of Chl protein fractions. However, the longer separation that showed a stronger separation of free Chl from PSI complexes which were moving towards the anode was not analysed by N-PAGE. Thus, for further FFE experiments with this buffer system, a separation time of 217 sec was used and a better separation could be obtained (*Figure 29* for spectroscopy data and *Figure 27* for native-gel). To sum up, the N-PAGE gel revealed that the

solubilization only contained PSI and antenna complexes that evenly distributed across the pH 6.5 step (*Figure 27*).

Furthermore, the protein complexes in the peak found in the cathodic region were investigated. Here, a complex composed of PSI and the Cytb$_6$f with molecular size of about 12 nm to 18 nm was expected (Yadav et al., 2017). The presence of protein complex particles in fractions 65 and 66 using dynamic light scattering (DLS) was investigated. In DLS, a polydisperse profile with a maximum molecular diameter of 18.2 nm was determined in both fractions with slightly different intensities (*Figure 30* A and B). Data indicated that the molecule was determined as a rotational symmetric particle with a diameter corresponding to the longest axis between both proteins (*Figure 30*). Thus, cathodic fractions consisted of a high percentage of PSI-Cytb$_6$f complexes.
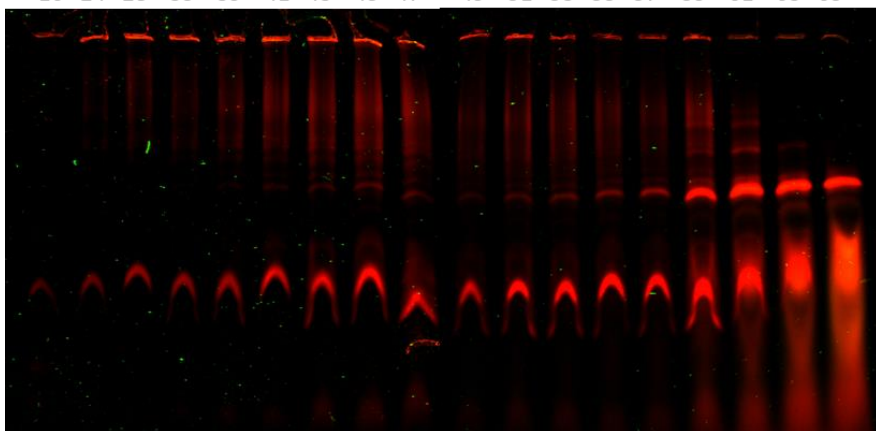

Figure 27. N-PAGE (fluorescence emission 700 nm and emission 800 nm) separations of concentrated protein complexes after FFE separation (fractions (35 – 69). Membrane complexes from the stroma lamellae were solubilised from freshly isolated chloroplasts of *A. thaliana* WT-col. FFE separations were done using the two-step Tris – Acetic acid pH 6.5 (E2 – E6) and pH 7 (E7 and E8) buffer system with β-DDM in E1 and E2. The solubilised complexes were separated by FFE, concentrated by centrifugal filtration and further analysed by N-PAGE (80 µM LDS was added to the cathode buffer). Fluorescence imaging was done by exciting at 685 nm and measuring the emission at 700 nm; and by exciting at 785 nm and measuring the emission at 800 nm.
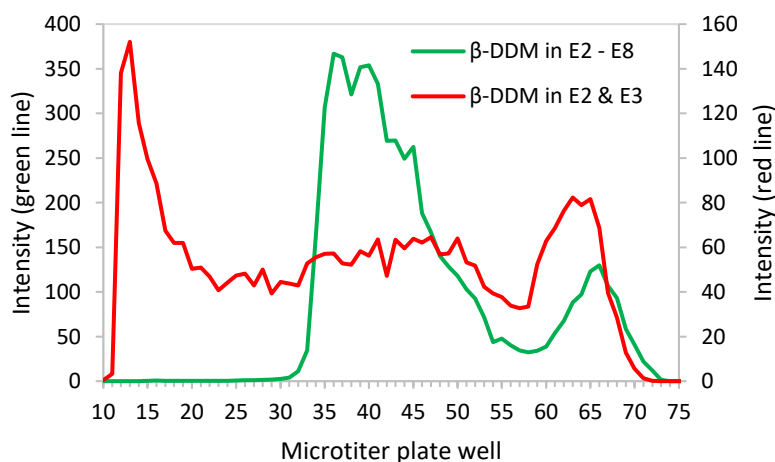

Figure 28. Fluorescence readings when exciting at 435 nm and emission at 680 nm. Fractions 10 – 75 are shown from the FFE separation of solubilised stroma lamellae membrane complexes from freshly isolated chloroplasts of *A. thaliana* WT-col. 150 µM β-DDM was added to all separation medium buffers of the FFE buffers ranging from pH 5.0-7.0 (green) or only to separation medium 1 and 2 (inlets E2 and E3) of the FFE buffers with pH steps 6.5 and 7.0 (red). Intensity values times 10^6.
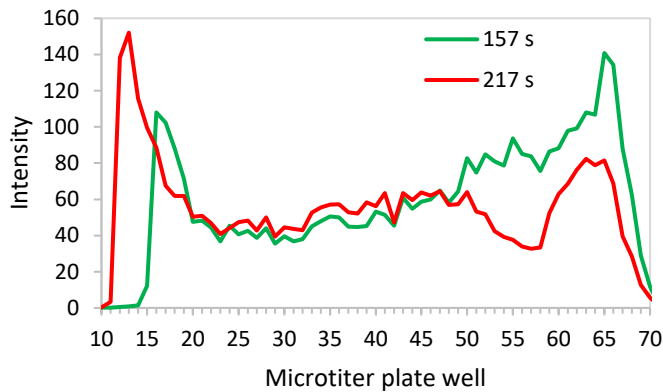
Figure 29. Fluorescence readings when exciting at 435 nm and emission at 680 nm. Fractions 10 – 75 are shown from the FFE separation of solubilised stroma lamellae membrane complexes from freshly isolated chloroplasts of *A. thaliana* WT-col. 150 µM β-DDM was added to separation medium 1 and 2 (inlets E2 and E3) of the FFE buffers with pH steps 6.5 and 7.0. To optimise the separation, two different separation times were tested, 157 s (green) and 217 s (red). Intensity values times 10^6.
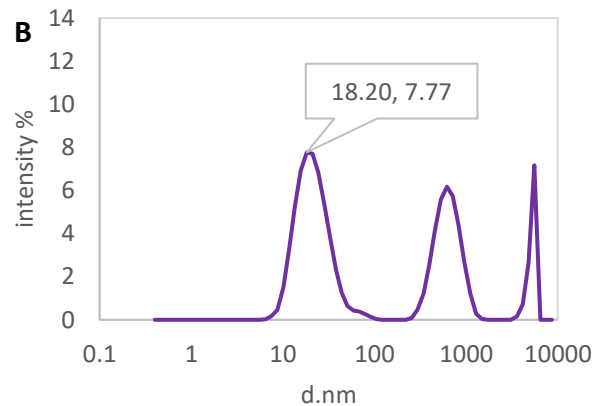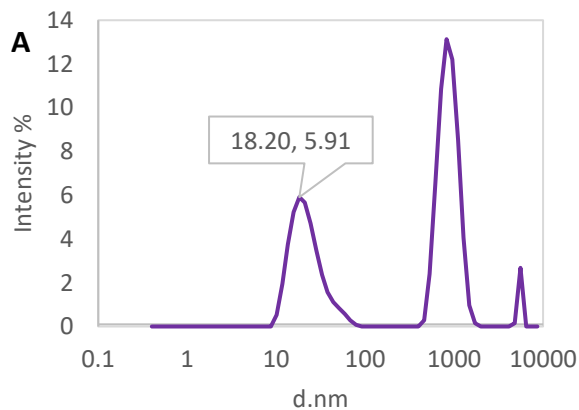

Figure 30. Dynamic light scattering (DLS) measurements of selected membrane complexes. Protein complexes were collected from the FFE separation of solubilised thylakoid stroma lamellae complexes from *A. thaliana* WT-col chloroplasts. The 10 mM acetic -acid pH 5 – 7 buffer system was used with 150 µM β-DDM added to separation media 1 and 2, the FFE separation time was 157 s. Fractions 65 **(A)** and 66 **(B)** were used for DLS measurements as these fractions are expected to contain the PSI-Cyt b$_6$f complex.

The effect of KCl on the native state of the membrane complexes during solubilization and subsequent FFE run

We tested next, if the integrity of the complexes was affected by the supplementation of a monovalent salt. The salt was added to both the media used to dissolve and solubilize the complexes as well as to the infusion buffer that is used to inject the sample into the separation chamber. Thylakoid stroma lamella complexes were solubilised from freshly harvested chloroplasts from *A. thaliana* WT-col plants as described in the isolation protocol under methods. Protein complexes of the thylakoid stroma lamella complexes were solubilised by 16 mM digitonin as described under solubilisation of thylakoid membrane protein complexes protocol in methods. Two different FFE separations were conducted in the 10 mM Tris – Acetic acid buffer system using a pH 7 throughout media inlets E2 to E6 and a pH 7.5 for loading of the solubilized samples in E7, and also pH 7.5 in E8 (*Table 6*, third column, in methods). In both experiments, separation media infused in anodic inlets E1 and E2 were supplemented with 150 μM β-DDM, and 10 mM KCl was either added to separation media 6 via inlet E7 or left out. Separation parameters according to "Procedure 1" (*Table 7* in methods) were used and a separation time of 217 s applied. Additionally, the influence of KCl was also tested for the effect on solubilisation on the thylakoid membrane proteins.

First, isolated chloroplast thylakoid membrane was isolated and adjusted to the same amount by using the same Chl a and b content in the solubilization mix. After solubilizing the same amount of chloroplast thylakoid membrane with or without 10 mM KCl, it was found that the amount of Chl-containing proteins that could be solubilized in the presence of KCl increased nearly by a factor of two (*Table 10*).

Table 10. The chlorophyll a and b concentration (μg/μl) of the isolated chloroplasts (WT-col) and the solubilised complexes used for the FFE separation to determine the effect of the presence of 10 mM KCl.

	Isolated chloroplasts	Solubilisation proteins used for FFE	Ratio of chl conc. of solubilized proteins to isol. chloroplasts
+ 10 mM KCl	3.91	1.18	0.30
No KCl	4.47	0.76	0.17

Secondly, it was tested whether the mobility of complexes was affected by the supplementation of KCl to the infusion buffer (E7) that is used to inject the sample into the FFE. Generally, the separation profile using only two pH steps 7 and 7.5 was very similar to the last experiment where the two-pH step system pH 7 and 6.5 was used (compare *Figure 28* and *Figure 31*). Again, the shift to more basic buffers with its subsequent increase in the mobility of strongly charged protein complexes in this experiment led to less protein complexes in the anodic region and a strong reduction of fluorescence in the anodic peak area (compare *Figure 28* and *Figure 31*). The loss of stronger negatively charged complexes was in addition caused by having chosen a first anodic buffer with low molarity (E2), that could not prevent their loss through slowing the mobility of highly charged complexes. The experimentation showed that by choosing a pH of 7.5 a fraction of the complexes revealed a reduced mobility in the cathodic part of the distribution profile (*Figure 31*). In addition, it was shown that in the absence of KCl an increase could be determined in the fluorescence trace in fractions 40 to 62. In contrast, an increase was determined in fractions 62 to 71 in the presence of KCl (*Figure 31*).
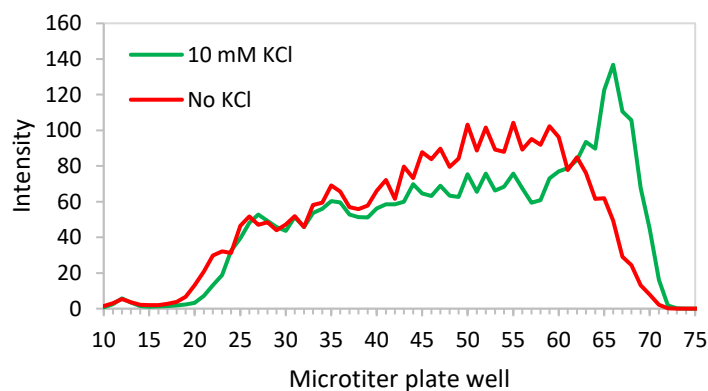

Figure 31. Fluorescence readings when exciting at 435 nm and emission at 680 nm. Fractions 10 – 75 are shown from the FFE separation of solubilised stroma lamellae membrane complexes from freshly isolated chloroplasts of *A. thaliana* WT-col. 150 µM β-DDM was added to separation medium 1 and 2 (inlets E2 and E3) of the FFE buffers and 10 mM KCl was added (green) or left out (red) from separation media 6 (inlet E7). Intensity values times 10^6.

Additionally, the complex composition was investigated between fraction 59 to 68 via using N-PAGE and fluorescence determination of the complexes by localization of their mobility in bands in the gel (*Figure 33*). Quantification of fluorescent bands from FFE fractions 59 to 67 upon N-PAGE separation of the complexes showed an overall increase in PSI bands towards fraction 63/64 in the absence of KCl. However, in the presence of KCl a continuous decrease in the same PSI band was observed (*Figure 34*). Interestingly, LHCII fluorescence followed the increase and decrease in PSI quantity. Data furthermore showed that the ratio of LHC to PSI proteins did not changed for fractions 61 to 65/67 in the absence or presence of KCl (*Figure 34*). However, this was not the case in the absence of KCl in fraction 59/60 where Chl fluorescence of LHCII increased to a stronger degree compared to other fractions (*Figure 34*). This indicated that in the absence of KCl in solubilization and FFE separation the overall increase in Chl fluorescence in fractions anodic of fraction 62 (*Figure 31*) correlated with an increase in LHC relative to PSI (*Figure 33*). In addition, quantification of complexes after N-PAGE separation showed that the group of higher molecular weight complexes increased continuously towards the anodic

fractions in the absence of KCl (*Figure 33* and quantification in *Figure 33*). This correlation between spectra and N-PAGE indicated that in the presence of KCl the increase of Chl fluorescence from fraction 65 to 70 (*Figure 31*) was not originating from PSI complexes (*Figure 33* and quantification in *Figure 33*). Therefore, even if overall fluorescence at 680 nm increased in the presence of KCl (*Figure 31*) the fluorescence yield from PSI and LHCII decreased upon N-PAGE separation (*Figure 33*). It was apparent that in the presence of KCl the amount of either free Chl-binding proteins such as LHC proteins and/or free Chl micelles was increasing. Free Chl molecules are typically solubilized in the detergent and separated to the native gel front. Hence, the most interesting finding in this experiment was that overall Chl fluorescence at 680 nm increased in the cathodic fractions in the presence of KCl but decreased in its absence. Moreover, in the presence of KCl this increase in fluorescence was not caused by an increase in PSI protein (comparing spectra *Figure 31*, green graph and quantification of N-PAGE in *Figure 34*). Thus, it can be assumed that KCl in the solubilization and/or FFE separation led to a higher accumulation of free Chl micelles at the cathode.

It remained unclear whether the increase in the release of Chl in the presence of KCl was related to the release of Chl bound to PSI proteins. Therefore, it was tested by DLS whether the molecular dimensions of the protein complexes changed in the cathodic fractions related to the overall fluorescence change (*Figure 31* and *Figure 32*). DLS revealed protein complexes with a polydisperse signal maximum of 18.2 nm in fractions 66/67 in the presence and of 21 nm in fractions 62/63 in the absence of KCl (*Figure 32*). This increase in the rotational diameter in the absence of KCl indicated that Chl remained bound to protein and most likely that the PSI-Cytb$_6$f-LHC complex were hence enlarged by binding more Chl binding LHC protein. In contrast, in the presence of KCl Chl was released from PSI-Cytb$_6$f-LHC complexes. This was associated with a fluorescence increase in the cathodic FFE fractions (*Figure 31*).
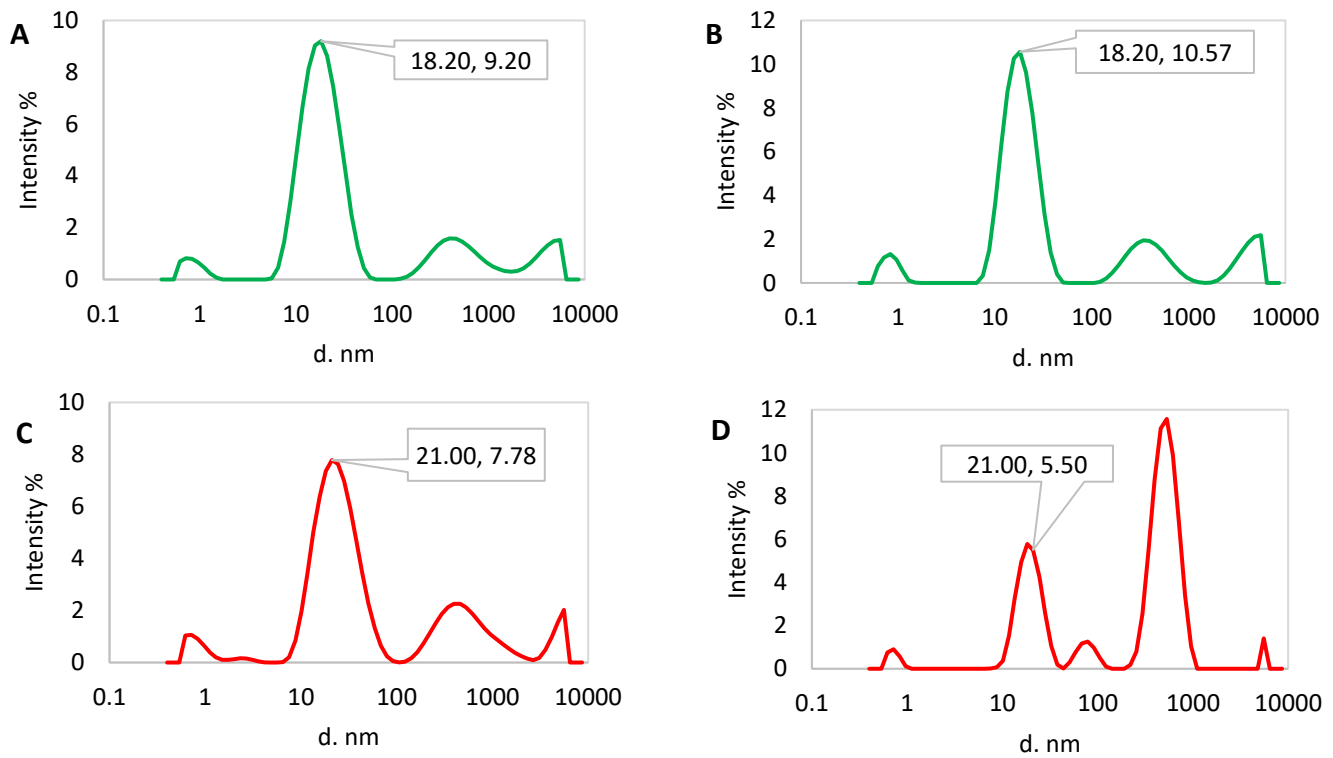
Figure 32. Dynamic light scattering (DLS) measurements of selected membrane complexes. Protein complexes were collected from the FFE separation of solubilised thylakoid stroma lamellae complexes from *A. thaliana* WT-col chloroplasts. Fractions 66 and 67 from the FFE separation with 10 mM KCl in green (A and B respectively) and the corresponding fractions 62 and 63 from the FFE separation with KCl in red (C and D respectively) are shown.
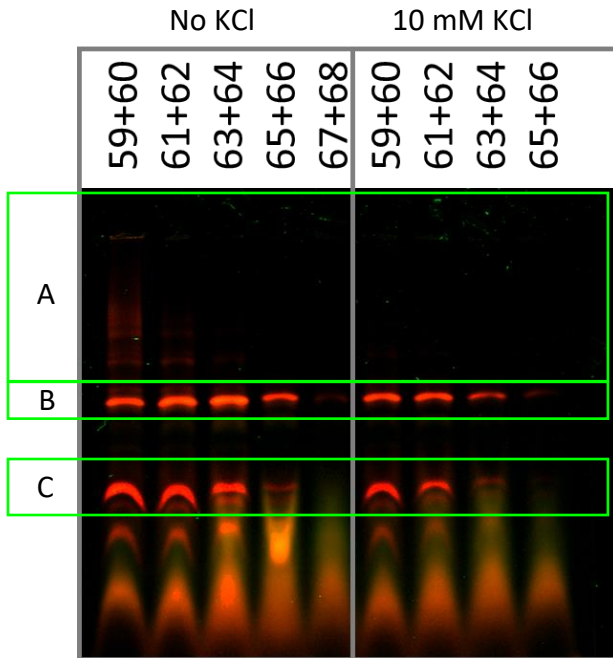
Figure 33. N-PAGE (fluorescence em700 and em800) separation of concentrated protein complexes after FFE separation (fractions 59 - 68). Membrane complexes from the stroma lamellae were solubilised from freshly isolated chloroplasts of *A. thaliana* WT-col. To compare the effect of the presence of KCl, 10 mM KCl was either left out (left) or added (right) to separation media 6 (inlet E7) of the FFE buffer used for solubilisation and electrophoretic separation. The solubilised complexes were separated by FFE, concentrated by centrifugal filtration using Sartorius 100K and further analysed by N-PAGE (80 µM LDS was added to the cathode buffer). Quantification analysis was done for the higher complexes (A), PSI (B) and LHCII (C) and is shown in *Figure 34.* The gel was imaged by exciting at 685 nm and recording the emission at 700 nm and exciting at 785 nm and recording the emission at 800 nm.
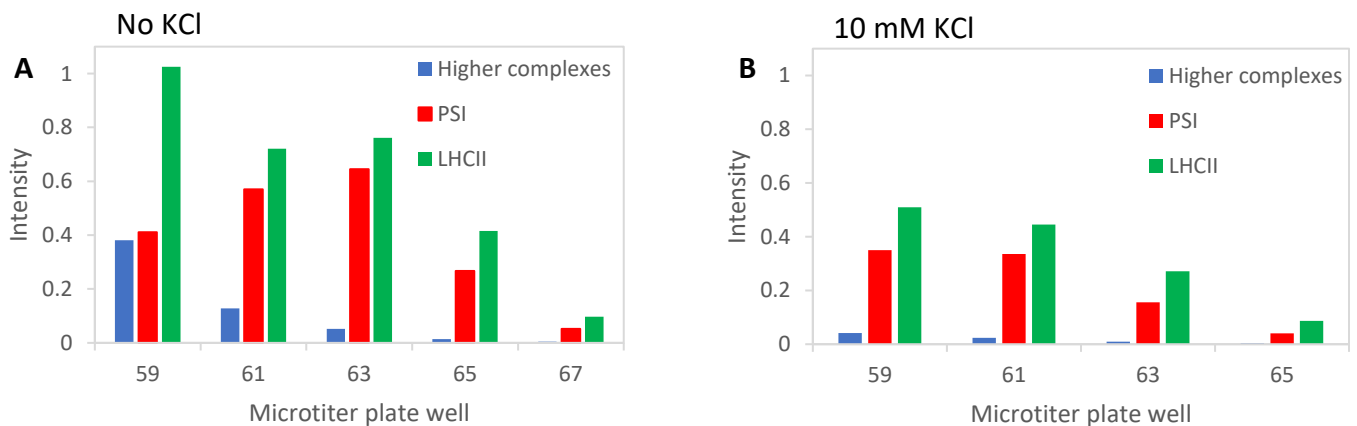

Figure 34. Quantification analysis of N-PAGE (fluorescence em700) separations of concentrated protein complexes after FFE separation (fractions 59 - 67). Membrane complexes from the stroma lamellae were solubilised from freshly isolated chloroplasts of *A. thaliana* WT-col. To compare the effect of the presence of KCl, 10 mM KCl was either omitted **(A)** or added **(B)** to separation media 6 (inlet E7) of the FFE buffer. The solubilised complexes were separated by FFE, concentrated by centrifugal filtration and further analysed by N-PAGE (40 µM LDS was added to the cathode buffer). Higher complexes are shown in blue, PSI in red and LHCII in green. Intensity values times 10^6. See *Figure 33.*

The effect of KCl on the native state of the membrane complexes during the FFE run only

Next, the effect of KCl on free Chl formation during FFE separation only was studied. An FFE separation was done in the presence and absence of 10 mM KCl in separation media 6 (E7) in order to investigate the effect of KCl on the assembly and charge state of the protein complexes. Chloroplasts were harvested freshly from of 18-week-old *A. thaliana* WT-col plants (see crude isolation of chloroplasts protocol in methods section), and thylakoid membranes were solubilised in the absence of KCl. FFE separation was performed by loading samples (solubilized in the absence of KCl) either in the presence or the absence of KCl in separation medium 6 infused via inlet E7. For the FFE separation, the 10 mM Tris – Acetic acid buffer system with three pH steps (pH 6.5 to 7.5) (*Table 6*, fourth column, in methods) was used and 'Protocol 2' (continuous flow) for the instrument parameters (see methods section *Table 7*). In contrast to the previous experiment, β-DDM was supplemented just to separation media 1 (inlet E2). Upon FFE separation, fractions were scanned directly in the microtiter plates for localization of Chl-containing protein complexes by excitation at 685 nm and recording of fluorescence at 700 nm using a near infrared scanning system. Subsequently, FFE fractions were concentrated by centrifugal filtration and analysed by N-PAGE. Protein complexes quantified after N-PAGE separation were scanned when excited at 685 nm and recording the emission at 700 nm. Additionally, the distribution of $Cytb_6$ containing complexes in the FFE fractions was analysed in gel-blot analysis.

Interestingly, under both conditions with and without KCl, liquid anodic fractions containing complexes with high mobility showed about an equally high intensity fluorescence at 700 nm upon when excited at 685 nm (*Figure 35*). However, in the presence of KCl, stroma thylakoid membranes showed an overall increased mobility during FFE separation. The highest anodic fractions were found at 22 and 28 and its fluorescence emission increased below fraction 45. Additionally, high Chl fluorescence was detected in the cathodic region above fractions 55, with a maximum seen at fraction 60 and fraction 62. In contrast, complexes separated in absence of KCl emitted about four times less fluorescence at the cathodic fractions (*Figure 35*). Additionally, its cathodic maximum moved closer to the cathode, namely, to fraction 66. Thus, protein complexes detected in this region showed a very low mobility and fluorescence intensity. Also, its anodic maxima shifted to fraction 23 and 29 (*Figure 35*).

To investigate which type of Chl protein complexes were detected through this analysis, protein complexes were further separated by N-PAGE. The distribution of complexes was investigated using the same 685 nm excitation and 700 nm emission scanning that had been applied for investigation of the distribution of the Chl-protein complexes upon FFE separation (*Figure 36*).
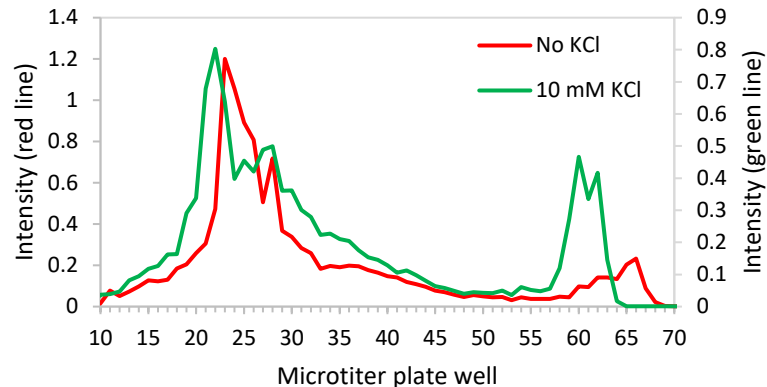
Figure 35. Fluorescence readings when exciting at 685 nm and emission at 700 nm. Fractions 10 – 70 are shown from the FFE separation of solubilised stroma lamellae membrane complexes from freshly isolated chloroplasts of *A. thaliana* WT-col. To compare the effect of the presence of KCl, 10 mM KCl was either left out **(red)** or added **(green)** to separation media 6 (inlet E7) of the FFE buffers. The solubilised complexes were separated by FFE, concentrated by centrifugal filtration and further analysed by N-PAGE, 80 µM LDS was added to the cathode buffer. Intensity values times 10^6.
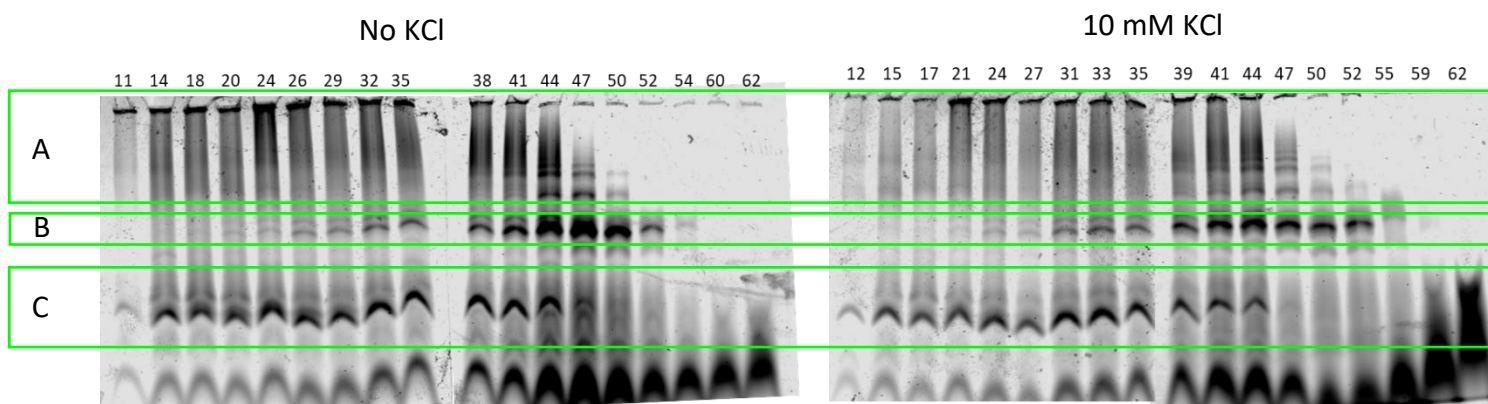

Figure 36. N-PAGE (fluorescence em700) separations of concentrated protein complexes after FFE separation (fractions 59 - 67). Membrane complexes from the stroma lamellae were solubilised from freshly isolated chloroplasts of *A. thaliana* WT-col. To compare the effect of the presence of KCl, 10 mM KCl was either omitted **(left)** or added **(right)** to separation media 6 (inlet E7) of the FFE buffer used for electrophoretic separation. The solubilised complexes were separated by FFE, concentrated by centrifugal filtration using Sartorius 100K and further analysed by N-PAGE (80 µM LDS was added to the cathode buffer). Quantification analysis of the higher complexes (A), PSI (B) and LHCII (C) is shown in *Figure 37.* The gels were imaged by exciting at 685 nm and recording the emission at 700 nm.

Generally, native-gel analysis indicated that PSI and PSI-LHCII complexes coexisted but that PSI-LHCII in fraction 24 to 44 moved closer to the anode due to its more negative charge (*Figure 36*). Additionally, PSI-LHCII complexes released most of its bound LHCII during N-PAGE. Moreover, gel analysis indicated that LHCII found in the anodic fractions 12 to 21 was strongly negatively charged. In the presence of KCl, Chl-containing micelles strongly accumulated in fractions 55 to 62 and were detectable in N-PAGE at the gel front (*Figure 36*). These results suggested that despite the absence of KCl during solubilization the addition of KCl in the FFE separation led to a strong increase in Chl fluorescence in the cathodic region. Thus, in the presence of KCl, more released Chl than in the absence of KCl is arrested at pH 7.5 in the cathodic region between fraction 55 to 62 than in the absence of KCl (*Figure 36*).
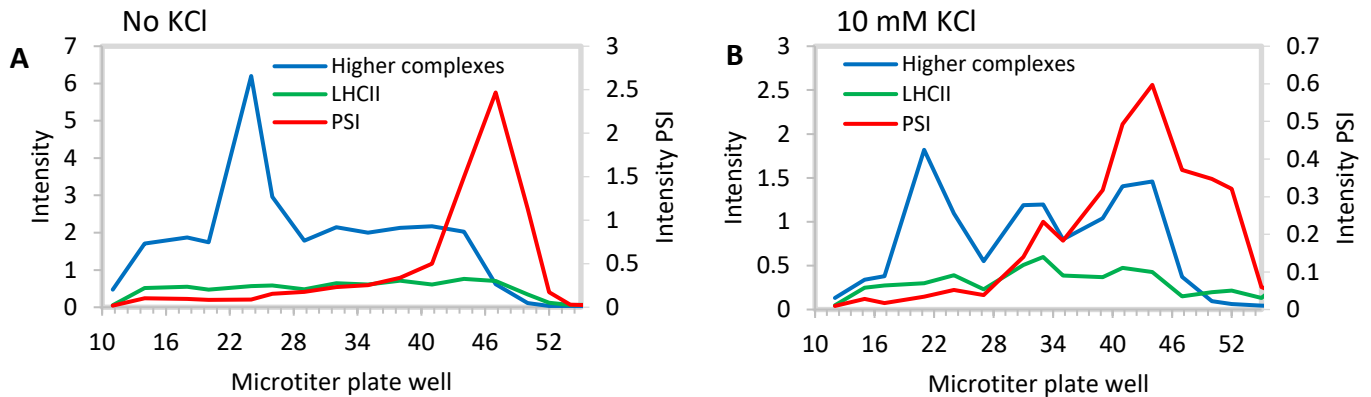
Figure 37. Quantification analysis of N-PAGE (fluorescence em700) separations of concentrated protein complexes after FFE separation (fractions 59 - 55). Membrane complexes from the stroma lamellae were solubilised from freshly isolated chloroplasts of *A. thaliana* WT-col. To compare the effect of the presence of KCl, 10 mM KCl was either omitted **(A)** or added **(B)** to separation media 6 (inlet E7) of the FFE buffer. The solubilised complexes were separated by FFE, concentrated by centrifugal filtration using Sartorius 100K and further analysed by N-PAGE, 40 µM LDS was added to the cathode buffer. Higher aggregates are shown in blue, PSI in red and LHCII in green. Intensity values times 10^5. See *Figure 36*.
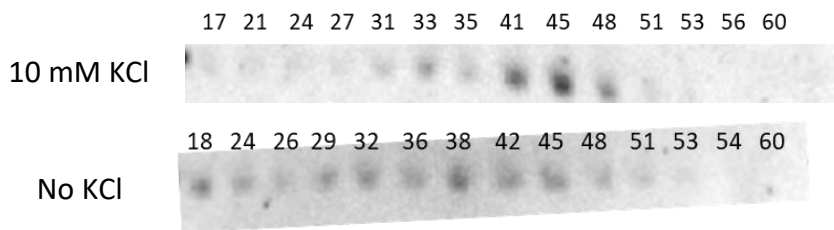
Figure 38. Gel-blot analysis of fractions 17 – 60 after FFE separation. Antibodies directed against the Cytb$_6$ subunit were used to determine the distribution of the Cytb$_6$f complex in FFE separations done with 10 mM KCl and without KCl in the separation 6 media of the FFE buffers (inlet E7). The thylakoid stromal lamellae membrane complexes solubilised from *A. thaliana* WT-col were separated by FFE before further separation by SDS-PAGE and gel-blot analysis. Quantification analysis shown in *Figure 39.*

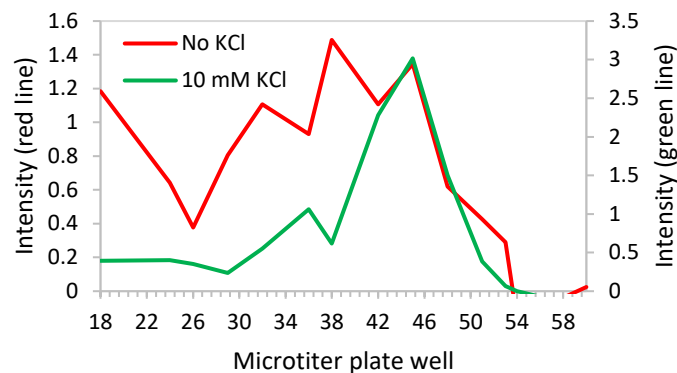**Figure 39. Quantification of chemiluminescent signal from gel-blot analysis.** Antibodies directed against the Cytb$_6$ subunit were used to determine the distribution of the Cytb$_6$f complex in FFE separations (fractions 18 to 60) done with 10 mM KCl (green) and without KCl (red) in the separation 6 media of the FFE buffers (inlet E7). The thylakoid stromal lamellae membrane complexes solubilised from *A. thaliana* WT-col were separated by FFE before further separation by SDS-PAGE and blot analysis. Chemiluminescence signal intensity values times 10^3. See *Figure 38*.

Furthermore, during N-PAGE separation PSI-LHCII complexes were identified in the cathodic region fractions of the FFE separation at around pH 7 for both conditions (*Figure 36*). Here, the PSI band was colocalized with free Chl dissolved in detergent at the gel front under both conditions. Interestingly, a higher concentration of PSI complex was identified in a band at about 720 kDa in the separation without KCl compared to that in the separation with KCl (*Figure 36* and *Figure 35*). Additionally, when KCl was absent, the increase in PSI between fractions 44 to 50 also showed more higher complexes, detached LHCII trimers, monomers and free Chls (*Figure 36* and quantification *Figure 37*). However, in the presence of KCl, the free Chl was found in a non-mobile or uncharged state in the cathodic fractions when detached from PSI complexes. It was found that in absence and presence of KCl PSI with the same molecular weight showed towards the anodic fractions decreasing fluorescence intensity. In the same way as for PSI, lower and more constant intensity of Chl fluorescence was found at the gel front. Also, Chl fluorescence was associated with a band in the molecular weight region resembling LHCII at about 240 kDa (*Figure 36*). The fluorescence of this band was about constant or only very slightly decreasing towards the anode, while the concentration of PSI fluorescence markedly decreased. This indicated that the ratio of PSI to LHCII decreased closer towards the anode.

In addition, gel-blot analysis revealed that in the presence and absence of KCl, in the cathodic region around fraction 45, a high amount of Cytb$_6$ was present (for gel-blot *Figure 38* and quantification *Figure 39*). This peak could under both conditions be overlaid with an increase in PSI in native-gel analysis (compare quantifications in *Figure 39* and *Figure 37*). Thus, it can be assumed that at the cathodic side a high amount of PSI-Cytb$_6$f complex accumulated. However, in the absence of KCl in the separation media (E7), the distribution of Cytb$_6$ was more spread towards the anode and showed maxima at fractions 38, 32 and 18 (*Figure 39*, red graph). Thus, KCl in the separation changes the proteins charge that could further lead to differences in complex formation and separation. After

analysing both KCl experiments it was concluded that, KCl would not be supplemented to any further thylakoid membrane solubilization and FFE separation.

Determining the difference between freshly isolated chloroplasts and frozen chloroplasts lysed with TMK buffer

In order to optimise the solubilisation and separation of the thylakoid stroma lamellae membrane complexes, an additional lysis step with TMK buffer was added to the isolation protocol. This step aimed to osmotically separate out the unwanted components of the chloroplast and to get a clearer separation of complexes of the photosynthetic membrane. A focus was set on the PSI and $Cytb_6f$ complexes. Additionally, it was tested if the freezing of isolated chloroplasts in liquid nitrogen (N_2) and storing them in -80 °C would change the amount and native state of protein complexes solubilized.

To study the effect of freezing and optimise the solubilisation process, chloroplasts were freshly harvested from 12-week-old *A. thaliana* WT-col plants (see isolation of chloroplasts with TMK lysis steps in methods section). Two samples of isolated chloroplasts were prepared:

1. Frozen sample: see isolation of chloroplasts and freezing in liquid nitrogen
2. Fresh sample: chloroplasts resuspended in separation media 6 (E7) of the FFE buffers after isolation

Thylakoid stroma lamella membrane complexes were solubilised (see solubilisation of thylakoid membrane protein complexes in methods section) and separated by continuous flow FFE (*Table 7* in methods) using the 10 mM Tris – Acetic acid pH 6.5 – 7.5 buffer system, with β-DDM supplemented into inlets E2 and E3 (*Table 6*, fourth column, in methods).

Table 11. The chlorophyll a and b concentration (µg/µl) of the isolated chloroplasts (WT-col) and the solubilised complexes used for the FFE separation to determine the effect of freezing chloroplasts before solubilization.

Sample	Isolated chloroplasts	Solubilized proteins used for FFE separation	Percentage (%) of Chl-containing complexes solubilised from isolated chloroplasts
Fresh	3.78	0.813	21.5
Frozen	2.88	1.147	39.8

Chloroplasts that were isolated and TMK treated were adjusted to the same Chl a and b content and subsequently solubilized. The percentage of Chl-containing complexes solubilised from the fresh sample was 21.5% (*Table 11*). In contrast, in the frozen sample almost double the amount of Chl-containing complexes, namely 39.8%, were solubilised (*Table 11*).
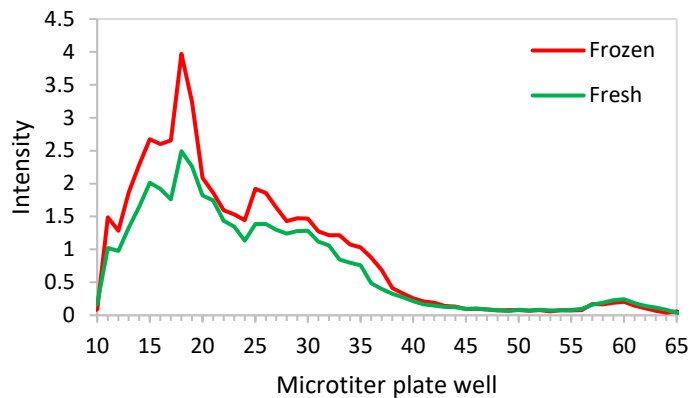
Figure 40. Fluorescence readings when exciting at 685 nm and emission at 700 nm. Fractions 10 – 65 are shown from the FFE separation of solubilised stroma lamellae membrane complexes from isolated chloroplasts of *A. thaliana* WT-col. Membrane complexes were solubilised from fresh **(green)** or frozen **(red)** chloroplasts. Intensity values times 10^6.
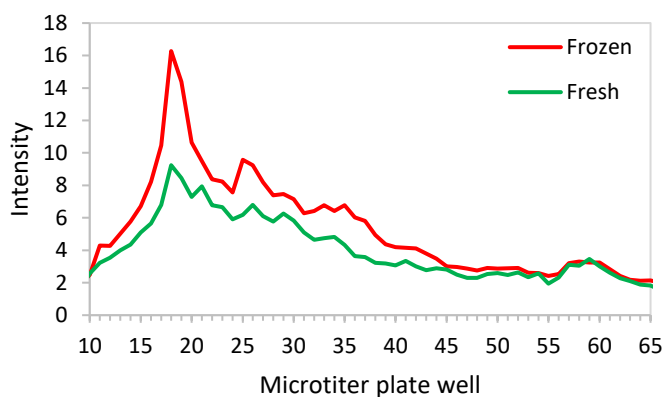

Figure 41. Fluorescence readings when exciting at 785 nm and emission at 800 nm. Fractions 10 – 65 are shown from the FFE separation of solubilised stroma lamellae membrane complexes from isolated chloroplasts of *A. thaliana* WT-col. Membrane complexes were solubilised from fresh **(green)** or frozen **(red)** chloroplasts. Intensity values times 10^2.

When comparing the FFE separations of membrane complexes solubilised from fresh and frozen chloroplasts, fluorescence readings at 700 nm (excited at 685 nm) of the microtiter plate showed a strong anodic peak in the region of fraction 18 (*Figure 40*). This strong intensity peak was also seen in the emission readings at 800 nm, when excited at 785 nm (*Figure 41*). The 700 nm emission showed higher intensity readings for the frozen sample in fractions 12 to 39 (*Figure 40*, red graph) compared to those of the fresh sample (*Figure 40*, green graph). Additionally, both samples showed very low relative emission in fractions 40 to 65. This indicated that most of the Chl-containing complexes were highly negatively charged and thus found closer to the anodic region, in fractions 12 to 39. The emission at 800 nm showed similar results (*Figure 41*). However, complexes had higher 800 nm emission intensities over a wider range, namely from fraction 11 to 45 in the frozen sample (*Figure 41*). The frozen sample showed a peak in fraction 18/19 with a 700 nm and 800 nm emission twice as strong as that of the fresh sample (*Figure 40* and *Figure 41*). This observation could be explained by the

fact that there was about twice the amount of Chl-containing complexes solubilised from the frozen chloroplasts than from the fresh chloroplasts (*Table 11*).
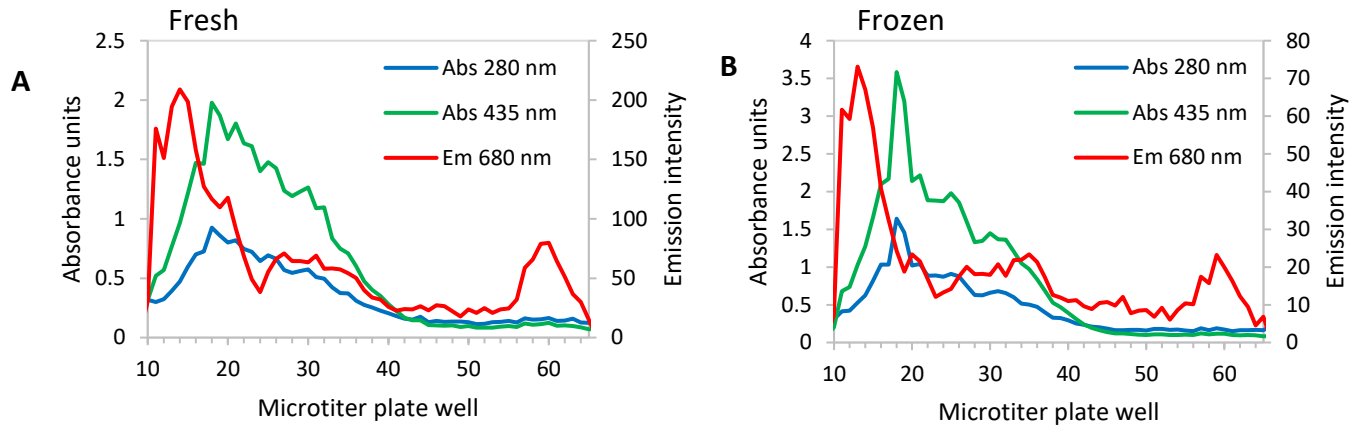

Figure 42. Spectroscopy readings of the FFE separations of membrane complexes solubilised from fresh and frozen chloroplasts of *A. thaliana* WT-col. Membrane complexes were solubilised from the thylakoid stroma lamellae and separated by continuous flow FFE. Complexes were either solubilised from freshly harvested chloroplasts **(A)** or from frozen chloroplasts **(B)**. Absorbance readings at 280 nm (blue) and 435 nm (green) are shown; as well as the fluorescence intensity when exciting at 435 nm and measuring the emission at 680 nm (red), emission values times 10^6.

The absorbance readings for the microtiter plate after FFE separation for the fresh sample showed a peak at fraction 19 for 435 nm and 280 nm (*Figure 42*). The absorbance readings at 435 nm were about twice as high as those at 280 nm (*Figure 42*). This means that there was a peak in Chl and protein concentration in this fraction. Similarly, the same was seen in the frozen sample, with a much narrower peak area. The peak in the frozen sample showed a sharper decrease in absorbance from fraction 20 to 32 than the decrease seen in the fresh sample. Fractions 41 to 66 for both the fresh and frozen samples showed equally a low absorbance at 435 nm and at 280 nm. Interestingly, the peak emission for 680 nm, when exciting at 435 nm decreased in fractions 13 to 15 for both samples. However, this did not overlap with the absorbance peaks. Additionally, both samples showed another relatively low 680 nm emission peak at fraction 60/61. From the N-PAGE separation it was evident that in both samples fractions 13 to 41 contain higher complexes of PSI and LHCII (*Figure 43*). Interestingly, in both samples, fractions 11 to 13/14 showed mostly free LHCII. Furthermore, in both samples, fractions 44 to 59 showed a high amount of free Chl micelle vesicles with little charge that accumulated in the cathodic region.
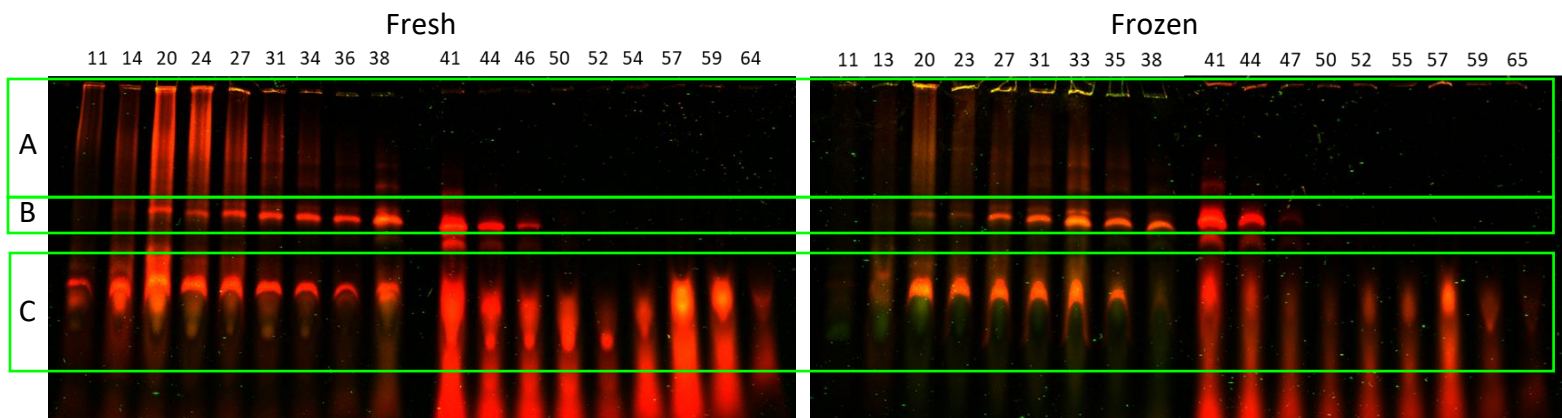
Figure 43. N-PAGE separations of concentrated protein complexes after FFE separation, fluorescence shown with excitation 685 nm and emission at 700 nm as well as excitation at 785 nm and emission measured at 800 nm. Membrane complexes from the stroma lamellae were solubilised from isolated chloroplasts of *A. thaliana* WT-col. Fractions 11 – 65 are shown from the FFE separation of solubilised stroma lamella membrane complexes from isolated chloroplasts of *A. thaliana* WT-col. Membrane complexes were solubilised from fresh or frozen chloroplasts. The solubilised complexes were separated by FFE, concentrated by centrifugal filtration using Sartorius 100K and further analysed by N-PAGE (80 μM LDS was added to the cathode buffer). Quantification analysis of the higher complexes (A), PSI (B) and LHCII (C) is shown in *Figure 44.*

Quantification of the N-PAGE separations showed that there is more LHCII found on the anodic side, around fraction 20, in the fresh sample than in the same fractions of the frozen sample (*Figure 44*). Additionally, in the frozen sample the peak for PSI was shifted closer towards the anode and was seen in fraction 33 (*Figure 44*). However, in the fresh sample the strongest PSI fluorescence peak was found in fraction 38 and its emission was 1.5 times smaller than in the frozen sample. This suggested that the PSI peak in the frozen sample contained complexes that were more charged than the complexes found in the fresh sample. The lower emission intensity seen in the fresh sample could indicate that there are fewer or alternatively more intact PSI complexes than in the frozen sample.

Size measurements for selected FFE fractions was done by using 60 μl of the fraction taken directly from the microtiter plate (see methods). The size measurements of fractions 14, 27, 34, 38 and 44 were recorded for the FFE fractions from the fresh sample separation. The results showed a range of sizes from 47.3 nm to 108.3 nm in diameter (*Table 12*). As the largest native complex has an expected diameter of not more than 50 nm these sizes are indicative of higher complexes/aggregates.
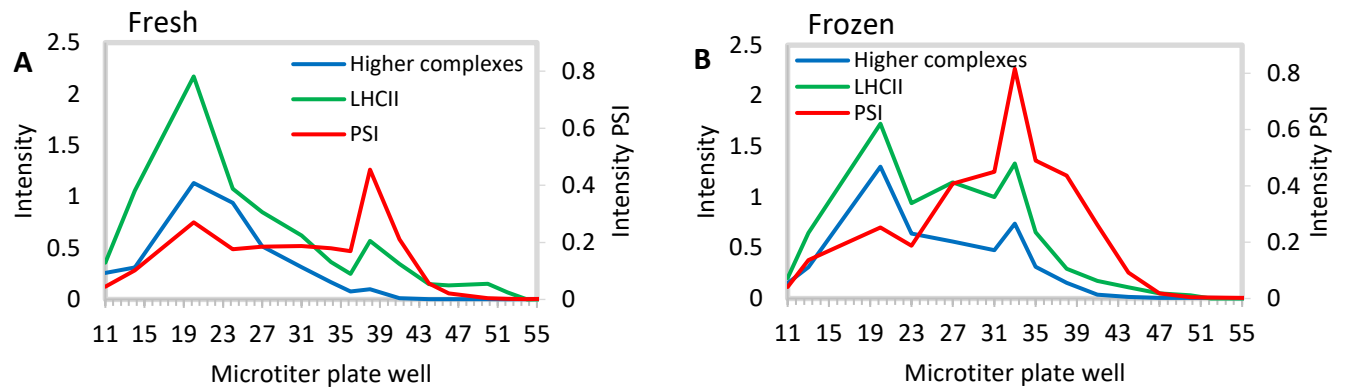
Figure 44. Quantification analysis of N-PAGE (fluorescence em700) separations of concentrated protein complexes after FFE separation. Membrane complexes from the stroma lamellae were solubilised from isolated chloroplasts of *A. thaliana* WT-col. Fractions 10 – 55 are shown from the FFE separation of solubilised stroma lamellae membrane complexes from isolated chloroplasts of *A. thaliana* WT-col. Membrane complexes were solubilised from fresh **(A)** or frozen **(B)** chloroplasts. The solubilised complexes were separated by FFE, concentrated by centrifugal filtration and further analysed by N-PAGE, 40 µM LDS was added to the cathode buffer. Higher aggregates are shown in blue, PSI in red and LHCII in green. Intensity values times 10^6. See *Figure 43*.

For zeta potential measurements, the fresh chloroplast FFE separation microtiter sample plate was used. To prepare the sample, 150 µl of sample was used from the microtiter plate and mixed with 600 µl 250 mM sorbitol solution to reach a final volume of 750 µl, which is the required volume for the sample cuvette. Zeta potential measurements were taken for the same fractions used for the size measurements and the results showed average zeta potentials from -17.6 mV to -30.6 mV (*Table 13*). All fractions analysed had very similar zeta potential values. Fractions 27 and 34 with values between -25,9 and -30.6 mV were most negatively charged. However, fraction 14 that moved closer towards the anode showed only an average zeta potential of -19,3 (*Table 13*). However, single measurements highly differentiated between analysed fractions. Therefore, this method might not be suitable to the fractions' heterogeneous complexity.

Table 12. Size measurements, obtained by Dynamic Light Scattering (DLS) experiments, of selected fractions from the FFE separation of solubilised thylakoid stroma lamellae membrane complexes of freshly harvested chloroplasts of *A. thaliana* WT-col.

FFE fraction	Size (d.nm)
14	70.62
27	64.47
34	50.27
38	47.3
44	108.3

Table 13. Zeta potential measurements of selected fractions from the FFE separation of solubilised thylakoid stroma lamellae membrane complexes of freshly harvested chloroplasts of *A. thaliana* WT-col.

FFE fraction	Reading number	Reported zeta potential (mV)	Average zeta potential (mV)
14	1	-16.7	-19.3
	2	-18.1	
	3	-22.1	
	4	-21.1	
	5	-22.2	
	6	-15.8	
27	1	-30.1	-25.9
	2	-19.9	
	3	-27.6	
34	1	-29.8	-30.6
	2	-36	
	3	-25.9	
38	1	-18.7	-20.3
	2	-16.7	
	3	-33.7	
	4	-27.7	
	5	-16	
	6	-9.27	
44	1	-18.4	-17.6
	2	-22.9	
	3	-24.3	
	4	-22.6	
	5	-14.4	
	6	-23.7	
	7	-25.1	
	8	-1.52	
	9	-5.41	

Optimised FFE separation of CEF mutants

Characterisation of photosynthetic membrane complexes composition in the CEF mutants, *crr2* and *pgr5,* were done using the optimised isolation and FFE protocols. Chloroplasts were harvested freshly from 13 to 14-week-old *A. thaliana* mutant plants (see isolation of chloroplasts with TMK lysis steps in methods) and thylakoid stroma lamella membrane complexes were solubilised (see solubilisation of thylakoid membrane protein complexes in methods). The solubilised complexes were separated by continuous flow FFE (*Table 7* in methods) using the 10 mM Tris – Acetic acid pH 6.5 – 7.5 buffer system with β-DDM supplemented in inlets E2 and E3 (*Table 6*, fourth column, in methods). Fluorescence and absorbance spectroscopy were recorded on the FFE microtiter plates. The separated native complexes were concentrated by centrifugal filtration and further studied by N-PAGE, SDS-PAGE and gel-blot analysis.

Table 14. The Chlorophyll (Chl) a and b concentrations (µg/µl) of the isolated chloroplasts and the solubilised complexes used for the FFE separations are shown. The ratio of the Chl a + b of the solubilised complexes to the isolated chloroplasts was calculated.

	WT isolated chloroplasts	WT solubilised complexes	*crr2* isolated chloroplasts	*crr2* solubilised complexes	*pgr5* isolated chloroplasts	*pgr5* solubilised complexes
Chl a	1.87	1.05	2.81	0.63	1.65	0.63
Chl b	0.70	0.35	1.07	0.23	0.60	0.21
Chl a + b	2.57	1.40	3.88	0.86	2.25	0.84
Percentage of Chl-containing complexes solubilised from isol. chloroplasts	54		22		37	

After harvest and isolation, the number of chloroplasts for each solubilization mix was adjusted according to their Chl a and b concentrations. The percentage of Chl-containing complexes solubilised from *crr2* (22%) was slightly lower than those solubilised from *pgr5* (37%) (*Table 14*). Additionally, both mutants showed considerably less solubilised Chl-containing complexes compared to the WT (54%) (*Table 14*).
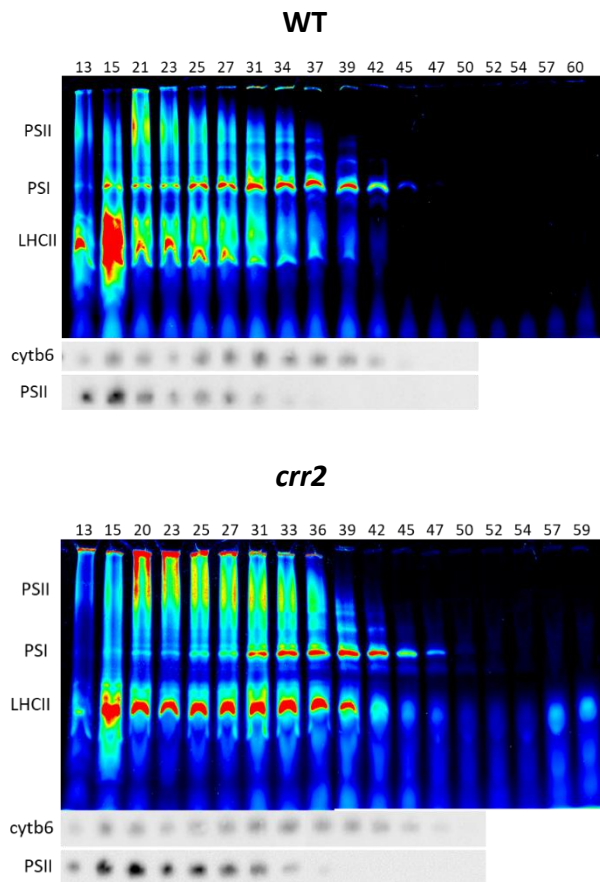
WT

Figure 45. Solubilization of membranes and separation of photosystem complexes by free-flow electrophoresis from *A. thaliana* wild-type (WT), *crr2*, and *pgr5*. Protein complexes were separated by free-flow electrophoresis and fractions collected in microtiter plates (fraction numbers 13-50). Protein complexes were concentrated by Amicon 100K and the retentate separated by native-PAGE (N-PAGE) and fluorescence emission detected at 700 nm when excited at 685 nm. Furthermore, protein composition of complexes was analysed by antibodies directed against Cytochrome b6 (Cytb6f) and D2 (PS II) using gel-blots. Quantification analysis (*Figure 47*) was done on the higher complexes containing PSII, PSI and LHCII; as well as for the gel-blots against Cytb6 and D2.
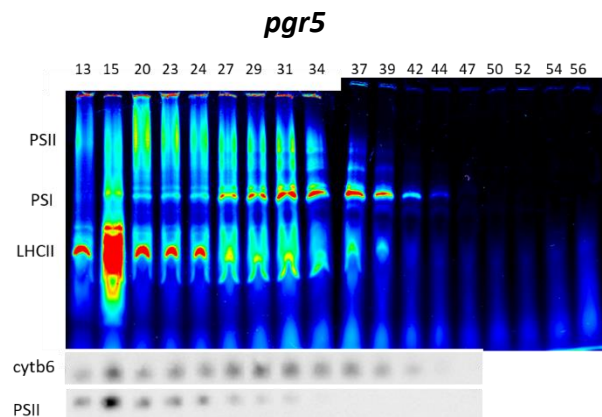
crr2

pgr5

WT

Figure 46. Solubilization of membranes and separation of photosystem complexes by free-flow electrophoresis from *A. thaliana* wild-type (WT), *crr2*, and *pgr5*. Protein complexes were separated by free-flow electrophoresis and fractions collected in microtiter plates (fraction numbers 13-50). Protein complexes were concentrated by Amicon 100K and the retentate separated by SDS-PAGE, the gels were then Coomassie stained.
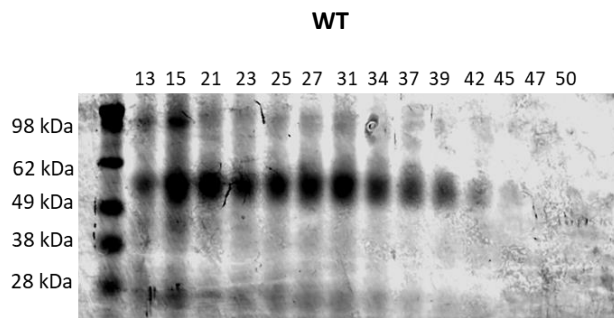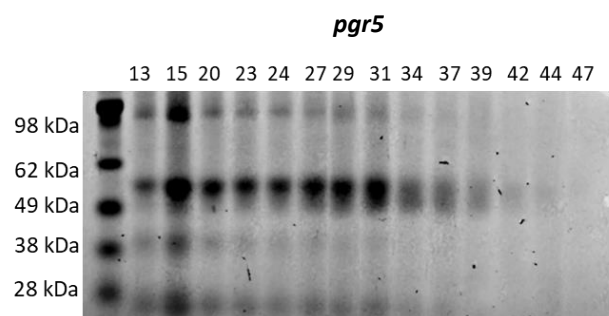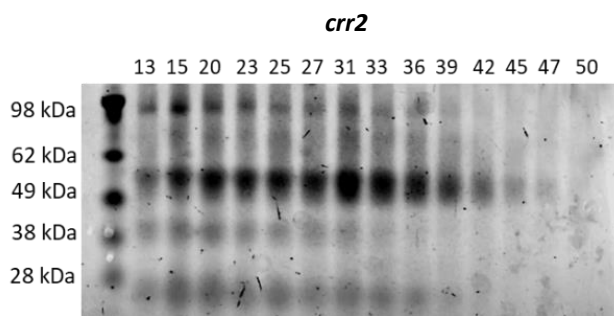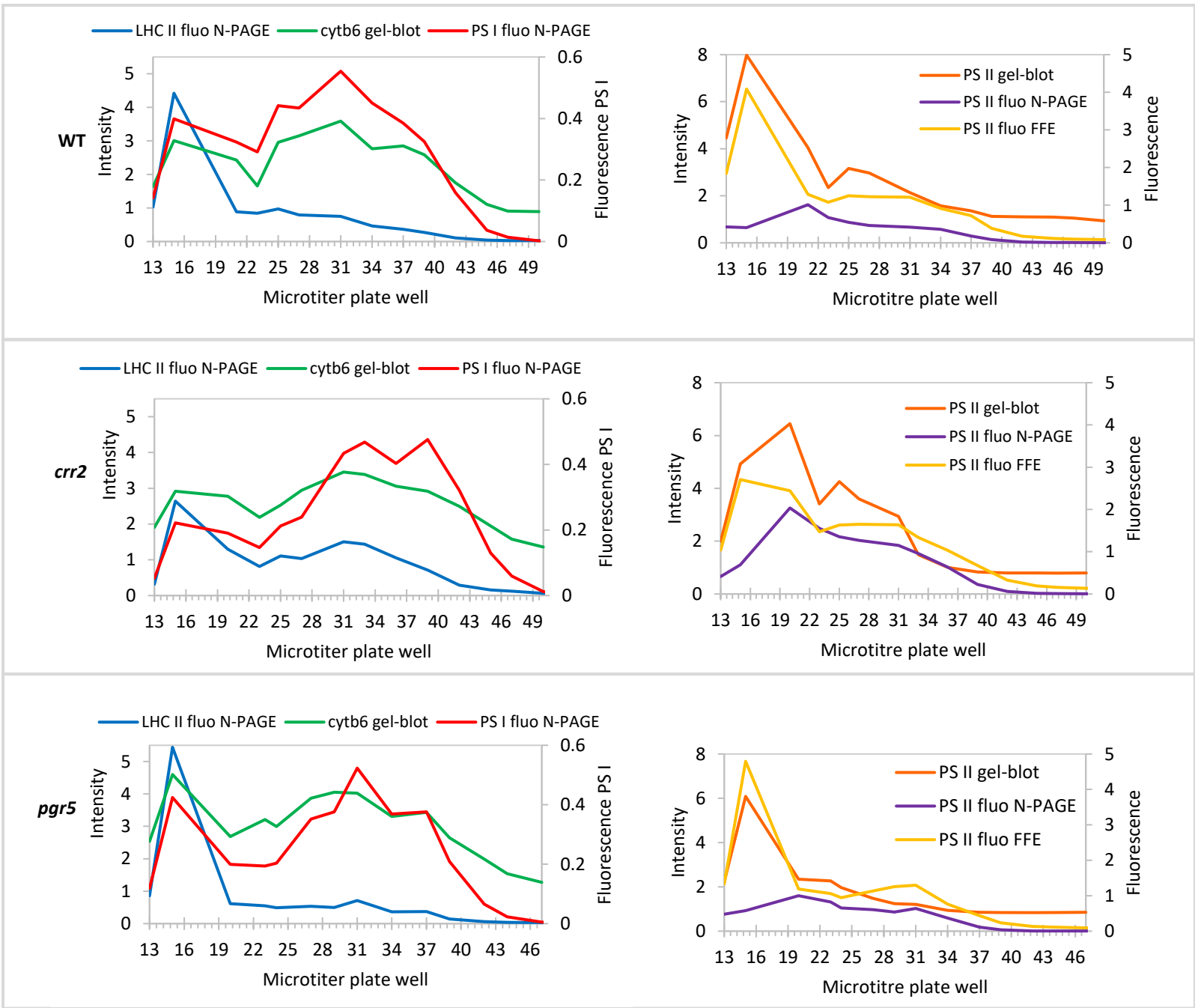
crr2

pgr5

Figure 47. Solubilization of membranes and separation of photosystem complexes by free-flow electrophoresis from *A. thaliana* wild-type (A), crr2 (B), and pgr5 (C). Protein complexes were separated by free-flow electrophoresis and fractions collected in microtiter plates (fraction numbers 13-50). Protein complexes were concentrated by Amicon 100K and the retentate separated by native-PAGE (N-PAGE). Furthermore, protein composition of complexes was analysed by fluorescence at 700 nm (PSI, PSII, LHCII) and 800 nm (PSI) and by antibodies directed against Cytochrome b6 (Cytb6) and D2 (PS II) using gel-blots. Signal intensity (values times 10^6) of protein bands was analysed by fluorescence (fluo) or chemiluminescence (gel-blot) scanning. LHCII fluo quantified from N-PAGE (blue), PSI fluo quantified from N-PAGE (red) and quantification analysis of chemiluminescence intensity from gel blotting for Cytb$_6$ (green) are shown; as well as quantification analysis of chemiluminescence intensity from gel blotting for D2 of PSII (orange), PSII fluo from the higher complexes of the N-PAGE (purple) and PSII from the fluo readings of the FFE microtiter plate at emission 700 nm (yellow). (See *Figure 45*).

Both the quantification data of the N-PAGE separations and gel-blots showed that PSI and Cytb$_6$f had similar distribution patterns in the FFE fractions for the WT and both CEF mutants (*Figure 47*). The peak for PSI and Cytb$_6$f was found at around fraction 31 in all three genotypes and then tapered down on either side as one moved closer towards the electrodes. The intensity changes of the PSI fluorescence signal and the Cytb$_6$ gel-blot signal were noticeably similar along the FFE fractions. In the native-gel it was clear that the *crr2* mutant had more of the higher complexes/aggregates between fractions 20 to 36 than both the WT and *pgr5* mutant (*Figure 45*). Additionally, the *crr2* mutant had considerably more LHCII in fraction 20 to 39 of the N-PAGE separation compared to WT and *pgr5* (*Figure 45*). Additionally, in *crr2* more D2 signal was seen in fractions 20 to 33 relative to WT and *pgr5* (*Figure 45*). WT and *pgr5* showed a more similar distribution of LHCII and D2 than *crr2* (*Figure 45*, gel-blot and N-PAGE). The stained SDS-PAGE showed that in *pgr5* was a lower overall protein concentration compared to *crr2* (*Figure 46*). Both the WT and the mutants showed more PSI monomers, with a molecular weight around 55 kDa in the cathodic region. However, LHC proteins around 25 kDa were detected most strongly in the anodic fractions and decreased towards the cathode. Also, PSI dimers, around 95 kDa for all three were detected most strongly in the anode. Interestingly, in *crr2* a band was detected in the range of 62 – 98 kDa, which was not evident both in the WT or *pgr5* separation (*Figure 46*). This unknown band in *crr2* showed the same intensity pattern as the PSI monomer band with a peak at fraction 31 (*Figure 46*).

To confirm the composition of the higher complexes found in the anodic fractions of the FFE separation, a N-PAGE with varying concentrations of β-DDM detergent added to the sample was run with selected fractions. The N-PAGE sample was run followed by the same sample with two different concentrations of β-DDM. Additionally, in order to investigate if LDS in the cathode buffer caused complexes to fall apart and release LHCII during N-PAGE, N-PAGE without LDS in the cathode buffer was conducted.

Figure 48. Characterisation of higher complexes solubilised from the thylakoid membrane of *A. thaliana* wild-type, *crr2*, and *pgr5*.
Higher complexes, concentrated by centrifugal filtration using Amicon 100K, found in the anodic fractions (21 − 27) of the FFE separation were further separated by N-PAGE with varying detergent treatments. The gel was analysed using both ex 685 nm / em 700 nm and ex 785 nm / em 800 nm for detection of fluorescent bands. All samples were treated with 5 mM digitonin, and additional β-DDM was added at different concentrations (A) 1.25 mM β-DDM and (B) 2.5 mM β-DDM. Quantification analysis is shown in *Figure 49.*

Figure 49. Characterisation of higher complexes solubilised from the thylakoid membrane of *A. thaliana* wild-type (1), *crr2* (2), and *pgr5* (3). Higher complexes, concentrated by centrifugal filtration using Amicon 100K, found in the anodic fractions (21 − 27) of the FFE separation were further separated by N-PAGE with varying detergent treatments. All samples were treated with 5 mM digitonin, and additional β-DDM was added at different concentrations (A) 1.25 mM β-DDM and (B) 2.5 mM β-DDM. Quantification analysis of the fluorescence at 700 nm of the bands in the N-PAGE is shown; higher complexes (blue), PSI (red), LHCII dimer (LHCII_d, in green), LHCII monomer (LHCII_m, in yellow) and free chlorophyll (Chl, in purple). Intensity values shown in millions. (See data *Figure 48*).

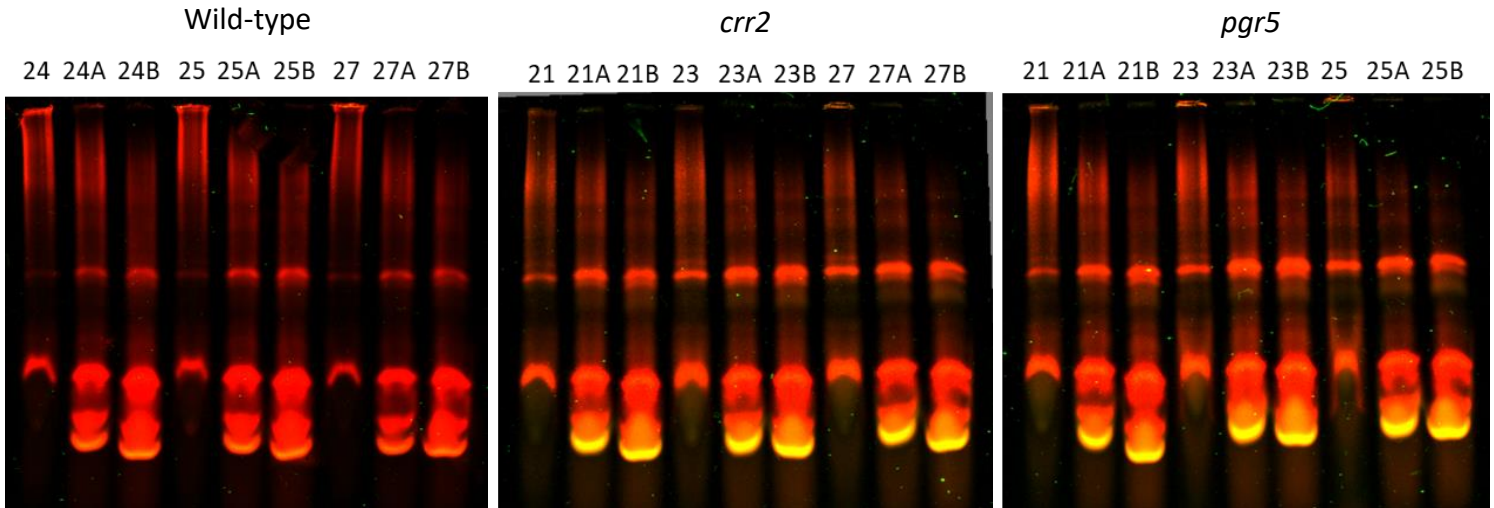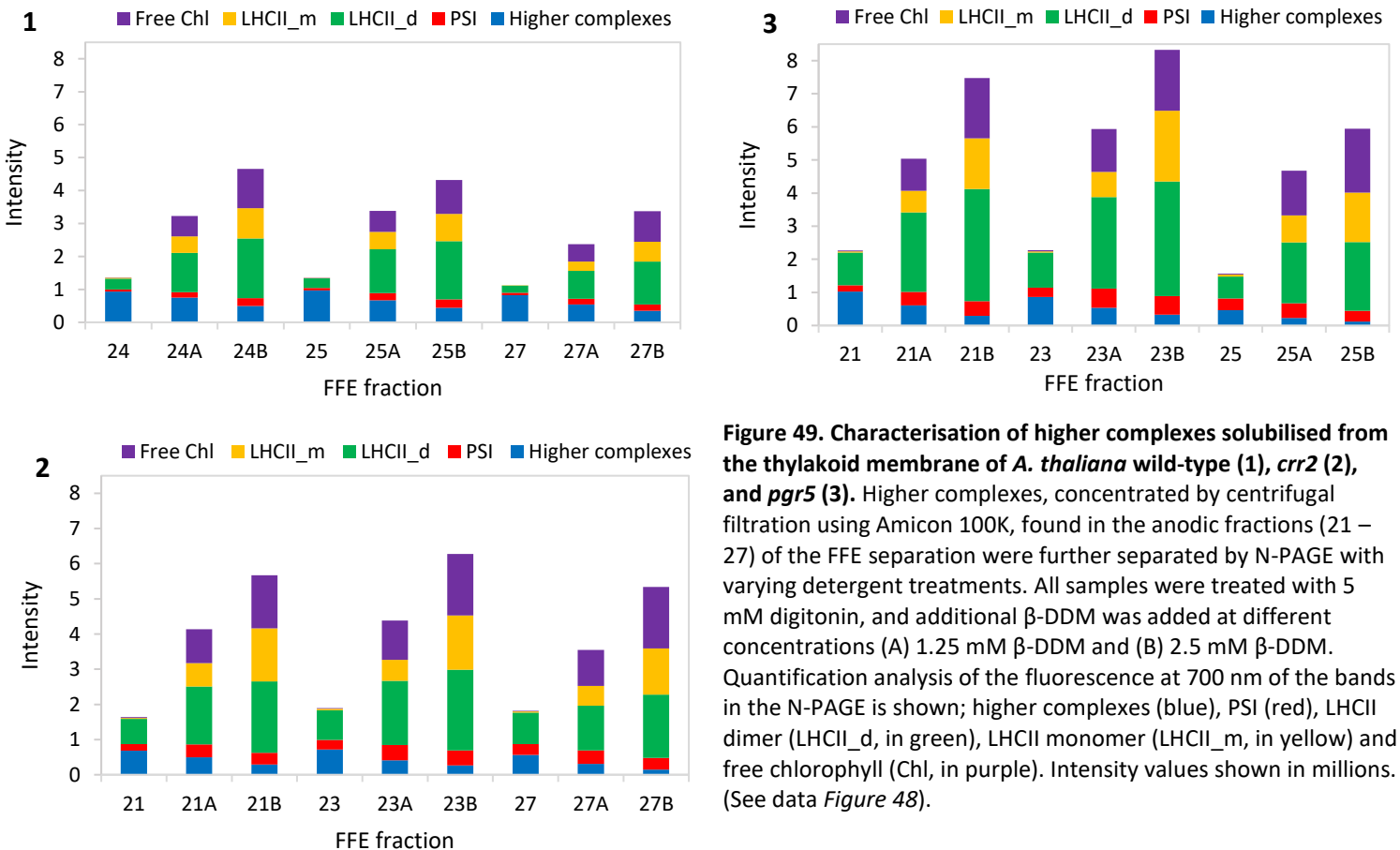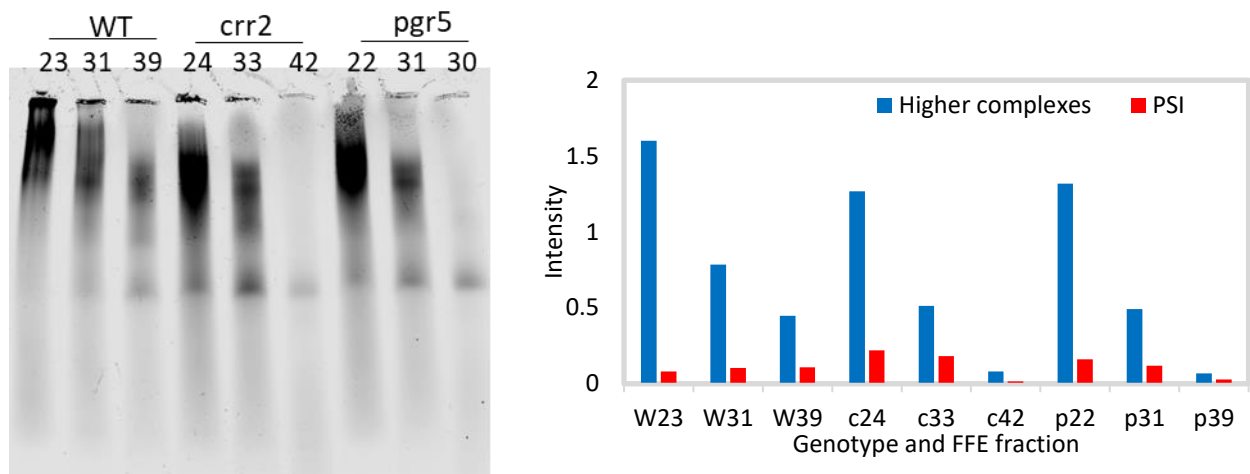**Figure 50. N-PAGE separation of selected membrane complexes without LDS in the cathode buffer. Characterisation of higher complexes solubilised from the thylakoid membrane of *A. thaliana* WT-gli (1), *crr2* (2), and *pgr5* (3).** Complexes concentrated by centrifugal filtration using Amicon 100K are shown for WT-gli (WT/W), *crr2* (c) and *pgr5* (p). Quantification analysis of the fluorescence at ex 685 nm/em 700 nm of the bands in the N-PAGE was shown; higher complexes (blue), PSI (red), and LHCII (green). Intensity values times 10^6.

Analysis of the composition of the higher complexes showed that complexes found in fractions 21 to 27 were the same in the WT and the two CEF mutants (*Figure 48*). Both mutants showed higher fluorescence of these higher complexes compared to the WT, with *pgr5* having the highest fluorescence (*Figure 49*). Noticeably, adding β-DDM caused the LHCII antenna proteins to detach from the main complex. From the N-PAGE separations, it was seen that the higher complexes found in the anodic region of the FFE separation contained mostly PSI and LHCII in its monomeric and dimeric state. Generally, the same complexes were found in all chosen anodic fractions of the three genotypes (*Figure 50*). This was expected, as those fractions showed the same emission spectra when analysing the liquid FFE fractions before N-PAGE (data not shown). However, there were more of the higher complexes in the WT, followed by *pgr5*, with *crr2* having the lowest concentration. Thus, this analysis revealed that higher aggregates were mostly containing complexes of PSI-Cytb$_6$f binding a large ratio of LHC proteins, whereas PSII just was evident in small amounts that could be verified by Western blotting.

Native-gels run without LDS in the cathode buffer showed in all three genotypes very high molecular weight bands at the anode around fraction 22 (*Figure 50*). Interestingly, fractions 31 to 40, that were closer to the cathode, also showed a smaller protein complex slightly below 720 kDa (*Figure 50*). With this gel analysis, it was evident that LHCII antenna were falling off from PSI complexes when LDS was present in the cathode buffer (comparing *Figure 50,* without LDS and *Figure 45*, with LDS). It was further concluded that the disassociation of LHCII from PSI complexes resulted in PSI complexes with

stronger fluorescence emission. This explained why the fluorescence emission recorded in the liquid state FFE sample before being analysed via N-PAGE did not show strong fluorescence emission (data not shown).

Absorbance spectroscopy *in vivo*

Absorbance measurements were performed on whole leaves harvested during the dark and light phases (see methods section), 'Protocol 1' was done first before optimisation and repeating the readings with 'Protocol 2'. In summary, the dark phase corresponded to leaves incubated dark for 16 hrs overnight. In contrast, the light phase corresponded to leaves incubated for a minimum amount of 4 hrs of light.

Figure 51. *In vivo* **absorbance spectroscopy of *A. thaliana* wild-type, *crr2* and *pgr5* leaves (protocol 1).** Leaves were harvested during the dark **(A)** and light **(B)** phases to determine the changes in NADPH levels (340 nm) and other changes caused by light induced reactions. The difference in absorbance for each mutant, *crr2* (green) and *pgr5* (red), is shown relative to wild-type (WT).

The *in vivo* absorbance spectroscopy indicated that from 290 nm to 360 nm and from 400 nm to 460 nm, *pgr5* showed a higher absorbance readings relative to WT than *crr2* (*Figure 52*). This difference was seen for both the dark and light phases (*Figure 51*). Interestingly, *pgr5* absorbed less from 360 nm to 400 nm and even less light between 520 nm to 640 nm than *crr2* relative to WT readings under both the dark and light conditions. In contrast, *crr2* absorbed more light in the same wavelength-regions relative to WT readings under both the dark and light phases. Interestingly, *pgr5* absorbed stronger at 340 nm, where NADPH excited, than *crr2* (*Figure 51*). Generally, the difference seen in the dark and light phases for both mutants were very similar. However, the absorbance levels were slightly amplified during the light phase.

The experiment was repeated, however this time 'Protocol 2' for the absorbance spectroscopy (see methods section) was followed. In this case, ten technical repeats were taken for each leaf. In addition, measured leaves were clamped at the stem to avoid loss of turgor pressure, which made measurements more comparable. In summary, the dark phase corresponded to leaves incubated dark for 16 hrs overnight. In contrast, the light phase corresponded to leaves incubated for a minimum amount of 4 hrs of light.
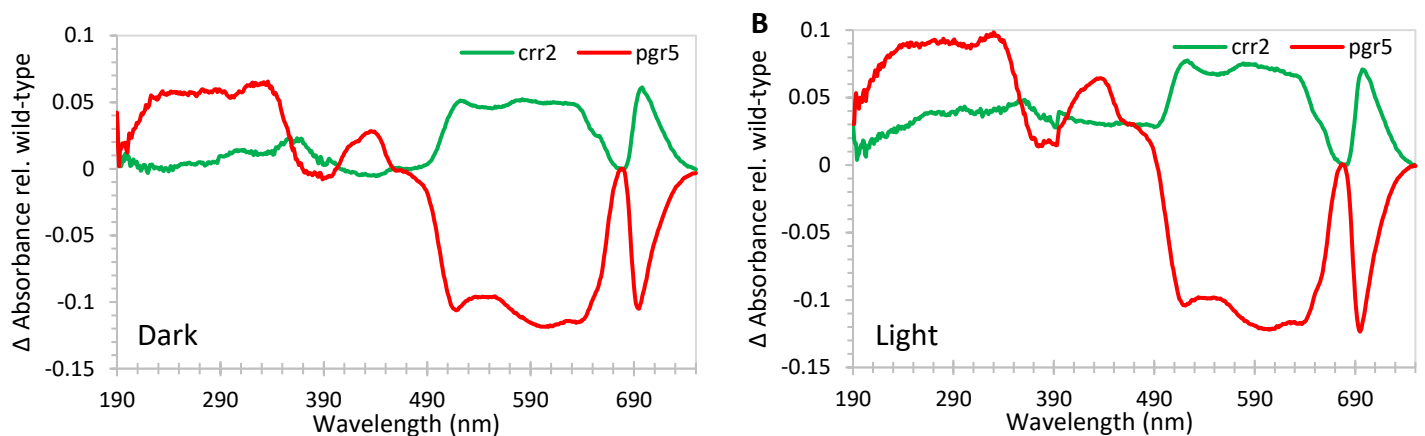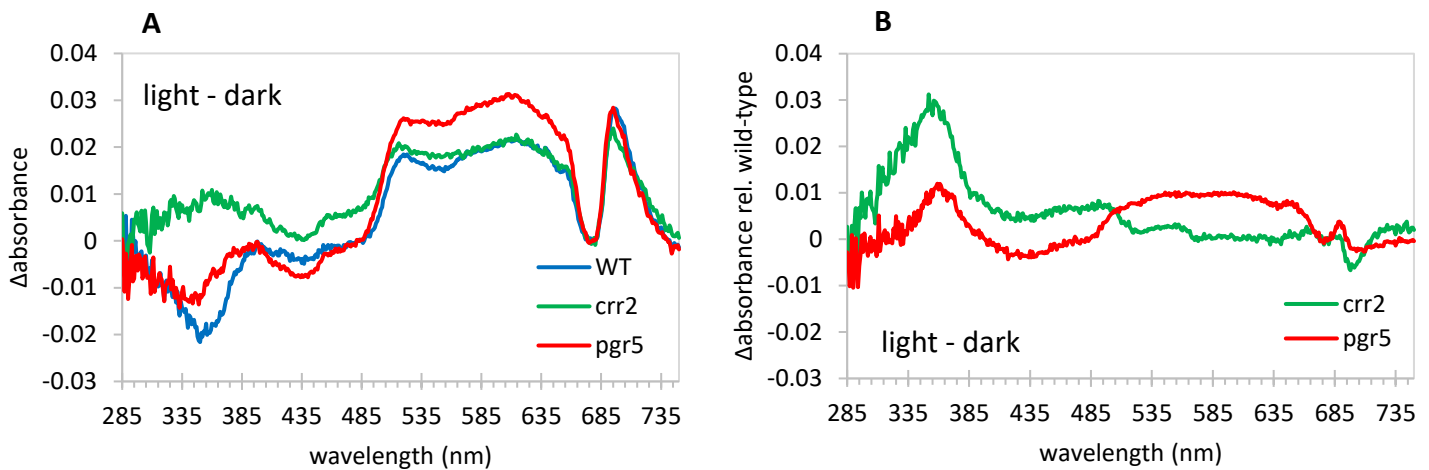

Figure 52. *In vivo* **absorbance spectroscopy of *A. thaliana* WT, *crr2* and *pgr5* leaves (protocol 2).** Leaves were harvested during the dark and light phases to determine the changes in NADPH levels (340 nm) and other changes caused by the light induced reactions. The difference in absorbance between the light and dark phases is shown **(A)** as well as the difference between the light and dark phase for each mutant relative to the WT **(B)**. WT (blue), *crr2* (green) and *pgr5* (red).

In order to determine absorbance changes that are caused by light illumination differential spectra of light and dark readings for WT, *crr2* and *pgr5* as well as *crr2* and *pgr5* relative to WT were calculated (*Figure 52*). *crr2* absorbed strongest from 285 nm to 500 nm, with a peak at 360 nm compared to WT and *pgr5.* However, *pgr5* absorbed higher than WT between 300 nm to 400 nm and stronger than WT and *crr2* between 515 and 660 nm. In contrast, *crr2* and WT showed similar absorbance readings in this region. At 340 nm, the wavelength at which NADPH gets excited, clear differences were observed. The *crr2* mutant absorbed ten-fold stronger than *pgr5*, both relative to WT (*Figure 52*).

As the second approach is more reliable than the first it can be concluded that under light illumination *crr2* has the highest absorbance at 340 nm compared to both WT and *pgr5*. This suggests that the mutant accumulated more NADPH during the light period. However, also *pgr5* leaves stronger absorbed at 340 nm compared to WT leaves. This further proposes that both *crr2* and *pgr5* produced more NADPH than the WT.

Discussion

A first look into the cyclic electron flow mutants: *crr2* and *pgr5*

The initial separation experiments of membrane complexes solubilised from *crr2* and *pgr5* showed in both mutants a prominent fluorescence peak at the anode. The peak was seen when measured at excitation 435 nm/emission 680 nm, excitation 685 nm/emission 700 nm and ex785nm/emission 800nm (*Figure 3*, *Figure 4*, *Figure 10* and *Figure 11*). When exciting at 435 nm and recording emission at 680 nm both PSII, PSI and LHCII can be detected. Furthermore, when exciting at 685 nm and recording the emission at 700 nm, the CP43 and CP47 reaction centre core proteins of PSII show fluorescence. Additionally, if PSI is coupled to LHCII it can absorb and fluoresce at 700 nm; however, it does that to a much lesser extent than PSII. Also, excitation energy could be quenched by PSI efficiently, resulting in a decrease in emission. Consequently, the anodic peak most likely represents PSII complexes. Moreover, with exciting at 785 nm and recording the emission at 800 nm, PSI can be detected. Thus, the cathodic region, that is only seen at the excitation 435 nm/emission 680 nm and excitation 785 nm/emission 800 nm is representative of PSI complexes (*Figure 11* and *Figure 4* respectively).

A cathodic peak was seen in both mutants except for the second separation for *pgr5*, where it was less defined and spread over several fractions (comparing *Figure 4* and *Figure 11*). This could have been caused by the presence of KCl in the first separation, which was seen in *pgr5* only. This is evidence that KCl influenced the native state of protein complexes found in the cathodic region of the *pgr5* separation. Additionally, fluorescence data of the anodic peak showed a clear drift of the *pgr5* complexes towards the anode relative to that of *crr2* (*Figure 3*, *Figure 4*, *Figure 10*). Moreover, the shift was also seen of the cathodic side. Consequently, the entire separation profile was shifted towards the anode in *pgr5.* This suggests that the shift could have been caused by a change in the charge of the separation chamber of the FFE instrument occurring between the separations of the two mutants. However, this was tested and seen to not be the case. Therefore, it could be possible that the difference in mobility of the Chl-binding proteins was caused by a variation in the net-charge state of the complexes. In the absence of the PGR5 protein, when the CRR2 protein was present and the NDH complex fully assembled, complexes were more negatively charged. In contrast, if PGR5 was present and CRR2 was absent and the NDH complex was unable to fully assemble, then fewer negative charges were assembled with the Chl-binding complexes. Furthermore, the anodic shift could also indicate that there were more protein complexes with higher lipid content in *pgr5*.

Next the characteristics of cathodic PSI-rich fractions was analysed. Therefore, the excitation difference spectra was recorded at an emission of 700 nm (*Figure 5*). It was observed that the *crr2* mutant showed a higher emission due to 430 nm excitation. This means that complexes contained more Chl a. Additionally, a fraction with a higher emission due to 480 nm excitation was found. It could be due to the presence of carotenoids and/or Chl b, which absorbs at these wavelengths. Carotenoids are excited at 480 nm and are known to be abundant in LHCII complexes (Liu et al., 2004). Therefore, it can be

deduced that *crr2* has more LHCII in the analysed fractions. This could be a compensatory mechanism for the absence of the NDH complex and subsequent retarded CEF.

The N-PAGE (excitation 685 nm/emission 700 nm) quantification analysis of both experiments confirmed that *crr2* did have more higher complexes compared to *pgr5* in the anodic region (*Figure 7* and *Figure 13*). However, the N-PAGE of the first experiment showed an undefined and diffused separation due to very low concentration of LDS used in the N-PAGE separation (*Figure 6*Figure x). Thus, only the N-PAGE of the second separation was interpreted. The native-gel showed that *pgr5* had more PSI complexes than *crr2* (*Figure 12*). Interestingly, the gel scan at excitation 633 nm/emission 670 nm showed in *crr2* the presence of a PSI complex found in the higher molecular weight region (*Figure 14*). This complex was not seen in *pgr5*. Additionally, there was at this wavelength much higher emission in the *crr2* fractions compared to *pgr5*. The reason for that remains elusive; however, it can be proposed that complexes bind to different amounts and/or forms of antenna proteins. In agreement with this finding, the fluorescence quantification of the native-gel at excitation 685 nm/emission 700 nm showed a difference in LHCII distribution (*Figure 13*). LHCII was distributed as only three maxima in *crr2*, whereas in *prg5* it was distributed as four. Thus, different LHCII protein complexes could be present in the respective mutants.

Detection of the $Cytb_6$ unit within the FFE fractions showed that both mutants showed a clear correlation between the migration of the cathodic PSI complexes and the $Cytb_6$ subunit (comparing *Figure 13* and *Figure 18*). Interestingly, in *pgr5* the $Cytb_6$f migrated more towards the anode (*Figure 18*). Therefore, it can be suggested that the Chl-containing complexes which showed the same shift previously, had co-migrated with $Cytb_6$f. Noticeably, the intensity of $Cytb_6$ in *pgr5* was significantly higher compared to *crr2* (*Figure 18*). Therefore, *pgr5* which contained more PSI complexes seen in the native gel could contain more PSI-$Cytb_6$f complexes than *crr2*.

When stained N-PAGE gel bands of cathodic fractions were analysed, two bands for PSI were seen (*Figure 15*). To determine the difference in composition of these two bands in *pgr5* and *crr2*, MS analysis was done. Data showed that both bands contained in both cases mostly PSI-$Cytb_6$f complexes (*Table 9* and *Table 8*). However, the upper band was found to be enriched in PSI, whereas the lower was enriched in $Cytb_6$f. Interestingly, the amount of peptide hits in *pgr5* was enhanced compared to *crr2*. Furthermore, PSII subunits namely CP47 and CP43, were found in the lower band of both mutants. These proteins are described as inner antennas of PSII. To confirm that it was exclusively antenna protein and not the PSII complexes, gel-blot analysis on the FFE fractions for the PSII D2 subunit was performed. From this analysis, it was evident that PSII was absent in these bands (*Figure 17*). Interestingly, it was shown that *pgr5* contained higher amounts of D2 in the anodic fractions compared to *crr2* (*Figure 18*). Therefore, it is apparent that more PSII complexes were solubilized from *pgr5* than *crr2*. This could be indicative of differences in the thylakoid membrane between the two mutants.

In addition, MS analysis also showed that PsbS was found with PSI-$Cytb_6$f (*Table 8*). Until now, PsbS is known as an energy quencher at PSII (Li et al., 2000). Thus, it can be suggested that it may function similarly at PSI.

In conclusion, both mutants indicated to have a PSI-Cytb$_6$f complex. Furthermore, there is evidence of a structural difference in the thylakoid membrane between the two mutants, which was seen in the amount and composition of PSI as well as higher complexes present in the different mutants.

Optimisation experiments for free flow electrophoresis

<u>β-DDM and digitonin vs. digitonin-only solubilization of the thylakoid membrane</u>

The difference in the solubilization of the thylakoid membrane by using different detergents was assessed. The treatment with 16 mM digitonin was expected to only solubilise the membrane complexes found in the stroma lamellae of the thylakoid membrane whereas the solubilisation with 10 mM digitonin and 94 µM β-DDM was suspected to solubilise a higher amount of stroma lamellae membrane complexes as well as the grana margins. Fluorescence analysis of the liquid FFE fractions at ex678/em700 showed that both solubilization showed a strong anodic peak, a plateau area and a much lower cathodic peak (*Figure 19*). These spectra indicated that both solubilisations resulted in an equal distribution of Chl-containing PSII, PSI and LHCII complexes. However, when β-DDM was added, the complexes showed a stronger shift towards the anode (*Figure 19*). This could suggest that complexes that were solubilized with β-DDM had a higher negative net-charge and thus showed higher mobility.

The analysis of the N-PAGE separation visualized that both treatments led to a difference in PSI distribution. According to a later experiment, it was the addition of LDS during the N-PAGE separation that led to a dissociation of complexes in the native-gel (*Figure 50*). Thus, protein bands in one fraction were regarded as one complex. β-DDM addition resulted in a more uniform distribution of PSI complexes from fraction 51 to 56, with a clear increase in intensity in fractions 51 to 57. In contrast, the treatment with only digitonin led to a very weak fluorescence intensity of PSI bands between fractions 51 to 57, and instead caused a stronger emission between fractions 59 to 65 (*Figure 20*). Interestingly, PSI bands closer to the cathode showed, under both treatments, a second band which moved at a lower molecular weight area. This band was increased in the solubilisation with only digitonin. In addition, when using only digitonin, gel analysis indicated that this PSI-Cytb$_6$f complexes were still connected to LHCII complexes. This observation suggests that both treatments solubilized PSI-Cytb$_6$f complexes to a different extent; and that digitonin only separated PSI-Cytb$_6$f-LHCII complexes. Furthermore, it can be assumed that the addition of Cytb$_6$f to PSI resulted in a more negative net-charge of the complex, which caused a slower migration in the FFE separation. Moreover, in the case where only digitonin was used, an increased fluorescence signal of higher complexes was quantified at the anodic side than when β-DDM was used (*Figure 21*). Interestingly, a decreased fluorescence of higher complexes in the anode when β-DDM was applied further resulted in a rise in LHCII and PSI fluorescence in fractions 51 to 57. Therefore, the addition of β-DDM appeared to solubilize more PSI-LHC complexes from higher complexes. In contrast, the treatment with only digitonin decreased the amount of PSI-LHCII solubilized from higher complexes and kept the higher complexes intact. In addition, native-gel analysis at excitation 785 nm/emission 800 nm indicated that free Chl micelles accumulated at a lower molecular weight area under both conditions; however,

increased in the solubilisation with only digitonin. The assumption that this band is free Chl is derived from the observation that Chl in detergent micelles leads to a long-wavelength shift of fluorescence (Gottstein and Scheer, 1983).

In summary, the experiment suggested that solubilization with only digitonin resulted in a gentler solubilization process that yielded more higher complexes and more intact PSI-Cytb$_6$f-LHCII complexes. Consequently, in further experiments thylakoid membranes were solubilized with only digitonin.

Comparing buffer systems: HiBa – Bistris with two pH steps at pH 4.9 and pH 6.9 versus Tris – Acetic acid ranging from pH 5 to pH 7

Different buffer systems used for FFE separations showed that the buffer components appeared to affect the movement of higher complexes/aggregates found in the anodic and cathodic fractions (*Figure 23*). This was caused by the fact that the molarity barrier in the Hiba – Bistris system slowed down complexes when the Tris concentration in the buffers increased from 10 mM to 20 mM. Additionally, the separation was influenced by the difference in pH steps that was used (two steps pH 4.9 and pH6.9 in the Hiba – Bistris system and a wide range of pH steps between pH 5 and pH 7 in the Tris – Acetic acid system). Interestingly, both N-PAGE analyses showed that protein complexes fluoresce stronger in the gel than when analysed in the liquid state (comparing *Figure 23* with *Figure 24*). This is most likely caused by the presence of LDS in the cathode buffer and its disassociating effect it has on protein complexes (*Figure 50*), leading to protein-interaction changes and detachment of antenna proteins as well as other unknown changes, which evidently increases the proteins fluorescence tremendously. It was shown by others that LHCIIs can form a quenched state with low fluorescence, whereas free LHCII increased its fluorescence lifetime significantly (Adams et al., 2018).

Most interestingly, the mobility of PSI and Cytb$_6$f correlated best in both buffer systems when comparing the Western blot analysis with PSI complexes in the N-PAGE separation of the FFE fractions (comparing *Figure 25* with *Figure 24*). This strongly indicates that PSI and Cytb$_6$f form a complex, as was suggested by (Yadav et al., 2017). This suggests that both buffer systems enable the isolating of the PSI-Cytb$_6$f complex. However, the bigger pH difference in the separation buffer of the Hiba – Bistris system showed to lead to a concentration of PSI-Cytb$_6$f complexes in fewer fractions (*Figure 25*Figure 25). This could mean that a smaller range of different PSI-Cytb$_6$f complexes can be accessed compared to the wider separation reached in the Tris – Acetic acid system. The wider PSI-Cytb$_6$f profile that was observed in the Tris – Acetic acid system suggests the existence of many different PSI-Cytb$_6$f complexes (*Figure 25*). Their difference in mobility during the FFE run could be influenced through having different binding partners such as different antenna complexes and/or auxiliary proteins. Additionally, it can be suggested that a very good correlation between the distribution of PSI bands and LHC bands can be determined with both separation buffer systems (*Figure 24*). However, N-PAGE analysis showed that bands at a lower molecular weight area that contained detergent solubilized free Chl, which showed fluorescence when detected at excitation 785 nm/emission 800 nm has to be subtracted from the LHC band signal (*Figure 24*). Additionally, the 630 nm emission analysis appeared to be an excellent tool to determine the distribution of free Chl micelles (*Figure 26*).

Overall, the data showed that there was a wider range of PSI-Cytb$_6$f complexes separated in the Tris-Acetic acid system. For this reason, the Tris – Acetic acid buffer system was selected for further FFE experiments.

Absence of β-DDM from separation media

Additionally, the absence of β-DDM in the FFE separation media and effect on protein complexes was studied. The N-PAGE separation without β-DDM with N-PAGE separations from previous experiments was compared. It was found that β-DDM does not influence the integrity, and thus fluorescence levels, of Chl-containing protein complexes (comparing *Figure 27* and *Figure 24*, B). However, the choice of only two pH steps of pH 6.5 and pH 7 in this experiment led to PSI complexes having migrated faster towards the anode than in the previous experiment, where are range pH steps between pH 5 and pH 7 were used (comparing *Figure 27* and *Figure 24*, B). Additionally, the increase in mobility resulted in a loss of anodic complexes (*Figure 27*). Thus, N-PAGE analysis revealed that the FFE separation resulted in different PSI-antenna complexes distributed across pH 6.5 (*Figure 27*). It was evident that higher PSI complexes were moving towards the anode. On the cathodic side, an accumulation of lower molecular weight PSI complexes was observed.

The absence of detergent in the separation media could have caused the increase in higher complexes at the anode and higher complexes/aggregates that were visible at the cathodic side. In comparison, those aggregates not able to enter the gel pocket were not seen in the cathodic fractions before (comparing *Figure 27* and *Figure 24*, B). Additionally, the absence of β-DDM could have resulted in a higher concentration of PSI complexes at the cathode by influencing their intrinsic charge and, subsequently, their mobility. This suggests that the absence of detergent caused a weaker solubilisation of the membrane, resulting in more higher complexes, and on the other hand could have possibly caused proteins to aggregate. Again, free Chl micelles in the native-gel analysis excitation 785 nm/emission 800 nm were found in the very anodic fractions (*Figure 29*). However, those free Chl micelles did not overlay completely with the fluorescence peak of PSI complexes (*Figure 29*). This indicated that the separation time was an effective parameter to direct separation of Chl-containing protein fractions.

In addition, DLS measurements were performed on selected anodic fractions, which showed a high fluorescent PSI complex in N-PAGE analysis (*Figure 27*). Those fractions indicated that the PSI complexes had a diameter of 18.2 nm (*Figure 30*). This suggests again that PSI found in the anodic fractions is in complex with Cytb$_6$f (Yadav et al., 2017). Thus, the absence of β-DDM did not influence the complexes' integrity. Therefore, in further experiments β-DDM was only supplemented to anodic separation buffers E2 and E3, in order to avoid aggregation, and was excluded from the other buffers.

Presence/absence of KCl in solubilization and/or FFE separation

Next, it was tested if the integrity of the complexes was affected by the supplementation of KCl during solubilization and FFE separation. It was seen that in the presence of KCl, more Chl-containing

complexes, with nearly two-fold more Chl content, were solubilised (*Table 10*). This could be caused by KCl's characteristic to affect the stability of the thylakoid membrane during the solubilisation procedure. Thereby the solubilisation of more membrane complexes could have been facilitated.

Furthermore, fluorescence analysis of FFE fractions at excitation 435 nm/emission 680 nm showed that by choosing a pH of 7.5 and pH7, complexes revealed a slower mobility in the cathodic part of the separation (*Figure 31*). Additionally, it was clear that in the presence of KCl, fluorescence emission was enhanced closer to the cathode (*Figure 31*). This observation suggested that the mobility of the protein complexes was lower when KCl was supplemented. This could have resulted from an increase in conductivity of the medium, which decreased the mobility of charged complexes. However, it could not be excluded that in the presence of KCl a stronger emission of fluorescence was caused by an increase in the concentration of non-charged Chl-containing proteins or accumulation of free Chl. In contrast, in the absence of KCl, an increase in fluorescence was seen closer towards the anode. This suggests that protein complexes in the absence of KCl showed a higher mobility. During N-PAGE analysis it was confirmed that in the presence of KCl less PSI-LHCII fluorescence was shown towards the cathode compared to the separation in absence of KCl (*Figure 33* and quantification *Figure 34*). Therefore, this gave a strong indication that the cathodic peak in the fluorescence measurement was caused by free Chl micelles only (*Figure 33*). In contrast, in the absence of KCl much more PSI-LHCII fluorescence was found towards the cathode (*Figure 33* and quantification *Figure 34*). In addition, PSI complexes towards the anode showed more higher complexes of PSI-LHCII (*Figure 33* and quantification *Figure 34*). Therefore, it is assumed that the addition of KCl in solubilization and FFE separation contributed to the solubilization of free Chl in the form of detergent-micelle vesicles that are neutral in net charge state. These detergent micelles could, due to their neutrality, be detected at the FFE fraction number where the sample was injected. However, in the absence of KCl, Chl appeared to remain bound to the charged protein complexes and thus were separated with the other solubilized complexes in the FFE separation. Chl molecules bound to PSI therefore showed less fluorescence as its absorbed energy was most likely quenched by the transfer to a reaction centre and/or released as heat.

Additionally, the rotational diameter of PSI-Cytb$_6$f-LHC complexes was investigated with DLS measurements. It was seen that in the presence of KCl the analysed complex had a diameter of 18.2 nm, whereas a more anodic fraction in the absence of KCl showed a diameter of 21 nm (*Figure 32*). This could suggest that in the absence of KCl more PSI-Cytb$_6$f complexes coupled to LHC proteins were present. Therefore, it was concluded that KCl in the solubilization and/or FFE separation can release Chls of LHC proteins that are functionally coupled to PSI molecules. This could further have a strong negative impact on the binding of LHC proteins to PSI complexes. During solubilization, KCl could saturate cationic amino acid side chains on the surface of the membrane protein complexes. Through this, proteins could be neutralized and consequently the binding of these proteins to the complex could be destabilized. During the separation by FFE, these proteins would then show a decreased mobility and accumulate near the cathode. However, the addition of KCl during the FFE separation could also saturate the same type of proteins without having any influence on the stability of the

assembly state of the protein complex. This charge saturation could also change the negativity of the holoprotein complexes and thus make them less mobile.

However, a clear differentiation between the effect of KCl on differential solubilization and FFE separation in the same experiment was not possible.

To test the influence of KCl during FFE separation only, the thylakoid membrane was solubilized in the absence of KCl and then separated in the presence and absence of KCl. The fluorescence at excitation 685 nm/emission 700 nm analysis of the FFE fractions showed that in the presence of KCl in the FFE separation complexes showed a stronger shift towards the anode than in the absence of KCl (*Figure 35*). Additionally, the presence of KCl resulted in a four times higher fluorescence emission of the cathodic peak compared to the FFE separation without KCl (*Figure 35*). N-PAGE analysis at excitation 785 nm/emission 800 nm of these fractions revealed that in the presence of KCl a much stronger amount of Chl micelles accumulated at the cathode (*Figure 36*). It was now very clear, that the addition of KCl in the separation caused a rise in the accumulation of free Chl micelles, which arrested at the injection site (*Figure 36*). Additionally, in the presence of KCl, a decrease in the fluorescence signal of PSI, higher complexes, LHCII trimers and monomers was detected compared to the FFE separation without KCl (*Figure 36* and quantification *Figure 37*). Moreover, the analysis of the distribution of complexes containing Cytb$_6$f showed that the presence of KCl resulted in more Cytb$_6$f-containg complexes at the cathode (*Figure 38* and quantification *Figure 39*). In contrast, the separation without KCl led to a more spread distribution of Cytb$_6$f-complexes towards the anode (*Figure 38* and quantification *Figure 39*). The cathodic accumulation in the presence of KCl could have been caused by the salt's capability to bind complexes and neutralize their state of charge. When their charge gets neutralised by the binding of KCl, protein complexes would be slowed down. Thus, it was assumed that the addition of KCl also affected the charge and consequently the separation of protein complexes.

From this experiment it was evident that the addition of KCl in the separation buffer used for injection favours the accumulation of Chl towards the cathode. Therefore, it can be concluded that in the presence of KCl Chls are decoupling more strongly from PSI-Cytb$_6$f-LHC complexes and then accumulate inside charge-neutral detergent micelles. It must be considered that an increase in Chl release from proteins leading to a change in charge could have also affected complexes' native states. Therefore, it was decided to not supplement any KCl – neither during solubilization nor during separation – to future FFE experiments.

In addition, the N-PAGE analysis of FFE separations under both conditions showed that PSI and PSI-LHCII coexisted (*Figure 36*). Interestingly, under both conditions less PSI fluorescence was seen towards the anode, whereas the fluorescence of LHCII complexes decreased only slightly but stayed rather constant (*Figure 36*). In accordance to a later experiment, the addition of LDS during the N-PAGE separation resulted in the dissociation of complexes in the native-gel (*Figure 50*). Thus, protein bands in one fraction were regarded as one complex. Therefore, it was suggested that the FFE separation was resulting in the separation of PSI complexes with different ratios of PSI to LHCII proteins.

N-PAGE analysis showed that the ratio of PSI to LHCII decreased from cathode towards the anode. Surprisingly, a strong difference was seen in the fluorescence imaging of Chl-containing complexes in the N-PAGE gel compared to the fluorescence data measured for the liquid state of the FFE fractions in the microtiter plate (comparing *Figure 35* and *Figure 36*). A high fluorescence signal in the N-PAGE corresponded to a low fluorescence signal in the liquid FFE state and vice versa. In the cathodic region of the FFE separation, this difference could be attributed to the effect of the LDS added to the cathode buffer used in the N-PAGE separation. It was shown in another experiment that LDS disrupts protein interactions, leading to dissection of complexes (*Figure 50*) and therefore leads to the significant increase in fluorescence found in N-PAGE analysis compared to low fluorescence found the liquid FFE fraction (*Figure 35* and *Figure 36*). Thus, these protein interactions are required to quench fluorescence.

The absence of more PSI and LHCII complexes on the native-gel at the anodic side (*Figure 36*) could have been due to a very strong interaction of large PSI-LHCII complex patches that could not be disrupted during N-PAGE. In agreement with this, protein patches that did not enter the gel but accumulated in the gel pockets increased at the anodic side. Those patches strongly fluoresced in both the native-gel and liquid FFE analysis (*Figure 35* and *Figure 36*). This indicated that total increase in fluorescence determined upon FFE separation of Chl-containing protein complexes correlated to an increase in very large PSI and LHCII protein complexes towards the anode in the N-PAGE separation. This observation suggests that those anodic patches of complexes fluoresce stronger in case one photosystem reaction centre is connected to a higher amount of antenna complexes. In contrast, the low fluorescence in the FFE fraction on the cathode implies that when LHCII is bound to PSI, fluorescence of LHCII is quenched for complexes containing a higher number of PSI relative to the number of LHCII. This explanation further implies that excitation energy that is absorbed by LHCII can be transferred to a PSI reaction centre in order to be eliminated. Alternatively, other proteins may be associated with PSI to quench the excited LHCII states. If this is the case, it could be concluded that FFE enabled a separation of PSI complexes associated with a differential amount of LHCII complexes and/or other auxiliary proteins. Interestingly, it was seen that cathodic PSI complex also binds higher amounts of Cytb$_6$f (comparing *Figure 37* and *Figure 39*), which could have an important impact on the complexes ability to use and destroy incoming light quanta.

In summary, it can be proposed that at the cathode, PSI complexes are separated that are connected to a low number of LHCII complexes per PSI, whereas towards the anode in FFE, PSI complexes with an increasing number of LHCII complexes per PSI complex are found.

But why should there exist different types of PSI-LHC complexes? Generally, all quanta that are harvested by the functionally linked LHCII molecules can contribute to charge separation at a reaction centre. A high light intensity translates into a high number of quanta per square area and time. In such a condition, in which light harvesting is leading to photochemistry, fluorescence will be quenched by an access of PSI molecules. This type of non-fluorescent PSI-LHCII complexes were identified in the cathodic region upon FFE separation. Here, a low number of LHCII complexes was identified per reaction centre. According to the model, this would imply that the number of PSI complexes separated

towards the cathode of FFE are high at an environmental high light state. In contrast, when the light intensity is low, a higher number of quanta can be harvested by a high number of LHCII complexes per a limited number of PSI. This complex was separated towards the anode and results at low light levels to an increased light-harvesting activity which leads to optimal photochemistry. However, when higher light is reaching these PSI-(LHCII)$_n$ complexes, the complexes reach a point of functional saturation of the reaction centre at which the functional capacity of PSI molecules to increase electron flow is limited by their turnover rate. This may either be a saturation of electron flow at the donor and/or acceptor sides. At high light quantity, the lower number of PSI connected to many LHCII can be regarded as functionally saturated. Any further increase of light quanta should now lead to an increase in fluorescence of those quanta that can't be delivered to the reaction centre. Therefore, fluorescence emission was high for the high molecular weight PSI complexes at the anodic FFE fractions. It could be nature's strategy to protect PSI from over-reduction and potential photodamage. Consequently, it is predicted that under natural growth conditions the concentration of these anodic PSI-LHCII complexes is increased at decreased light intensity in order to upregulate energy transfer and modulate electron flow. On the other hand, cathodic PSI-LHCII complexes with a smaller amount of antenna are increased at enhanced light intensity in order to quench excess light energy and modulate optimal photochemistry. According to this principle, it could be that the number of LHCII complexes that are associated per reaction centre are an effective means to regulate electron flow. Whether the number of LHCII complexes that are associated with PSI follows a characteristic pattern or whether regulation leads to a continuous change in the number of LHCII complexes requires further clarification.

The effect of solubilising from frozen chloroplasts compared to fresh chloroplasts

It is evident that freezing of chloroplasts enables the solubilisation of more Chl-containing complexes (*Table 11*). This may be caused by freezing weakening the integrity of the lipid membrane, thereby allowing the digitonin to access and solubilise more of the thylakoid stroma lamella membrane complexes. A two-fold increase was seen in the emission intensities of the fluorescence spectroscopy data between the frozen and fresh samples (*Figure 40* and *Figure 41*). This can be attributed to this difference in the concentration of the solubilised proteins, which was also two-fold higher in the frozen sample. It was clear that the freezing of the chloroplasts did not affect the composition of the native complexes. Both samples were found to have PSI with LHCII separated during FFE and subsequent N-PAGE (*Figure 43*). Furthermore, both separations resulted in free Chl micelles found near the cathode. However, this was enriched in the fresh sample. More LHCII was found in the fresh sample's anodic FFE fractions after N-PAGE. This may be indicative that antenna proteins have been lost due to freezing of the chloroplasts.

The migration of PSI in the frozen sample compared to the fresh sample clearly showed that PSI was more negatively charged in the frozen sample (*Figure 43*). The shift in the PSI peak may possible have been due to a loss of lipids as a result of freezing. The loss of lipids would have allowed for more binding sites for the ions present in the separation media. If this was the case, it would have resulted in a greater negative net charge of the PSI complexes, causing the complexes to migrate faster than in the

case of the fresh sample. It is alternatively speculated that the PSI complexes had more lipids associated with them. This would have increased their negative net charge state, as it is known that lipids are negatively charged. Freezing of chloroplasts may reduce membrane fluidity, thereby resulting in clumps of un-solubilised thylakoid membranes containing PSI complexes. However, the DLS measurements to determine the size of the complexes in the fresh sample also showed fractions of un-solubilised membrane complexes (*Table 12*). Thus, this may have just been enriched in the frozen sample.

The anodic peak seen in the emission data for both separations appears to be free antenna or could be a lot of antenna bound to relatively little PSI (*Figure 40* and *Figure 41*). Where the emission is much lower, the absorbance peak is most likely PSI-LHCII complexes with a lower ratio to PSI, thus there could be fluorescence quenching. In the cathodic region, free Chl micelles were found, so it seems that the lysis of intact chloroplasts osmotically with TMK increases the amount of free Chl. Also, it appeared that free Chl showed higher fluorescence in fresh samples than that of the frozen sample. Thus, it is suggested that Chl molecules from fresh chloroplasts are in a more intact state.

In conclusion, freezing of chloroplasts did not affect the composition of the native complexes. However, differences were seen in the migration during FFE of the native complexes from the fresh and frozen samples. In order to keep the studied complexes as native as possible, it was decided to continue experimentation using fresh chloroplasts.

Zeta potential measurements were done to determine the net charge of the complexes solubilised from the fresh chloroplasts and separated by FFE (Table 13). As the readings were very noisy and inconsistent, it was suspected that it was due to having too low a concentration of protein complexes in the sample, therefore it was not possible to say with certainty from this data what the net charges of the complexes were. Size measurements using DLS indicated that complexes have a varied size and confirms the importance of using FFE for these separation of membrane patches.

Membrane complexes of the cyclic electron flow mutants: *crr2* and *pgr5*

It was evident that if the complexes in the mutants were the same as the WT in terms of Chl concentration, then fewer complexes were solubilised from the two CEF mutants compared to the WT. Furthermore, fewer complexes were solubilised from the *crr2* mutant than from *pgr5* (*Table 14*). This could be indicative of a difference in the structure of the thylakoid membrane of the mutants. One hypothesis could be that the mutants remodel the thylakoid membrane structure to compensate for the retarded CEF.

As seen before, there was co-migration of PSI with $Cytb_6f$. This was evident from the N-PAGE quantification and the gel-blot quantification (*Figure 47*). From this data, it was seen that most of the PSI-$Cytb_6f$ complexes were found closer to the cathode, which means that these complexes were less charged than the higher complexes found in the anodic region. The PSI-$Cytb_6f$ complexes showed the same migration trends in all three genotypes. Evidently, the absence of PGR5 (*pgr5)* or the NDH

complex (*crr2*) did not affect the formation of the PSI-Cytb$_6$f complex. It can be suggested that the PSI-Cytb$_6$f complex is a vital complex in photosynthesis and is not altered to compensate for the CEF mutations.

Interestingly, *crr2* showed to have more of the higher molecular weight region complexes compared to *pgr5* and the WT (*Figure 45*). This difference was seen even though fewer Chl-containing complexes were solubilised from *crr2.* Furthermore, *crr2* showed to have more LHCII closer towards the cathodic region than *pgr5* and WT (*Figure 45*). The LHCII complexes in *crr2* thus have a lower charge state and are more abundant than those found in WT and *pgr5.* From this, as suggested in the preliminary separations, it can be deduced that the thylakoid membrane structure of *crr2* differs from *pgr5* and the WT. In support of this conclusion, it was found that *crr2* had more PSII in the stroma thylakoids compared to *pgr5* and the WT (*Figure 45* and *Figure 47*). It is known that the absence of the NDH complex leads to retarded CEF (Shikanai, 2016). The increase in PSII seen in *crr2* could be indicative of a need for more LEF in the stroma thylakoids to compensate for this retarded CEF. When considering the before mentioned hypothesis about separating PSI-(LHCII)$_n$ complexes on the anodic side, it can be seen that *crr2* increased these complexes relative to WT and *pgr5*. This further suggests, that *crr2* adapts to growth light conditions by increasing these complexes which have been suggested to be important under low light conditions (Ueda et al., 2012; Yamori et al., 2011). Consistent with this hypothesis it has been shown that at low light conditions the NDH complex is needed to reduce the electron transport chain for efficient photochemistry.

The SDS-PAGE analysis of the FFE fractions revealed a band in the range of 62 to 98 kDa that was only found in *crr2* (*Figure 46*)*.* The appearance of this protein could have been due to a concentration variance between the three genotypes. Alternatively, this could be a protein that formed part of the native-complexes in the N-PAGE. It is possible that the NDH complex inhibits/prevents the binding of this protein to the holocomplex, or that it is not needed in the presence of the NDH complex. If so, when NDH is absent, as is the case in *crr2*, this protein could bind and migrate with the larger PSI complexes in the FFE. Moreover, it may be that *crr2* requires this protein in order to form the higher molecular weight region complexes found to be enriched relative to WT. The distribution of this protein followed that of the PSI monomers, so it could be that this protein is in complex with PSI. However, further analysis is needed in order to determine what this protein is and if it is in fact in complex with PSI.

The mutants and the WT were found to have the same higher molecular weight region complexes in the anodic region (*Figure 48*). Noticeably, the addition of β-DDM to these higher complexes resulted in the detachment of LHCII proteins. This revealed that these higher complexes contained PSI and different states of LHCII. The composition of these complexes did not differ between the genotypes. However, it was seen that the complexes from the mutants showed higher fluorescence (*Figure 48*). This could mean that the mutants contained more of the higher complexes than the WT. This once again supports the hypothesis that the mutants have structural differences in the thylakoid membrane compared to WT.

It was clear that these higher complexes contained PSI-Cytb$_6$f with many LHC proteins and very little PSII. It was confirmed by N-PAGE done without LDS in the running buffer that theses complexes were falling apart into individual components because of the detergent (*Figure 50*). In conclusion, the higher complexes consisted of PSI-Cytb$_6$f with large amounts of LHC proteins bound and very little PSII.

NADPH measurement in leaves of *crr2* and *pgr5*

NADPH is the terminal electron acceptor for LEF and absorbs at 340 nm. NADPH levels can thus be used as a relative indication of the amount of LEF occurring in a section of the leaf. However, it must be brought into consideration that *in vivo* absorbance measurements do not allow for the differentiation of NADPH absorption and absorption due to other cell components. By acquiring dark phase and light phase measurements it became more clear which differences in absorbance were due only to light changes. Only the data from the second data set were interpreted. This was due to the second readings being more consistent as the effect of the turgor pressure changes was eliminated. After light incubation both mutants showed higher absorbance at 340 nm relative to WT (*Figure 52*, A). This observation could indicate that both mutants were doing more LEF than the WT. Moreover, *crr2* showed higher absorbance at 340 nm relative to *pgr5* and was consequently deemed to be performing more LEF. If this was the case, that could mean that the *crr2* was doing more LEF to compensate for the absence of the NDH complex and that this compensation was not as drastic in the absence of the PGR5 protein.

However, to confirm these results, further spectroscopy would need to be done – such as pulse modulated spectroscopy on isolated chloroplasts (*in vitro*) to determine total NADPH levels. The concentration of the chloroplasts would need to be equal, as it is not possible to rely on Chl concentration as the complexes differ in their antenna composition.

A difference in the absorbance for *pgr5* relative to WT was seen in the range of 500 nm to 665 nm (*Figure 52*, B). In this range, *pgr5* was seen to have a higher absorbance than *crr2* and the WT. Here, WT and *crr2* were found to have very similar absorbance readings. It is not certain what this difference in absorbance was caused by, but it could have been a change in carotenoid concentrations to attempt to provide a way to dissipate excess electrons. Alternatively, it could be evidence of a different mechanism for *pgr5* to cope with the surplus light energy. Therefore, the absence of PGR5 lead to increased absorbance in the range of 500 nm to 665 nm. It may be proposed that in the absence of PGR5, complexes with increased absorbance at this range compensate for photoprotection. An increase in photoprotection that is needed in the absence of PGR5 is supported by the finding that CEF regulated via PGR5 is needed under high light stress (Munekage et al., 2002). However, it can be suggested that a deficiency in only the NDH complex does not require the same measures as the absence of PGR5. Additionally, a difference in the absorbance for *crr2* relative to WT was seen in the range of 285 nm to 500 nm (*Figure 52*, B). Here, *pgr5* and WT were found to absorb in the same way, but *crr2* showed increased absorbance. Using the same logic as before, the absence of the NDH complex led to increased absorbance in this wavelength range. Subsequently, it can be proposed that

NDH is able to absorb more light of higher energy than that of the WT and *pgr5*. This is consistent with the mutants' increase in PSI-LHCII complexes seen in the native-gel (*Figure 45*).

Overall, it is proposed that in the absence of the NDH complex, light at higher energy wavelengths is absorbed more strongly, this could be achieved via the enrichment of the PSI-(LHCII)$_n$ complexes. These complexes have a higher LHCII to PSI ratio and are thus able to capture more light. Furthermore, in the absence of PGR5 more complexes which absorb at low energy wavelengths are present relative to WT. Also, *crr2* may be executing more LEF than *pgr5.*

Main conclusions regarding the cyclic electron flow mutants

The PSI-Cytb$_6$f is a key complex for photosynthesis and can be isolated using FFE. There is strong evidence that the thylakoid membrane structure and PSI complex composition differs between the two CEF mutants and the wild-type plant. Finally, the absence of NDH appeared to increase complexes, such as PSI-(LHCII)$_n$ absorbing increasingly at high light energies. In contrast, the deficiency in PGR5 increased complexes absorbing at low light energies. Carotenoids are known to absorb at low energy wavelengths and thus *pgr5* seems to have more complexes that can be used in photoprotection.

Future experiments

The overall conclusions drawn from these experiments showed that there could be a difference in the thylakoid membrane structure between the two CEF mutants. In order to confirm this and analyse the differences further, electron microscopy would need to be done. Moreover, gel-blot analysis for the different antenna proteins could provide further insight into why the difference in LHCII migration differs so much in *crr2* compared to WT and *pgr5.* Additionally, to confirm that there are structural differences between the two CEF mutants, FFE separation profiles of *A. thaliana* structural mutants that have for example CURVATURE THYLAKOID1 proteins overexpressed or knocked could be investigated.

Bibliography

Adams, P.G., Vasilev, C., Hunter, C.N., Johnson, M.P., 2018. Correlated fluorescence quenching and topographic mapping of Light-Harvesting Complex II within surface-assembled aggregates and lipid bilayers. Biochim. Biophys. Acta BBA - Bioenerg. 1859, 1075–1085. https://doi.org/10.1016/j.bbabio.2018.06.011

Banerjee, P., Joo, J.B., Buse, J.T., Dawson, G., 1995. Differential solubilization of lipids along with membrane proteins by different classes of detergents. Chem. Phys. Lipids 77, 65–78. https://doi.org/10.1016/0009-3084(95)02455-R

Bellafiore, S., Barneche, F., Peltier, G., Rochaix, J.-D., 2005. State transitions and light adaptation require chloroplast thylakoid protein kinase STN7. Nature 433, 892–895. https://doi.org/10.1038/nature03286

Cooper, G.M., 2000. Chloroplasts and Other Plastids. Cell Mol. Approach 2nd Ed.

DalCorso, G., Pesaresi, P., Masiero, S., Aseeva, E., Schünemann, D., Finazzi, G., Joliot, P., Barbato, R., Leister, D., 2008. A Complex Containing PGRL1 and PGR5 Is Involved in the Switch between Linear and Cyclic Electron Flow in Arabidopsis. Cell 132, 273–285. https://doi.org/10.1016/j.cell.2007.12.028

Drop, B., Yadav K.N., S., Boekema, E.J., Croce, R., 2014. Consequences of state transitions on the structural and functional organization of Photosystem I in the green alga *Chlamydomonas reinhardtii*. Plant J. 78, 181–191. https://doi.org/10.1111/tpj.12459

Fromme, P., Jordan, P., Krauß, N., 2001. Structure of photosystem I. Biochim. Biophys. Acta BBA - Bioenerg. 1507, 5–31. https://doi.org/10.1016/S0005-2728(01)00195-5

Galetskiy, D., Susnea, I., Reiser, V., Adamska, I., Przybylski, M., 2008. Structure and Dynamics of Photosystem II Light-Harvesting Complex Revealed by High-Resolution FTICR Mass Spectrometric Proteome Analysis. J. Am. Soc. Mass Spectrom. 19, 1004–1013. https://doi.org/10.1016/j.jasms.2008.03.014

Galka, P., Santabarbara, S., Khuong, T.T.H., Degand, H., Morsomme, P., Jennings, R.C., Boekema, E.J., Caffarri, S., 2012. Functional Analyses of the Plant Photosystem I-Light-Harvesting Complex II Supercomplex Reveal That Light-Harvesting Complex II Loosely Bound to Photosystem II Is a Very Efficient Antenna for Photosystem I in State II. Plant Cell 24, 2963–2978. https://doi.org/10.1105/tpc.112.100339

Garavito, R.M., Ferguson-Miller, S., 2001. Detergents as Tools in Membrane Biochemistry. J. Biol. Chem. 276, 32403–32406. https://doi.org/10.1074/jbc.R100031200

Gottstein, J., Scheer, H., 1983. Long-wavelength-absorbing forms of bacteriochlorophyll a in solutions of Triton X-100. Proc. Natl. Acad. Sci. 80, 2231–2234. https://doi.org/10.1073/pnas.80.8.2231

Grieco, M., Suorsa, M., Jajoo, A., Tikkanen, M., Aro, E.-M., 2015. Light-harvesting II antenna trimers connect energetically the entire photosynthetic machinery — including both photosystems II and I. Biochim. Biophys. Acta BBA - Bioenerg. 1847, 607–619. https://doi.org/10.1016/j.bbabio.2015.03.004

Heinz, S., Rast, A., Shao, L., Gutu, A., Gügel, I.L., Heyno, E., Labs, M., Rengstl, B., Viola, S., Nowaczyk, M.M., Leister, D., Nickelsen, J., 2016. Thylakoid Membrane Architecture in *Synechocystis* Depends on CurT, a Homolog of the Granal CURVATURE THYLAKOID1 Proteins. Plant Cell 28, 2238–2260. https://doi.org/10.1105/tpc.16.00491

Hoober, J.K., 2016. Photosynthesis, in: Plant Cells and Their Organelles. John Wiley & Sons, Ltd, pp. 300–350. https://doi.org/10.1002/9781118924846.ch11

Iwai, M., Takizawa, K., Tokutsu, R., Okamuro, A., Takahashi, Y., Minagawa, J., 2010. Isolation of the elusive supercomplex that drives cyclic electron flow in photosynthesis. Nature 464, 1210–1213. https://doi.org/10.1038/nature08885

Izawa, S., Good, N.E., 1966. Effect of Salts and Electron Transport on the Conformation of Isolated Chloroplasts. II. Electron Microscopy. PLANT Physiol. 41, 544–552. https://doi.org/10.1104/pp.41.3.544

Johnson, G.N., 2011. Physiology of PSI cyclic electron transport in higher plants. Biochim. Biophys. Acta BBA - Bioenerg. 1807, 384–389. https://doi.org/10.1016/j.bbabio.2010.11.009

Kang, 2002. Highly Sensitive and Fast Protein Detection with Coomassie Brilliant Blue in Sodium Dodecyl Sulfate-Polyacrylamide Gel Electrophoresis. Bull. Korean Chem. Soc. 23, 1511–1512. https://doi.org/10.5012/bkcs.2002.23.11.1511

Kouřil, R., van Oosterwijk, N., Yakushevska, A.E., Boekema, E.J., 2005a. Photosystem I: a search for green plant trimers. Photochem. Photobiol. Sci. 4, 1091. https://doi.org/10.1039/b505519a

Kouřil, R., Zygadlo, A., Arteni, A.A., de Wit, C.D., Dekker, J.P., Jensen, P.E., Scheller, H.V., Boekema, E.J., 2005b. Structural Characterization of a Complex of Photosystem I and Light-Harvesting Complex II of *Arabidopsis thaliana* [†]. Biochemistry 44, 10935–10940. https://doi.org/10.1021/bi051097a

Kouril, R., Zygadlo, A., Arteni, A.A., Wit, C.D. de, Dekker, J.P., Jensen, P.E., Scheller, H.V., Boekema, E.J., 2005. Structural characterization of a complex of photosystem I and light-harvesting complex II of Arabidopsis thaliana. Biochemistry 44, 10935–10940. https://doi.org/10.1021/bi051097a

Kragh-Hansen, U., le Maire, M., Møller, J.V., 1998. The Mechanism of Detergent Solubilization of Liposomes and Protein-Containing Membranes. Biophys. J. 75, 2932–2946. https://doi.org/10.1016/S0006-3495(98)77735-5

Krause, F., 2006. Detection and analysis of protein–protein interactions in organellar and prokaryotic proteomes by native gel electrophoresis: (Membrane) protein complexes and supercomplexes. ELECTROPHORESIS 27, 2759–2781. https://doi.org/10.1002/elps.200600049

Li, X.-P., Björkman, O., Shih, C., Grossman, A.R., Rosenquist, M., Jansson, S., Niyogi, K.K., 2000. A pigment-binding protein essential for regulation of photosynthetic light harvesting. Nature 403, 391–395. https://doi.org/10.1038/35000131

Liu, Z., Yan, H., Wang, K., Kuang, T., Zhang, J., Gui, L., An, X., Chang, W., 2004. Crystal structure of spinach major light-harvesting complex at 2.72 Å resolution. Nature 428, 287–292. https://doi.org/10.1038/nature02373

Malvern instruments, 2014. DLS - An Introduction in 30 Minutes.pdf.

Malvern instruments, 2003. Zetasizer_Nano_user_manual_Man0317-1.1.pdf.

Munekage, Y., Hashimoto, M., Miyake, C., Tomizawa, K.-I., Endo, T., Tasaka, M., Shikanai, T., 2004. Cyclic electron flow around photosystem I is essential for photosynthesis. Nature 429, 579–582. https://doi.org/10.1038/nature02598

Munekage, Y., Hojo, M., Meurer, J., Endo, T., Tasaka, M., Shikanai, T., 2002. PGR5 Is Involved in Cyclic Electron Flow around Photosystem I and Is Essential for Photoprotection in Arabidopsis. Cell 110, 361–371. https://doi.org/10.1016/S0092-8674(02)00867-X

Porra, R.J., Thompson, W.A., Kriedemann, P.E., 1989. Determination of accurate extinction coefficients and simultaneous equations for assaying chlorophylls a and b extracted with four different solvents: verification of the concentration of chlorophyll standards by atomic absorption

spectroscopy. Biochim. Biophys. Acta BBA - Bioenerg. 975, 384–394.
https://doi.org/10.1016/S0005-2728(89)80347-0

Privé, G.G., 2007. Detergents for the stabilization and crystallization of membrane proteins. Methods 41, 388–397. https://doi.org/10.1016/j.ymeth.2007.01.007

Reisinger, V., Eichacker, L.A., 2008. Solubilization of membrane protein complexes for blue native PAGE. J. Proteomics 71, 277–283. https://doi.org/10.1016/j.jprot.2008.05.004

Sanders, C.R., Kuhn Hoffmann, A., Gray, D.N., Keyes, M.H., Ellis, C.D., 2004. French Swimwear for Membrane Proteins. ChemBioChem 5, 423–426. https://doi.org/10.1002/cbic.200300830

Shikanai, T., 2016. Chloroplast NDH: A different enzyme with a structure similar to that of respiratory NADH dehydrogenase. Biochim. Biophys. Acta BBA - Bioenerg. 1857, 1015–1022. https://doi.org/10.1016/j.bbabio.2015.10.013

Shikanai, T., 2014. Central role of cyclic electron transport around photosystem I in the regulation of photosynthesis. Curr. Opin. Biotechnol. 26, 25–30. https://doi.org/10.1016/j.copbio.2013.08.012

Shikanai, T., Endo, T., Hashimoto, T., Yamada, Y., Asada, K., Yokota, A., 1998. Directed disruption of the tobacco *ndhB* gene impairs cyclic electron flow around photosystem I. Proc. Natl. Acad. Sci. 95, 9705–9709. https://doi.org/10.1073/pnas.95.16.9705

Speers, A.E., Wu, C.C., 2007. Proteomics of Integral Membrane ProteinsTheory and Application. Chem. Rev. 107, 3687–3714. https://doi.org/10.1021/cr068286z

Steinbeck, J., Ross, I.L., Rothnagel, R., Gäbelein, P., Schulze, S., Giles, N., Ali, R., Drysdale, R., Sierecki, E., Gambin, Y., Stahlberg, H., Takahashi, Y., Hippler, M., Hankamer, B., 2018. Structure of a PSI–LHCI–cyt b $_6$ f supercomplex in *Chlamydomonas reinhardtii* promoting cyclic electron flow under anaerobic conditions. Proc. Natl. Acad. Sci. 115, 10517–10522. https://doi.org/10.1073/pnas.1809973115

Suorsa, M., Jarvi, S., Grieco, M., Nurmi, M., Pietrzykowska, M., Rantala, M., Kangasjarvi, S., Paakkarinen, V., Tikkanen, M., Jansson, S., Aro, E.-M., 2012. PROTON GRADIENT REGULATION5 Is Essential for Proper Acclimation of Arabidopsis Photosystem I to Naturally and Artificially Fluctuating Light Conditions. Plant Cell 24, 2934–2948. https://doi.org/10.1105/tpc.112.097162

Tagawa, K., Tsujimoto, H.Y., Arnon, D.I., 1963. ROLE OF CHLOROPLAST FERREDOXIN IN THE ENERGY 49, 6.

Ueda, M., Kuniyoshi, T., Yamamoto, H., Sugimoto, K., Ishizaki, K., Kohchi, T., Nishimura, Y., Shikanai, T., 2012. Composition and physiological function of the chloroplast NADH dehydrogenase-like complex in *Marchantia polymorpha*: *Chloroplast NDH in* Marchantia. Plant J. 72, 683–693. https://doi.org/10.1111/j.1365-313X.2012.05115.x

Weber, G., Wildgruber, R., 2008. Free-Flow Electrophoresis System for Proteomics Applications, in: Schmitt-Kopplin, P. (Ed.), Capillary Electrophoresis. Humana Press, Totowa, NJ, pp. 703–716. https://doi.org/10.1007/978-1-59745-376-9_28

Wimley, W.C., 2003. The versatile β-barrel membrane protein. Curr. Opin. Struct. Biol. 13, 404–411. https://doi.org/10.1016/S0959-440X(03)00099-X

Yadav, K.N.S., Semchonok, D.A., Nosek, L., Kouřil, R., Fucile, G., Boekema, E.J., Eichacker, L.A., 2017. Supercomplexes of plant photosystem I with cytochrome b6f, light-harvesting complex II and NDH. Biochim. Biophys. Acta BBA - Bioenerg. 1858, 12–20. https://doi.org/10.1016/j.bbabio.2016.10.006

Yamori, W., Sakata, N., Suzuki, Y., Shikanai, T., Makino, A., 2011. Cyclic electron flow around photosystem I via chloroplast NAD(P)H dehydrogenase (NDH) complex performs a significant physiological role during photosynthesis and plant growth at low temperature in rice: NDH-dependent cyclic electron flow around PSI. Plant J. 68, 966–976. https://doi.org/10.1111/j.1365-313X.2011.04747.x

Yamori, W., Shikanai, T., 2016. Physiological Functions of Cyclic Electron Transport Around Photosystem I in Sustaining Photosynthesis and Plant Growth. Annu. Rev. Plant Biol. 67, 81–106. https://doi.org/10.1146/annurev-arplant-043015-112002

Yokono, M., Takabayashi, A., Akimoto, S., Tanaka, A., 2015. A megacomplex composed of both photosystem reaction centres in higher plants. Nat. Commun. 6. https://doi.org/10.1038/ncomms7675